HEME-BASED OXYGEN SENSORS OF COMMENSAL, SYMBIOTIC,

AND PATHOGENIC BACTERIA

APPROVED BY SUPERVISORY COMMITTEE

Dr. Marie-Alda Gilles-Gonzalez, Ph.D.

Dr. Vanessa Sperandio, Ph.D.

Dr. Thomas Wilkie, Ph.D.

Dr. Wade Winkler, Ph.D.

DEDICATION

To those who have been primarily responsible for overseeing my scientific education: Marie-Alda Gilles-Gonzalez, Gonzalo Gonzalez, and Peter J. Ratcliffe. My sincerest thanks.

This work was funded by the National Science Foundation.

HEME-BASED OXYGEN SENSORS OF COMMENSAL, SYMBIOTIC, AND PATHOGENIC BACTERIA

by

JASON ROBERT TUCKERMAN

DISSERTATION

Presented to the Faculty of the Graduate School of Biomedical Sciences

The University of Texas Southwestern Medical Center at Dallas

In Partial Fulfillment of the Requirements

For the Degree of

DOCTOR OF PHILOSOPHY

The University of Texas Southwestern Medical Center at Dallas

Dallas, Texas, USA

May, 2010

HEME-BASED OXYGEN SENSORS OF COMMENSAL, SYMBIOTIC,

AND PATHOGENIC BACTERIA

JASON ROBERT TUCKERMAN

The University of Texas Southwestern Medical Center at Dallas, 2010

MARIE-ALDA GILLES-GONZALEZ, Ph.D.

Direct oxygen sensors are proteins that serve as “on-off switches” to cause reversible and adaptive changes in the activities of other proteins or genes, with great specificity in response to fluctuations in oxygen concentration. The heme-based oxygen sensors are a large class of direct oxygen sensors that feature direct binding of oxygen to a sensory

heme-containing domain. This heme-binding region couples to a regulatory domain within the same polypeptide. The types of functionalities controlled by these oxygen-specific switches are diverse, and include the regulation of protein activities, gene expression, and second messenger elaboration. A primary focus of this work was the biochemical characterization of a pair of heme-based oxygen sensors involved in the control of the bacterial second messenger cyclic diguanylic acid (c-di-GMP) in *Escherichia coli*. We discovered that these enzymes, designated DosC and DosP, serve as a diguanylate cyclase and c-di-GMP phosphodiesterase pair that associate with components of the *E. coli* RNA degradosome *in vivo*. Importantly, one member of these degradosomes, PNPase, is a direct, high-affinity target of c-di-GMP. These findings imply that specialized oxygen-sensing degradosomes exist in *E. coli*. In these oxygen-sensing degradosomes cellular oxygen levels regulate PNPase processing of specific RNA transcripts via c-di-GMP.

A secondary focus of this work was the characterization of a novel two-component system in *M. tuberculosis* involved in the non-replicating persistent phase of this bacterium in a typical TB infection. Here, the activities of two heme-containing histidine kinases, DosT and DevS, were discovered to be inhibited specifically by oxygen. As DosT and DevS are

the primary regulators of the dormancy survival regulator (DosR/DevR) transcription factor, these results contributed a molecular explanation for the numerous observations linking oxygen and DevR to the dormancy phenotype of *M. tuberculosis* seen both *in vitro* and *in vivo*.

TABLE OF CONTENTS

PRIOR PUBLICATIONS

Tuckerman JR, Gonzalez G, & Gilles-Gonzalez MA. Oxygen Controlled RNA Degradosomes via c-di-GMP. (*Submitted*).

Tuckerman JR, Gonzalez G, Sousa EH, Wan X, Saito JA, Alam M, & Gilles-Gonzalez MA. An oxygen-sensing diguanylate cyclase and phosphodiesterase couple for c-di-GMP control. *Biochemistry* (2009) 48:9764-74.

Wan X, **Tuckerman JR**, Saito JA, Freitas TA, Newhouse JS, Denery JR, Galperin MY, Gonzalez G, Gilles-Gonzalez MA, & Alam M. Globins synthesize the second messenger bis-(3'-5')-cyclic diguanosine monophosphate in bacteria. *J Mol Biol*. (2009) 388:262-70.

Gilles-Gonzalez MA, Gonzalez G, Sousa EH, & **Tuckerman JR**. Oxygen-sensing histidine-protein kinases: assays of ligand binding and turnover of response-regulator substrates. *Methods Enzymol*. (2008) 437:173-89.

Sousa EH, **Tuckerman JR**, Gonzalez G, & Gilles-Gonzalez MA. DosT and DevS are oxygen-switched kinases in *Mycobacterium tuberculosis*. *Protein Sci*. (2007) 16:1708-19.

Sousa EH, **Tuckerman JR**, Gonzalez G, & Gilles-Gonzalez MA. A memory of oxygen binding explains the dose response of the heme-based sensor FixL. *Biochemistry* (2007) 46:6249-57.

Tuckerman JR, Zhao Y, Hewitson KS, Tian YM, Pugh CW, Ratcliffe PJ, & Mole DR. Determination and comparison of specific activity of the HIF-prolyl hydroxylases. *FEBS Lett*. (2004) 576:145-50.

Masson N, Appelhoff RJ, **Tuckerman JR**, Tian YM, Demol H, Puype M, Vandekerckhove J, Ratcliffe PJ, & Pugh CW. The HIF prolyl hydroxylase PHD3 is a potential substrate of the TRiC chaperonin. *FEBS Lett*. (2004) 570:166-70.

Dunham CM, Dioum EM, **Tuckerman JR**, Gonzalez G, Scott WG, & Gilles-Gonzalez MA. A distal arginine in oxygen-sensing heme-PAS

domains is essential to ligand binding, signal transduction, and structure. *Biochemistry* (2003) 42:7701-8.

Dioum EM, Rutter J, **Tuckerman JR**, Gonzalez G, Gilles-Gonzalez MA, & McKnight SL. NPAS2: a gas-responsive transcription factor. *Science* (2002) 298:2385-7.

Tuckerman JR, Gonzalez G, Dioum EM, & Gilles-Gonzalez MA. Ligand and oxidation-state specific regulation of the heme-based oxygen sensor FixL from *Sinorhizobium meliloti*. *Biochemistry* (2002) 41:6170-7.

Tuckerman JR, Gonzalez G, & Gilles-Gonzalez MA. Complexation precedes phosphorylation for two-component regulatory system FixL/FixJ of *Sinorhizobium meliloti*. *J Mol Biol*. (2001) 308:449-55.

Chang AL, **Tuckerman JR**, Gonzalez G, Mayer R, Weinhouse H, Volman G, Amikam D, Benziman M, & Gilles-Gonzalez MA. Phosphodiesterase A1, a regulator of cellulose synthesis in *Acetobacter xylinum*, is a heme-based sensor. *Biochemistry* (2001) 40:3420-6.

LIST OF FIGURES

LIST OF TABLES

LIST OF ABBREVIATIONS

ATP	Adenosine 5'-triphosphate
Ax PDE-A1	*Gluconacetobacter xylinus* (formerly *Acetobacter xylinum)* phosphodiesterase A1
Bj FixL	*Bradyrhizobium japonicum* sensor kinase FixL
*Bpe*GReg	*Bordetella pertussis* globin-coupled regulator
CHAPS	(3-[(3-cholamidopropyl)dimethylammonio]-1-propanesulfonate)
cAMP	3'→5' cyclic adenylic acid
c-di-GMP	3'→5' cyclic diguanylic acid
Deoxy	Ferrous (Fe^{2+}) heme without exogenous ligand
DevS	*Mycobacterium tuberculosis* sensor kinase DevS
DevR	*Mycobacterium tuberculosis* response regulator DevR
DGC	Diguanylate cyclase
DosC	*Escherichia coli* direct oxygen sensing cyclase
$DosC_H$	DosC truncation containing only heme domain residues 2-160
DosP	*Escherichia coli* direct oxygen sensing phosphodiesterase
$DosP_H$	DosP truncation containing only heme domain residues 1-147
DosT	*Mycobacterium tuberculosis* sensor kinase DosT
DTT	Dithiothreitol
EAL	Cyclic di-GMP phosphodiesterase domain
EDTA	Ethylenediaminetetraacetic acid

GAF	Protein domain named after cGMP-regulated nucleotide phosphodiesterases, adenylate cyclases, and FhlA
GCS	Globin-coupled sensor
GGDEF	Diguanylate cyclase domain
GTP	Guanosine 5'-triphosphate
HemAT-*Bs*	*Bacillus subtilis* methyl-accepting chemotaxis protein HemAT
HNOB	Heme-nitric oxide-binding domain
IPTG	Isopropyl-β-D-thiogalactoside
LB	Luria-Bertani broth
MBP	*Escherichia coli* maltose-binding protein
Met	Ferric (Fe^{3+}) heme without exogenous ligand
Oxy	Ferrous (Fe^{2+}) heme ligated to O_2
PAS	Sensory domain named after the eukaryotic proteins Period, Arnt, and Simple-minded
PDE	Cyclic di-GMP phosphodiesterase
PMSF	Phenylmethylsulfonyl fluoride
Rm FixL	*Sinorhizobium meliloti* (formerly *Rhizobium meliloti*) sensor kinase FixL
SDS	Sodium dodecyl sulfate
SG	Sensory globin domain
SW Mb	Sperm whale myoglobin

PART ONE: STUDIES ON O_2-REGULATED C-DI-GMP SIGNALING

CHAPTER ONE

Introduction and Literature Review

(1.1) Sensory Transduction by Heme-based O_2 Sensors.

Oxygen signal transduction is critically important to many organisms and cell types. In mammals, many processes are under the control of O_2. For example, the production of erythrocytes and development of peripheral vasculature are regulated by a pair of hormones—erythropoietin (Epo) and vascular endothelial growth factor (VEGF), respectively—whose levels are controlled by O_2 (*1-3*). An O_2-sensitive signaling system also controls ventilation in response to both acute and chronic hypoxemia (*4-6*). Disrupted O_2 signaling also likely plays a role in the development and progression of many of cancers, as many neoplastic processes—including aspects of cell survival, angiogenesis, glucose metabolism, and invasiveness—are regulated by the O_2-sensitive transcriptional activator HIF (hypoxia-inducible factor) (*7-9*). Bacteria likewise rely on O_2-dependent signaling mechanisms.

Indeed, the very capacity of a whole class of bacteria—the facultative anaerobes—to switch between aerobic and anaerobic lifestyles highlights the ability of these organisms to perceive and adapt to fluctuations in environmental O_2 levels (*10-13*).

What are the molecular mechanisms that underlie adaptations to changes in O_2 tension? One of the most direct strategies so far identified features biological heme-based O_2 sensors. In a heme-based O_2 sensor, reversible binding of O_2 to a regulatory heme-binding domain controls a neighboring transmitter region of the same protein (Figure 1.1A) (*14, 15*). As a class of heme proteins, these direct O_2 sensors are distinct from the carriers of O_2 and the catalysts of oxygen-atom and electron transfer reactions (*14, 15*). To date, at least four different regulatory heme-binding domains (PAS, GAF, sensory globin, and HNOB) and five transmitter regions (histidine kinase, methyl carrier protein, guanylate cyclase, diguanylate cyclase, and c-di-GMP phosphodiesterase) have been identified (Figure 1.1B) (*15-18*). As biochemical tools, heme-based sensors provide excellent models for study of oxygen signal transduction, with the iron center supplying a built-in probe of the sensor's status and the transmitter reporting the switching potential of any state of the heme (*15*).

The first heme-based sensor discovered was the histidine kinase FixL from the nitrogen-fixing symbionts *Rhizobium meliloti* and *Bradyrhizobium japonicum* (*19, 20*). Here, an N-terminal heme-containing PAS (H-PAS) domain couples to a C-terminal histidine protein kinase such that binding of O_2 to the H-PAS switches off the kinase activity. Dissociation of O_2 from the FixL heme, such as occurs during the migration of *Rhizobia* into the increasingly microaerobic environments of the plant root nodules that they colonize, leads to autophosphorylation of the kinase and subsequent transfer of the phosphoryl group to the cognate response regulator FixJ. Phospho-FixJ binds to *nif* and *fix* promoter elements, resulting in the increased transcription of genes necessary for nitrogen fixation, anaerobic respiration, and denitrification (Figures 1.2, 1.3, 1.4) (*20, 21*).

(1.2) Cyclic-di-GMP Signaling.

Among the most numerous and widely distributed genes in bacteria are those that code for proteins with GGDEF and/or EAL domains (*22*). These domains are responsible for the synthesis and degradation of the bacterial second messenger cyclic diguanylic acid (c-di-GMP) (Figure 1.5). In *Gluconacetobacter xylinus*, where c-di-GMP was first discovered, this

dinucleotide second messenger allosterically activates a cellulose synthase enzyme to polymerize UDP-glucose to cellulose (*23, 24*). In fact, a single *G. xylinus* can polymerize to cellulose up to 200,000 glucose molecules per second (*25*). The cellular level of c-di-GMP depends on a balance between the activity of a diguanylate cyclase (GGDEF-domain-containing) and a c-di-GMP specific phosphodiesterase (EAL-domain-containing) (Figure 1.5) (*26, 27*). The diguanylate cyclase (DGC) synthesizes c-di-GMP from 2 molecules of GTP, whereas the phosphodiesterase (PDE) hydrolyzes c-di-GMP to linear pGpG (Figure 1.5) (*28-30*). The thick cellulose pellicle generated by *G. xylinus* represents a rudimentary biofilm that provides a specialized protective environment for a "multicellular" *G. xylinus* community (Figure 1.6). There is increasing interest in biofilms because they are known to protect bacteria from antibiotic exposure and to exacerbate some chronic infections in humans (*31*).

Since the pioneering work on *G. xylinus* and bioinformatic studies suggesting that the GGDEF/EAL-domain enzymes for c-di-GMP synthesis and degradation occur in many bacterial species, interest in this second messenger has been revived, and our understanding of it has grown (*22, 32-36*). Nevertheless, fundamental questions remain unanswered about

the c-di-GMP homeostatic mechanism. For example, what signals regulate the activities of the diguanylate cyclases (DGC) and c-di-GMP phosphodiesterases (PDE)? That such signals exist is indicated by the recognizable signaling domains in these proteins that accompany their enzymatic domains (*16, 20, 22, 29, 37*). Even so, relatively few studies have directly addressed the coupling of signaling domain to a DGC or PDE activity (*38-44*). The first demonstration of coupling of an environmental signal to a c-di-GMP processing enzyme was done for the *G. xylinus* c-di-GMP phosphodiesterase *Ax* PDE-A1. In *Ax* PDE-A1, binding of O_2 to the heme iron of a heme-PAS domain was found to switch off its PDE activity (Figure 1.6) (*38*). The inhibition of this PDE activity by O_2 was consistent with the observation that, in static cultures of *G. xylinus*, the cellulose pellicle is produced at the air-liquid interface by the most aerated cells. In these cells, the inhibition of PDE-A1 by O_2 leads to an increase of c-di-GMP and activation of cellulose synthesis. Cells anchored to the cellulose pellicle would stay near the surface where they have access to nutrients as well as sufficient O_2 for respiration. Bacteria of the genus *Gluconacetobacter* are obligate aerobes. For *G. xylinus*, production of cellulose is costly, in terms of both carbon sources and

energy. Shutdown of cellulose production when O_2, and therefore energy, is low may be a way of conserving resources.

Another important question regards the *in vivo* targets of c-di-GMP. The range of c-di-GMP's influence was recently shown to include metabolite-binding regions in mRNAs that regulate specific transcripts (*45*). Though few protein targets have been identified for c-di-GMP, the example of the *G. xylinus* cellulose synthase represents an important precedent that this molecule can serve as an allosteric effector of target proteins (*23, 46-52*).

The numbers of GGDEF/EAL proteins encoded by bacteria pose yet another puzzle: why are so many of these proteins needed in some species if GGDEF domains reliably manifest a DGC activity and EAL domains a c-di-GMP-dedicated PDE activity (*27, 29, 30*)? The *Escherichia coli* K12 genome, for example, encodes 12 proteins with a GGDEF domain, 10 with an EAL, and 7 with both GGDEF and EAL (*53, 54*). By contrast to this relatively large number of c-di-GMP-dedicated enzymes, *E. coli* possesses a single adenylate cyclase and a single cAMP phosphodiesterase (*55, 56*). Nevertheless, for several bacterial species, a phenotypic change has been shown to result from the deletion of a single DGC or PDE (*41, 57-59*). Why should this be so, if several other related

enzymes in the same cell could, in principle, complement the deletion? Though physiological conditions such as temperature, media, and growth phase have been identified that influence the expression of *E. coli* genes encoding GGDEF/EAL proteins, this still leaves much of their redundancy unexplained (*53, 54*). One hypothesis is that the specific interactions of environmental signals with sensory domains in GGDEF/EAL proteins might guide their c-di-GMP generation to specific sites in the cell, instead of a common cellular pool.

The presence or absence of c-di-GMP at a specific site would in turn be governed by the physiological state of an organism and its environment. In such a scheme, a physiological signal would again be an essential part of a DGC or PDE response. Oxygen appears to be a highly important signal ligand for regulating DGCs and PDEs. As noted above, the first demonstrated regulation of a GGDEF/EAL-class enzyme by an environmental signal was the discovery of the O_2-switched PDE activity in *Ax* PDE-A1 (*38*). Subsequent work has shown that the synthesis of c-di-GMP in *G. xylinus* is also regulated by O_2, though indirectly, from the oxidation state of the diguanylate cyclase *Ax* DGC-2, a flavin-containing DGC (*42*). Both *Ax* PDE-A1 and *Ax* DGC-2 are found in close association with the cellulose synthase. In fact, this large complex likely represents a

compartmentalized c-di-GMP signaling circuit (Figure 1.7). In this system, where both the synthesis (by DGC-2) and degradation (by PDE-A1) of c-di-GMP are regulated by an environmental signal (O_2), the target of the c-di-GMP, *i.e.* the cellulose synthase, resides in the same macromolecular complex. Signaling complexes, such as the cellulose synthase and associated molecules in *G. xylinus*, may be more widespread as ways to compartmentalize c-di-GMP signaling circuits within individual bacterial cells.

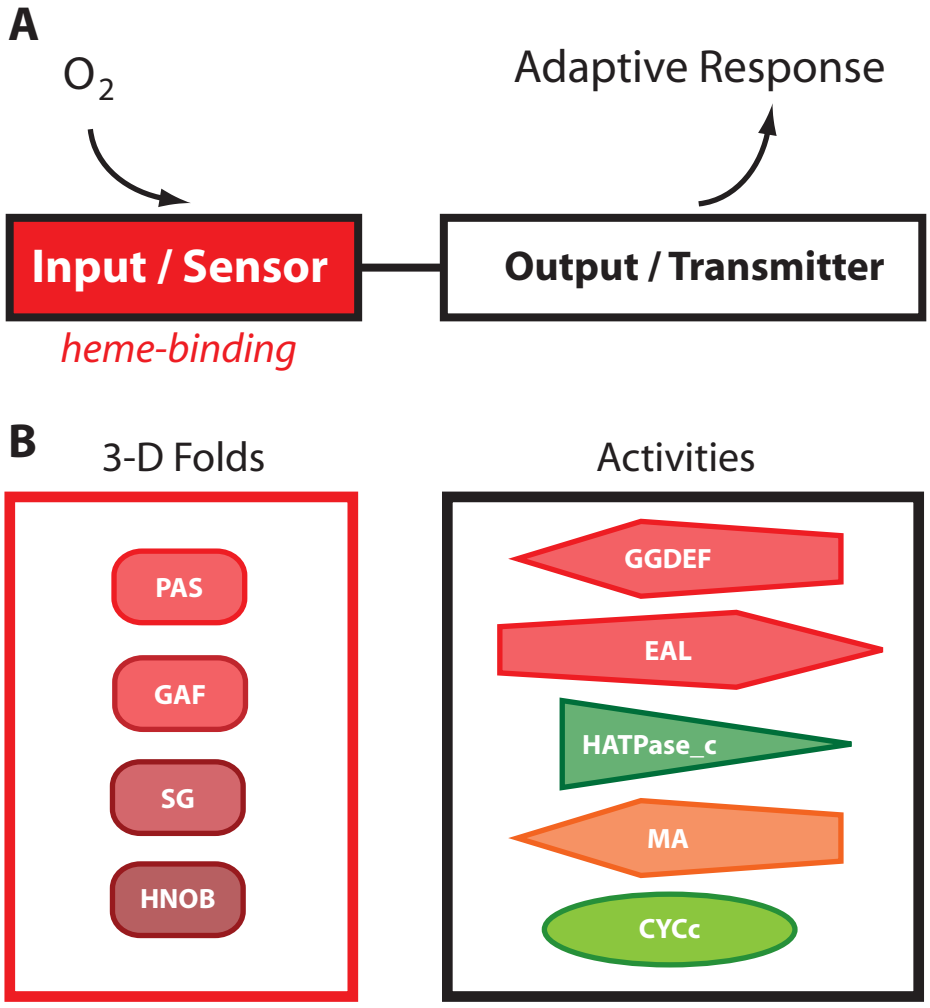

Figure 1.1. **Modularity of heme-based oxygen sensors. (A)** Representative domain organization of a heme-based oxygen sensor. **(B)** Heme-containing sensory modules and transmitter regions identified to date for heme-based oxygen sensors. Shapes and abbreviations correspond to the domain designations in the SMART database. PAS, Per-Arnt-Sim; GAF, c**G**MP-regulated cyclic nucleotide phosphodiesterases, **a**denylate cyclases, and bacterial transcriptional regulator **F**hlA domains; SG, sensory globin (not in SMART database); HNOB, heme-nitric oxide binding (not in SMART database); GGDEF, diguanylate cyclase; EAL, c-di-GMP phosphodiesterase; HATPase_c, histidine kinase; MA, methyl-accepting chemotaxis domain; CYCc, adenylyl/guanylyl cyclase.

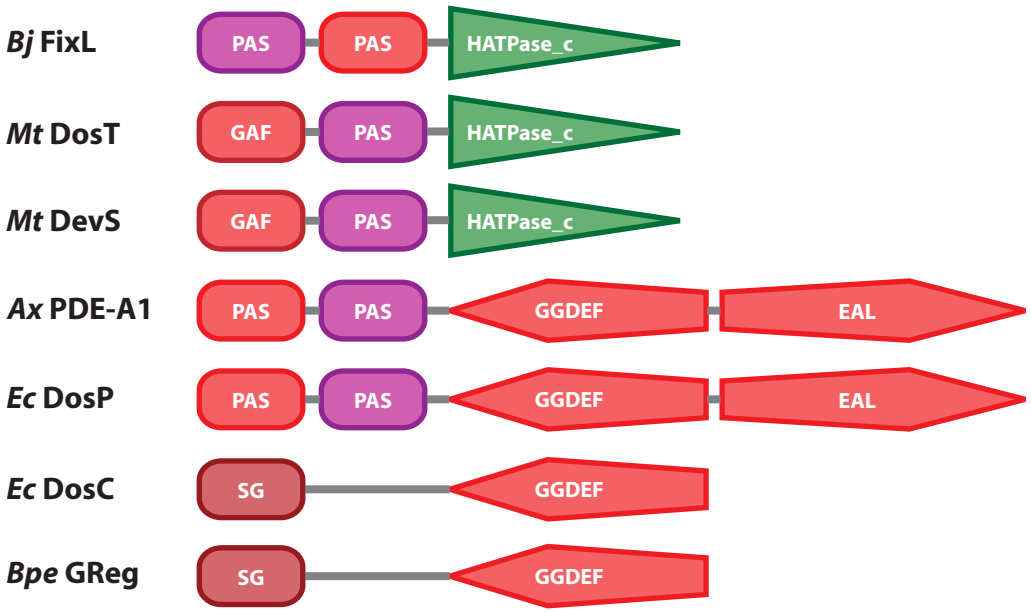

Figure 1.2. **Heme-based oxygen sensors described in this study.** *Bj, Bradyrhizobium japonicum; Mt, Mycobacterium tuberculosis; Ax; Acetobacter xylinum; Ec, Escherichia coli; Bpe, Bordetella pertussis.*

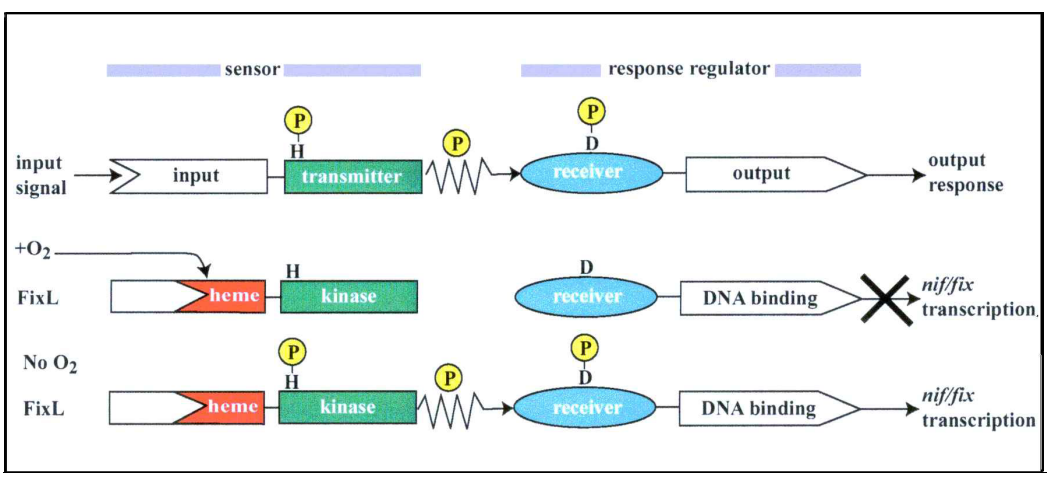

Figure 1.3. **The FixL / FixJ two-component regulatory system.** In two-component regulatory systems, an input signal is transduced to generate an output response by the successive transfer of a phosphoryl group from a sensor kinase to its cognate response regulator. For the sensor kinase FixL, the sensory module is a heme-binding PAS domain that inhibits autophosphorylation when O_2 binds and permits enzymatic activity when O_2 dissociates. The output response is transcriptional activation at nitrogen-fixation promoters. The FixL/FixJ two-component system ensures that genes required for nitrogen fixation are efficiently repressed under aerobic conditions. The phosphorylation site histidine in FixL and aspartate in FixJ are denoted "H" and "D", respectively.

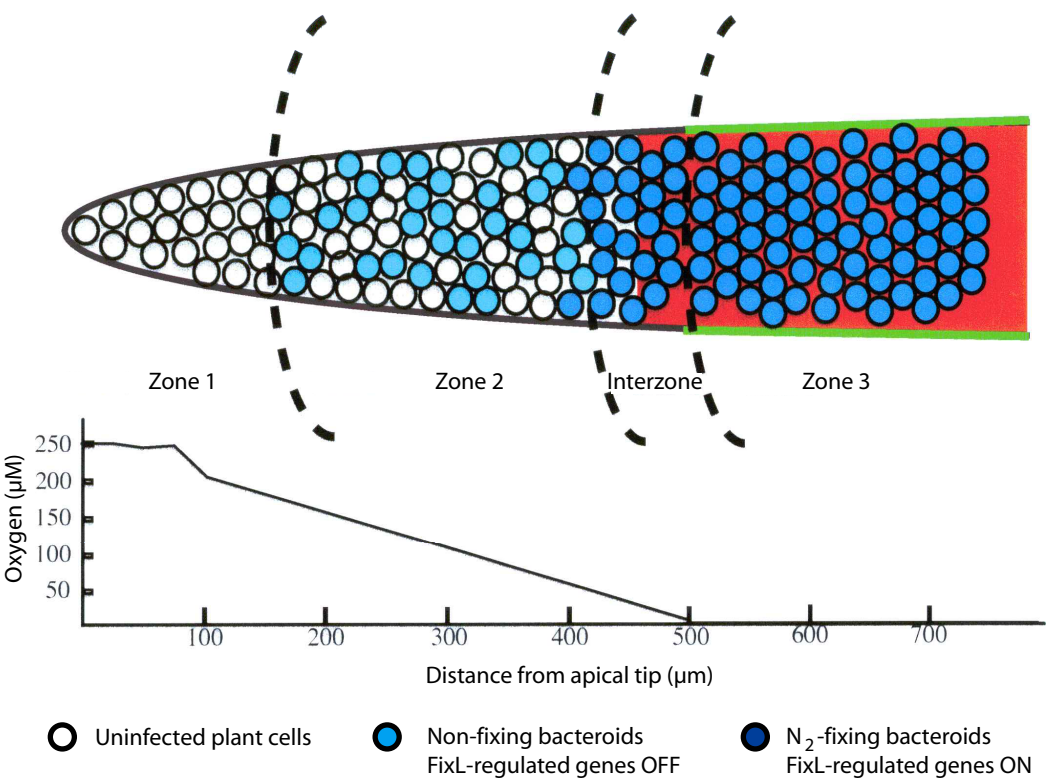

Figure 1.4. **Influence of oxygen concentration on the expression of nitrogen-fixation genes within a developing symbiotic root nodule.** Induction of nitrogen-fixation genes occurs in the interzone and in zone 3, where $[O_2] < 50$ μM. This figure was adapted from the results of Batut and colleagues (Soupene E, Foussard M, Boistard P, Truchet G, & Batut J., *Proc Natl Acad Sci USA* (1995) 92:3759-3763) (*102*).

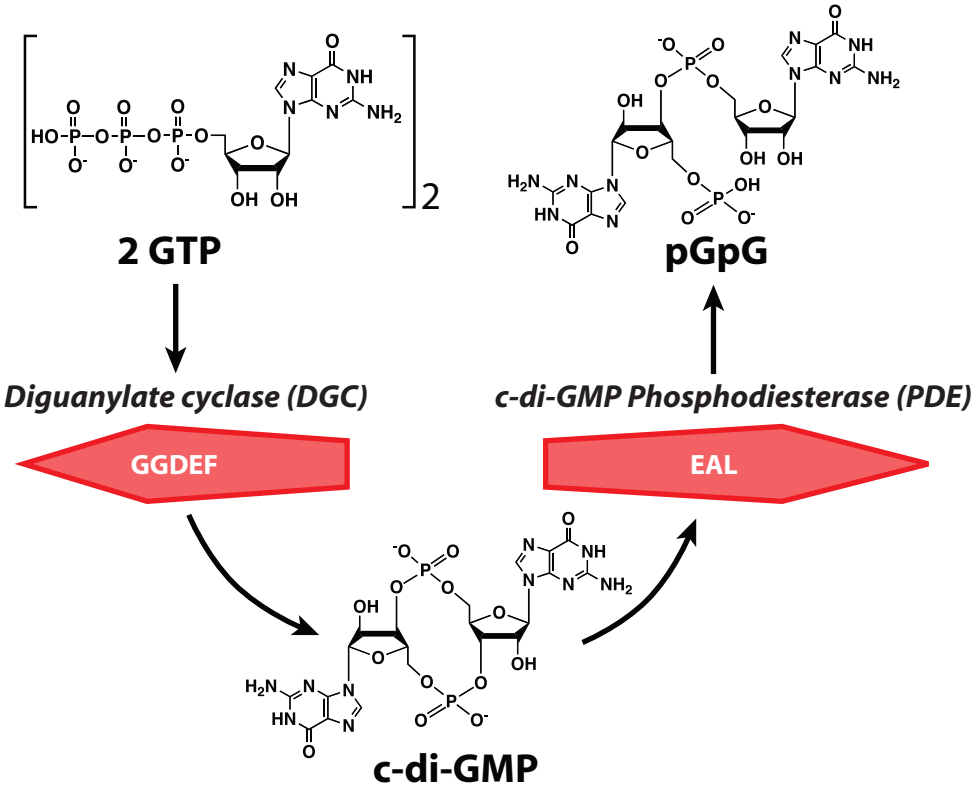

GGDEF		GGDEF + EAL		EAL	
dosC	*yeaJ*	***dosP***	*yhjK*	*rtn*	*ylaB*
yaiC	*yeaP*	*yciR*		*ycgF*	*yliE*
ycdT	*yedQ*	*yegE*		*ycgG*	*yoaD*
ydaM	*yfiN*	*yfeA*		*ydiV*	*yahA*
ydeH	*yliF*	*yfgF*		*yhjH*	
yeaI	*yneF*	*yhdA*		*yjcC*	

***Figure 1.5*. Cyclic-di-GMP signaling.** The top panel illustrates the enzymes and protein domains involved in synthesizing and degrading c-di-GMP. Synthesis is catalyzed by a diguanylate cyclase (GGDEF-domain containing) while degradation is catalyzed by a c-di-GMP phosphodiesterase (EAL-domain containing). The bottom panel lists the 29 genes in *E. coli* that encode either a GGDEF or EAL domain. Seven of the 29 genes code for proteins predicted to contain both GGDEF and EAL domains.

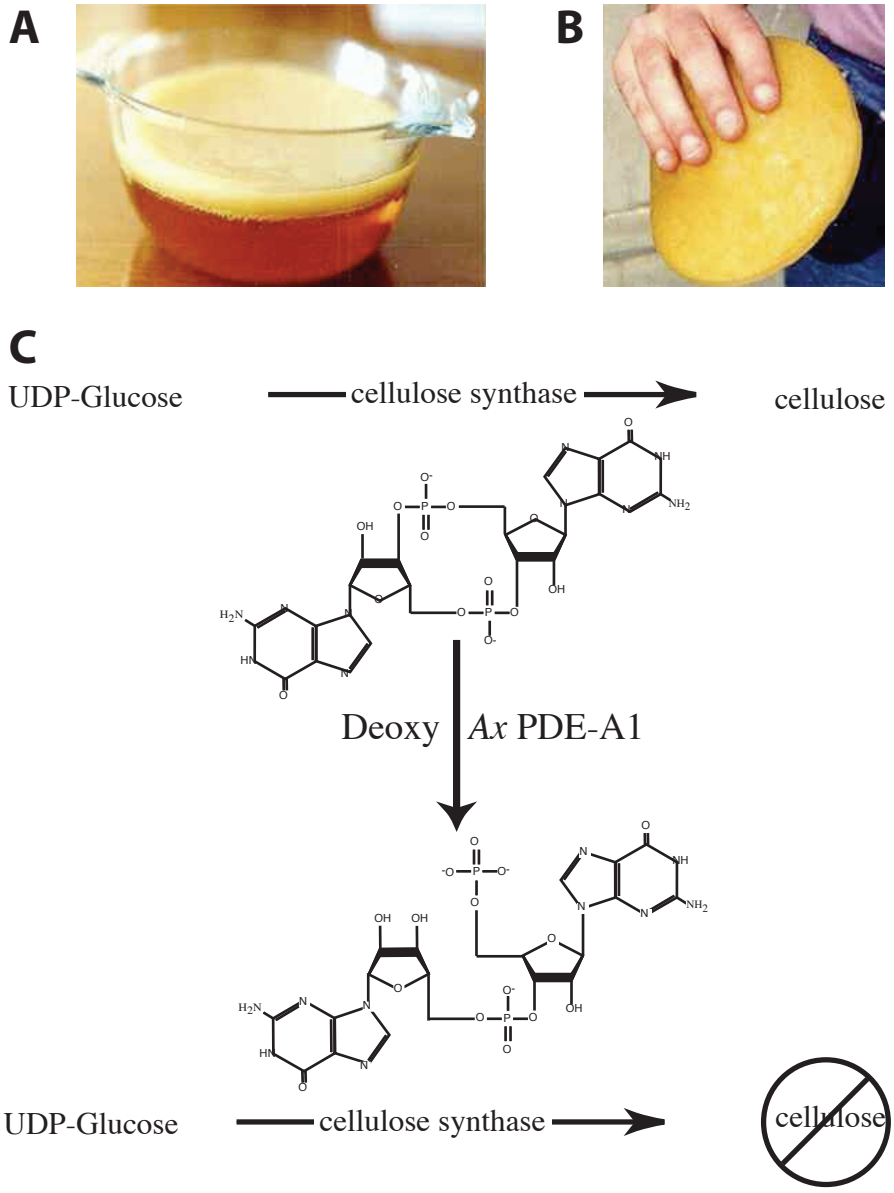

Figure 1.6. **Influence of O_2 and c-di-GMP on cellulose synthesis by *Gluconacetobacter xylinus*. (A, B)** Static cultures of *G. xylinus* form a cellulose pellicle at the air-liquid interface. **(C)** The second messenger c-di-GMP is required for allosteric activation of the *G. xylinus* cellulose synthase. Deoxy-*Ax*PDE-A1 actively converts c-di-GMP to the inert pGpG to inhibit cellulose synthesis within the anaerobic liquid phase. Oxygen binding to the *Ax*PDE-A1 heme domain inhibits PDE activity and permits the persistence of c-di-GMP in cells at the air-liquid interface.

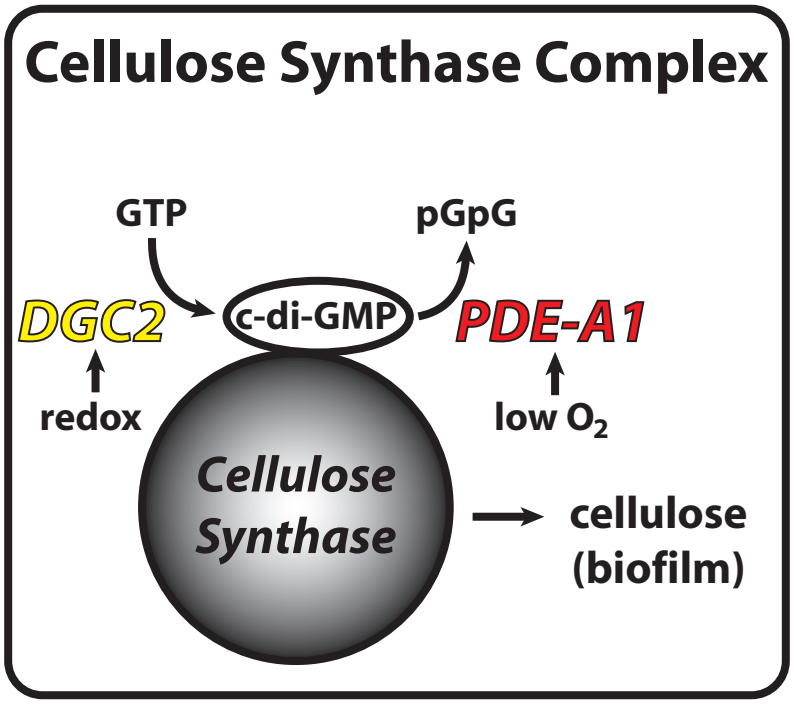

***Figure 1.7*. The *G. xylinus* cellulose synthase signaling complex.** Here, a redox controlled DGC and an O_2 regulated PDE establish the local levels of c-di-GMP available to the target cellulose synthase. Descriptions of *Ax*DGC2 and *Ax*PDE-A1 are from Qui Y, Rao F, Luo Z, & Liang ZX. *Biochemistry* (2009) 48: 10275-10285 (*42*); and Chang AL, Tuckerman JR, Gonzalez G, Mayer R, Weinhouse H, Volman G, Amikam D, Benziman M, & Gilles-Gonzalez MA. *Biochemistry* (2001) 40: 3420-3426 (*38*), respectively.

CHAPTER TWO

Materials and Methods

(2.1) Genetic Manipulations. The designs of oligonucleotide primers for amplifying regions of the *dosCP* operon were based on the *E. coli* genome sequence published by Blattner and colleagues (*60*). *E. coli* genomic DNA served as the template in polymerase chain reactions (PCR). The PCR primers appended a *NsiI* or *NdeI* restriction site to the 5' end and a *HindIII* or *NotI* site to the 3' end of each amplified DNA. The amplified products with *dosCP* and $dosC_H$ (codons 2-160) were cloned as *NsiI-NotI* fragments into an *E. coli pUC19*-based expression vector such that the final plasmids conferred ampicillin resistance and *tac*-promoter control of the recombinant genes. The *E. coli malE* gene was fused to the 5'-end of *dosC* by cloning the *dosCP*-coding sequence as a *NsiI-NotI* fragment into the *E. coli* vector pMAL-c2e (New England Biolabs), where *NsiI* and *NotI* restriction sites were engineered into the polylinker.

In all cases, cloning of the correct fragments was confirmed by DNA sequencing (McDermott Center for Human Growth and Development, University of Texas Southwestern Medical Center).

The cloned *E. coli pnp* gene, in pGC400, was a generous gift from Dr. George Jones (Emory University). This plasmid encodes the wild-type *pnp* gene under the control of a T7 promoter and confers ampicillin resistance.

A plasmid containing the *E. coli malE* gene (pMAL-c5e) was purchased from New England Biolabs and used for the production of recombinant maltose-binding protein (MBP).

(2.2) Gene Expression and Protein Purification. The *dosCP* operon was overexpressed in *E. coli* strain MC1061 in a Bioflow 3000 4-L fermentor with continuous supplementation of LB and glucose. This fermentor features automatic control of temperature via electrical heating and circulation of chilled water so that any programmed temperature is reached within 2 min and maintained automatically within 0.1 ^{o}C. It was initially set to 37 °C. The pH was programmed for 7.5 and was automatically maintained within 0.2 units of this value by precise additions of neat NH_4OH to neutralize bacterial catabolites. The O_2 electrode was calibrated by agitating the medium vigorously with air and setting that point as 100% air saturation once the electrode reading stabilized. The O_2 concentration was set to 4 % O_2 (i.e. 20 % of atmospheric O_2) and

maintained by automatic adjustments of the agitation rate and the percentage of O_2 in a feed of air and pure O_2. When the cultures reached 30 g/L of wet cells, isopropyl β-D-1-thiogalactopyranoside (IPTG) was added to a final concentration of 1.0 mM, and the fermentor temperature was changed to 27 °C. The cells were harvested 20 h later. The *dosC*$_H$ region, encoding a globin-coupled sensor domain, and the *malE:dosCP* fusion were expressed in shaker cultures of *E. coli* strains MC1061 and TG1, respectively. The media initially consisted of LB with 200 μg/mL ampicillin and 0.2 % (w/v) glucose. When the cultures reached $A_{600} \sim 0.5$, gene expression was induced with 1.0 mM IPTG and the temperature was reduced to 27 °C. The cells were harvested 4 – 8 h post-induction.

All subsequent protein purification steps were at 4 °C, with monitoring of the proteins from their bright-red color or absorption spectra (Cary 4000 UV-Vis spectrophotometer, Varian) (Figure 2.1). The *dosCP*-overexpressing cells were lysed by sonicating the harvested cell pellet in lysis buffer [50 mM Tris-HCl pH 8.0, 150 mM NaCl, 5.0 mM dithiothreitol (DTT), 1.0 mM EDTA, 0.050 mg/mL lysozyme, and 0.17 mg/mL PMSF]. After 40 min of centrifugation at 70,000 rpm, the cleared lysate was brought to 0.40 M $(NH_4)_2SO_4$ and loaded onto a phenyl sepharose fast-flow column (GE Healthcare) equilibrated with 0.40 M $(NH_4)_2SO_4$ in FS-

buffer [50 mM Tris-HCl, 150 mM NaCl, 5.0 mM DTT, 1.0 mM EDTA, pH 8.0]. The column was washed sequentially with FS-buffer containing 0.40, 0.20, and 0.10 M $(NH_4)_2SO_4$ prior to elution of the bound DosC:DosP complex with FS-buffer without $(NH_4)_2SO_4$. The recovered DosC:DosP complex was loaded onto a 1 meter x 25 mm Superdex S200 column (GE Healthcare) pre-equilibrated with 50 mM Tris-HCl, 50 mM NaCl, and 5.0 % (v/v) glycerol, pH 8.0. The collected fractions were analyzed for their purity and protein contents from their spectra, from Bradford protein assays (Bio-Rad), and from Coomassie-stained SDS-PAGE gels (*61*). The heme content of purified proteins was quantified by a pyridine hemochromagen assay, with hemin as the standard (Section 2.3) (*62*).

Separation of DosP from DosC was possible using anion-exchange chromatography (DEAE Sepharose, GE Healthcare). After separation, the isolated DosP remains soluble while DosC becomes insoluble.

Cells overproducing $DosC_H$ were sonicated in the same lysis buffer described above, except for replacement of DTT with β-mercaptoethanol (10 mM). After 40 min of centrifugation at 70,000 rpm, the cleared lysate was brought to 1.2 M $(NH_4)_2SO_4$ and centrifuged at 12,000 rpm for 15 min. The pellet was discarded, and the supernatant was slowly brought to 2.4 M $(NH_4)_2SO_4$. After 15 min of centrifugation at 12,000 rpm, the protein

pellets were stored at –80 °C. Later the protein pellets were resuspended in two volumes of 20 mM Tris-HCl, 10 mM β-mercaptoethanol, pH 8.0, and a small fraction of undissolved materials was removed by 15 min of centrifugation at 12,000 rpm. The supernatant was desalted through a Sephadex G25 column pre-equilibrated in 20 mM Tris-HCl, 10 mM β-mercaptoethanol, pH 8.0 and then applied to a DEAE-Sepharose 10 cm (h) x 3 cm (d) column pre-equilibrated with the same buffer. After thorough washing of the column with the loading buffer, the $DosC_H$ was slowly eluted from buffer supplemented with 150 mM NaCl. The eluted $DosC_H$ was concentrated, purified to homogeneity by gel-filtration chromatography (Superdex S200, 1 meter x 25 mm, GE Healthcare), and stored at –80 °C.

For MBP-DosC, the harvested cells (~ 24 g) were resuspended in 40 mL of lysis buffer (50 mM Tris-HCl pH 8.0, 150 mM NaCl, 5 mM $MgCl_2$, 1 mM DTT, 5 % (v/v) glycerol), centrifuged at 5000 rpm for 15 min, and the resulting cell pellets were frozen initially on dry ice and then overnight at –20 °C. Twelve grams of frozen cells were resuspended in 35 mL of lysis buffer supplemented with 42 mg lysozyme and 7 mg PMSF and incubated on ice for 20 min. The cells were then completely disrupted by sonication, centrifuged at 70,000 rpm for 35 min, and the supernatant was

applied directly onto an amylose-resin matrix [9 cm (h) x 2 cm (d), New England Biolabs] pre-equilibrated with lysis buffer. After extensive washing with wash buffer [50 mM Tris-HCl pH 8.0, 200 mM NaCl, 1 mM EDTA, 1 mM DTT], the bound MBP-DosC was eluted with wash buffer containing 10 mM maltose. Glycerol was added to the eluted MBP-DosC to a final concentration of 5 % (v/v), and the purified protein was frozen with liquid N_2 and stored at –80 °C. As a control, *E. coli* maltose-binding protein (MBP) was overproduced and purified using the same series of steps described for the isolation of recombinant MBP-DosC.

The expression and purification of *E. coli* PNPase was essentially as described previously by Jones and colleagues (*63*). Briefly, a frozen inoculum of *E. coli* BL21(DE3)pLysS containing pGC400 was used to inoculate 2-L of LB containing ampicillin (50 μg/mL) and chloramphenicol (34 μg/mL) at 37 °C. The culture was induced with 1 mM IPTG when A_{600} = 0.5 and harvested 3 hours post-induction by centrifugation for 10 min at 10,000*g* and 4 °C. Following harvest, cell pellets were resuspended in 20 mL of Buffer A [50 mM Tris-HCl pH 8.0, 5 mM $MgCl_2$, 1 mM DTT, and 5 % glycerol] and centrifuged again as described above. The cell pellets were frozen initially on dry ice and then overnight at –20 °C. The cell pellets were thawed by suspension in 20 mL of cold Buffer A supplemented with

28 mg lysozyme, 28 mg CHAPS, and 50 mg PMSF. After gentle mixing, DNase I (500 U, RNase-free, New England Biolabs) was added and the suspensions were incubated on ice for 60 min. The suspensions were then centrifuged for 15 min at 15,000*g* and 4 °C. The supernatants were removed and subjected to phosphorolysis with 10 mM with potassium phosphate, pH 8.0, in dialysis tubing, where dialysis was for 60 min at 37 °C against 1-L buffer A containing 10 mM potassium phosphate, pH 8.0.

After phosphorolysis, the dialyzed PNPase-containing suspension was purified by phenyl sepharose (Phenyl Sepharose 6 Fast Flow (high sub), GE Healthcare), anion exchange (Q-Sepharose Fast Flow, Pharmacia), and gel filtration (Superdex S-200, GE Healthcare) chromatographies. The purified PNPase was stored as an ammonium sulfate suspension in 3 M $(NH_4)_2SO_4$ with 50 mM Tris-HCl, pH 8.0, at 4 °C.

(2.3) Pyridine Hemochromogen Assays. Assays of heme content were according to the procedure of Appleby (*62*). Briefly, multiple dilutions of hemeprotein were prepared in a solution of alkaline pyridine [4.2 M pyridine in 0.2 M NaOH]. This treatment removes the heme group from the protein and results in a hexacoordinated heme iron, where pyridine occupies both axial heme iron positions. When hemin (also in alkaline

pyridine) is used as a standard, comparison of the absorbances at 556 nm allows one to calculate the amount of heme (in moles) present in a given hemeprotein preparation (ε_{556} = 33.9 $mM^{-1}cm^{-1}$). A measurement of the total protein concentration is usually with the Bradford or BCA protein assays, with bovine serum albumin as the standard.

(2.4) Absorption Spectra, Ligand-Binding, and Autoxidation. Unless otherwise noted, all determinations of UV-Vis absorption and ligand-binding were for 2-5 μM protein in 0.10 M sodium phosphate pH 7.5 at 25 °C. Absorption spectra were monitored with a Cary 4000 UV-Vis spectrophotometer (Varian). Laser-flash photolysis and stopped-flow measurements were made with an LKS.60 laser kinetic spectrometer fitted with a PiStar stopped-flow drive unit. (Applied Photophysics, Leatherhead U.K.). For sample excitation, the LKS.60 spectrometer was coupled to a Quantel Brilliant B Nd:YAG laser with second-harmonic generation. Ligand-binding kinetics were followed at a wavelength of maximum difference between the starting and final species. Each association rate constant was calculated from a linear plot of $k_{observed}$ versus ligand concentration including at least four ligand concentrations.

Binding of O_2, CO, and NO was measured for the ferrous forms of the hemeproteins, and binding of imidazole and cyanide was measured for their ferric forms. Association rates for O_2 (80 - 1280 μM) and NO (30 - 240 μM) were measured by laser-flash photolysis at two wavelengths (412 - 417 nm and 433 - 435 nm). Association rates for CO (30 - 960 μM) were measured by both stopped-flow and laser-flash photolysis at two wavelengths (419 nm and 433 - 435 nm). Association rates for imidazole (0.25 - 4.0 mM) and cyanide (12.5 - 50 mM) were measured by stopped-flow at 390 and 420 nm, respectively. The O_2 dissociation rate constant was measured by stopped-flow at both 412 nm and 433-435 nm by mixing oxy-protein in 50-256 μM free O_2 with a solution of 2.0 mM sodium dithionite. The CO dissociation rate constant was measured by ligand replacement in the stopped-flow at 421 nm by mixing carbonmonoxy-protein in 10 - 30 μM free CO with a 1.0 – 2.0 mM solution of NO. The cyanide dissociation rate constant was measured as follows: met-DosC_H was equilibrated with 1.0 mM KCN, passed through a desalting column (Biospin, Bio-Rad) pre-equilibrated with 0.10 M sodium phosphate and 0.20 M imidazole pH 7.5, and whole absorption spectra were recorded for the transition from cyanomet to imidazolemet-DosC_H. The spectra were deconvoluted into cyanomet and imidazolemet components by multiple

linear regression, and the rates were calculated from the change in the fraction of imidazolemet-DosC_H over time.

The equilibrium dissociation constants for binding of O_2 and CO were measured directly by mixing the deoxy-protein with 1.0 - 1280 μM O_2 or 1.0 - 960 μM CO dissolved in buffer (0.10 M sodium phosphate pH 7.5). Linear combinations of whole basis spectra for the deoxy, oxy, and carbonmonoxy states of the protein were used to determine its saturation at varying O_2 and CO concentrations. K_d and Hill constant were calculated by fitting the saturation versus ligand-concentration curve (R^2 > 0.99) to the Hill equation in Excel.

(2.5) Diguanylate Cyclase Assays. Assays of diguanylate cyclase activity were done for 1 - 5 μM DosC or *Bpe*GReg in 20 mM sodium phosphate pH 7.5, 10 mM $MgCl_2$, and 2.0 mM DTT at 30 °C. To start the reactions, GTP ([α-^{32}P], Perkin-Elmer) was added to 500 μM. At the appropriate times, an aliquot of the reaction mixture was removed and added to an equal volume of 0.10 M EDTA pH 8.0. Stopped time points were heated at 95 °C for 5 min, centrifuged, and 1 - 2 μL of the supernatant was spotted onto polyethyleneimine-cellulose thin-layer chromatography plates (PEI-TLC, Merck KGaA; Darmstadt, Germany) and

developed in a 1.5:1.0 mixture of KH_2PO_4 (1.5 M, pH 3.6) : $(NH_4)_2SO_4$ (4.0 M, pH 3.6). Under these conditions, GTP migrates with R_f = 0.58, pGpG with R_f = 0.34, and c-di-GMP with R_f = 0.18. The dried TLC plates were imaged with a storage phosphor screen (Kodak K-HD) and a Personal Molecular Imager FX phosphorimager (Bio-Rad), and quantified with Quantity One software version 4.4.0 (Bio-Rad).

(2.6) Cyclic-di-GMP Synthesis and Purification. Radioactive and non-radioactive c-di-GMP was synthesized enzymatically from [α-^{32}P]-GTP (Perkin-Elmer) or GTP (Roche) using *Bpe*GReg (*41*). Overnight completed reactions were heated at 95 °C for 10 min, centrifuged to remove the precipitated *Bpe* GReg, and the supernatant was loaded onto a Sep-Pak C18 cartridge (Waters; Milford, MA). The column was washed with 3 volumes of 0.15 M KH_2PO_4 and eluted with acetonitrile. The solvent from the eluted c-di-GMP was evaporated by drying under a stream of N_2. The crystalline c-di-GMP was resuspended in 10 mM Tris-HCl pH 8.0 and stored at –20 °C. The c-di-GMP purity was determined by HPLC and the concentration was calculated from the 253-nm absorption (ε_{253} = 23,700 M^{-1} cm^{-1}) (Figure 2.2).

(2.7) C-di-GMP Phosphodiesterase Assays. Deoxy-DosP was prepared by reducing the purified protein with DTT in an anaerobic glove bag (Coy; Grasslake, MI). Oxy-DosP was prepared by bubbling air into samples of deoxy-DosP. Assays of phosphodiesterase activity were done for 0.20 – 1.0 μM DosP in 20 mM sodium phosphate, 10 mM $MgCl_2$, and 2 mM DTT, pH 7.5 at 30 °C. To start the reactions, c-di-GMP (unlabeled or ^{32}P-labeled) was added to a final concentration 10-100 μM. At the appropriate times, an aliquot of the reaction mixture was removed and added to an equal volume of 0.10 M EDTA pH 8.0. Stopped time points were heated at 95 °C for 5 min and centrifuged to remove the precipitated DosP. Radioactive samples were processed, imaged, and quantified as described above for the DGC assays. Non-radioactive samples (10 μL) were loaded onto an Adsorbosphere Nucleotide-Nucleoside reversed-phase HPLC column (Alltech, 250 x 4.6 mm) equipped with an Adsorbosphere Nucleotide-Nucleoside guard column (Alltech/Grace, 7.5 x 4.6 mm). The mobile phase consisted of (A) 0.15 M NaH_2PO_4, pH 5.2, and (B) 40 % (v/v) acetonitrile balanced with 0.15 M NaH_2PO_4 pH 5.2. A linear gradient from 0 % to 35 % buffer B for 10 min at 1 mL/min was used to separate the pGpG product from the c-di-GMP substrate.

(2.8) RNA Purification and Analysis. RNAs were isolated from whole *E. coli* cells or from DosC-DosP degradosomes using TRI-Reagent (Ambion). Electrophoresis of RNA samples was either on polyacrylamide or agarose gels. Samples for polyacrylamide gel electrophoresis were prepared in 1 x urea-PAGE loading buffer [100 mM Tris-HCl pH 8.0, 50 mM EDTA, 5 % (v/v) glycerol, 10 M urea, 0.01 % bromophenol blue, 0.01 % xylene cyanole] and run on gels (6 % or 10 % polyacrylamide) containing 1 x TBE [89 mM Tris base, 89 mM boric acid, 2 mM EDTA] and urea (8 M) at 40 W constant power. The running buffer was 1 x TBE. Following electrophoresis, the gels were incubated in 1 x SYBR-Gold nucleic acid stain (Invitrogen, in 1 x TBE) for 10 – 20 min at 23 °C and visualized by trans-illumination (VersaDoc Model 3000 imaging system, Bio-Rad). Samples for agarose gel electrophoresis were prepared in 1 x agarose loading buffer [90 mM Tris-borate, 7 M urea, 2 mM EDTA, 13 % ficoll (w/v), 0.1 % bromophenol blue; pH 8.3] and heated to 65 °C for 10 min prior to electrophoresis on gels (~ 1 % agarose in 1 x TBE) containing ethidium bromide (0.00015 % w/v), where the running buffer was 1 x TBE. After electrophoresis for ~ 2 h at 40 mA constant current, RNAs were visualized by UV trans-illumination (VersaDoc Model 3000 imaging system, Bio-Rad).

(2.9)Western Blotting. Western blotting succeeded the electrophoresis of samples on SDS polyacrylamide gels (8 – 15 %). Following electrophoresis, these gels were soaked in transfer buffer [25 mM Tris-HCl, 200 mM glycine, 20 % methanol] for 2 – 5 min. Prior to sample transfer, PVDF membranes (Immobilon-P, Millipore) were prepared by incubation for 60 sec in methanol, 60 sec in ddH_2O, and then > 5 min in transfer buffer. Sample transfer was in a Trans-Blot SD semi-dry transfer cell (Bio-Rad) at 12 V for 60 min, where the "sandwich" was composed of (from bottom to top): 3 sheets of Whatman 3mm paper, the PVDF membrane, the polyacrylamide gel, and then 3 sheets of Whatman 3mm paper. Following sample transfer, membranes were blocked for 1 h in 5 % nonfat milk in TBST [15.4 mM Tris-HCl, 137 mM NaCl, 0.001 % (v/v) Tween 20] at 23 °C. Primary antibodies were diluted in 5 % nonfat milk/TBST and incubated with the membranes overnight at 4 °C. After washing the membranes 3 – 5 times with TBST, secondary antibodies (1:5000 to 1:10,000 dilution in 5 % nonfat milk/TBST) were incubated with the membranes for 1 h at 23 °C. After washing the membranes 5 times with TBST, membranes were overlaid with ECL reagent (GE Healthcare) for 5 min at 23 °C and then detected by chemiluminescence either by

exposure to film (Hyperfilm ECL, GE Healthcare) or with an imaging system (VersaDoc Model 3000 imaging system, Bio-Rad). Rabbit polyclonal antibodies against *E. coli* polynucleotide phosphorylase (PNPase) were generous gifts from Dr. A. J. Carpousis.

(2.10) Immunoprecipitation. Antigen(Ag)–antibody(Ab) complexes were formed by incubating the MBP-DosC complex (Ag) with 5 μL of rabbit-α-PNPase (Ab) in 50 μL of interaction buffer [50 mM Tris-HCl, 50 mM NaCl, 5 mM DTT, 0.5 mM EDTA, pH 8.0] for 3 h at 23 °C. A 20 % (v/v) Protein-A Sepharose bead slurry (Protein-A Sepharose CL-4B, Amersham-Pharmacia) was prepared by weighing out 0.0314 g of beads and allowing them to swell for > 1 h at 23 °C in 314 μL of wash buffer [50 mM Tris-HCl (pH 8.0), 50 mM NaCl, and 0.5 mM EDTA] with agitation. The swollen beads were centrifuged (now ~ 100 μL of pelleted beads) and washed by resuspension in wash buffer + 0.02 % (w/v) bovine serum albumin for > 1 h at 23 °C with agitation. Following two additional wash steps with wash buffer, the beads were resuspended with wash buffer such that the final volume was 500 μL. Pull-down was accomplished by mixing the above 50 μL Ag-Ab interaction solution with 70 μL of the 20 % (v/v) bead slurry and 30 μL ddH_2O on ice for 4 h with agitation, followed by centrifugation to

pellet the captured Ag-Ab complex. The supernatants were collected and stored for subsequent analysis of PNPase content and activity. The pellets were washed 2X with wash buffer and then treated with 1X protein gel loading buffer, heated at 95 °C, and analyzed by Western blotting.

(2.11) PNPase Assays. Real-time measurements of PNPase poly(A) polymerizing activity contained 50 mM Tris-HCl (pH 8.0), 250 mM NaCl, 5 mM $MgCl_2$, 5 mM DTT, 8 x SYBR Gold, 0.5 mM ADP, 0.4 μg/mL PNPase, and c-di-GMP where appropriate in a 200 μL reaction volume at 23 °C. Reactions were monitored with a Fluoromax-3 spectrofluorimeter (Jobin Yvon Horiba) with excitation at 490 nm and emission at 540 nm. Phosphate-exchange assays were essentially as reported previously (*64*). Briefly, reactions contained 100 mM Tris-HCl (pH 8.0), 4 mM $MgCl_2$, 2 mM sodium phosphate (pH 7.0), 0.8 mM ADP, $^{32}P_i$ (5 μCi), 16.7 μg/mL PNPase, and 10 μM c-di-GMP where appropriate in a 30 μL reaction volume at 23 °C. At the appropriate times, 2.5 μL of the reaction was removed and added to 2.5 μL of 0.1 M EDTA (pH 8.0). One microliter of the stopped reactions were spotted onto polyethyleneimine TLC plates (Merck KGaA), developed with 0.75 M sodium phosphate (pH 3.5), and imaged with a phosphorimager (Personal Molecular Imager FX, Bio-Rad).

(2.12) C-di-GMP Photolabeling. A method for crosslinking c-di-GMP to proteins with UV light was adapted from a report by Benziman and colleagues (*65*). Briefly, equilibration of [^{32}P] c-di-GMP with PNPase (~ 1 μg) was for 20 min at 23 °C in 15 μL of crosslinking buffer [33 mM Tris-HCl (pH 8.0), 100 mM NaCl, and 10 mM $MgCl_2$]. Each sample was then placed on ice for 10 min, followed by transfer to the bottom of a single well of a 96-well polystyrene flat bottom culture plate (Corning). Crosslinking was accomplished with UV light (254 nm) by placing the culture plate 2 cm above a UV transluminator (Spectroline UV Transluminator Model TE-912S; 120 V, 80 Hz, 1 A; Spectronics Corp.) and 2 cm below a hand-held UV lamp (Model UVG-54 Mineralight lamp; 115 V, 60 Hz, 0.16 A; UVP Inc.) for 20 min in a cold room (4 °C). Samples were prepared for electrophoresis by the addition of 5 μL of 4X protein gel loading buffer [100 mM Tris-HCl (pH 6.8), 1 % (w/v) SDS, 10 mM EDTA, 40 % glycerol, 0.4 % (v/v) β-mercaptoethanol, and 0.1 % (w/v) bromophenol blue]. Following polyacrylamide gel electrophoresis (10 %), gels were dried and imaged by autoradiography with a storage phosphor screen (Kodak K-HD) and a Personal Molecular Imager FX phosphorimager (Bio-Rad).

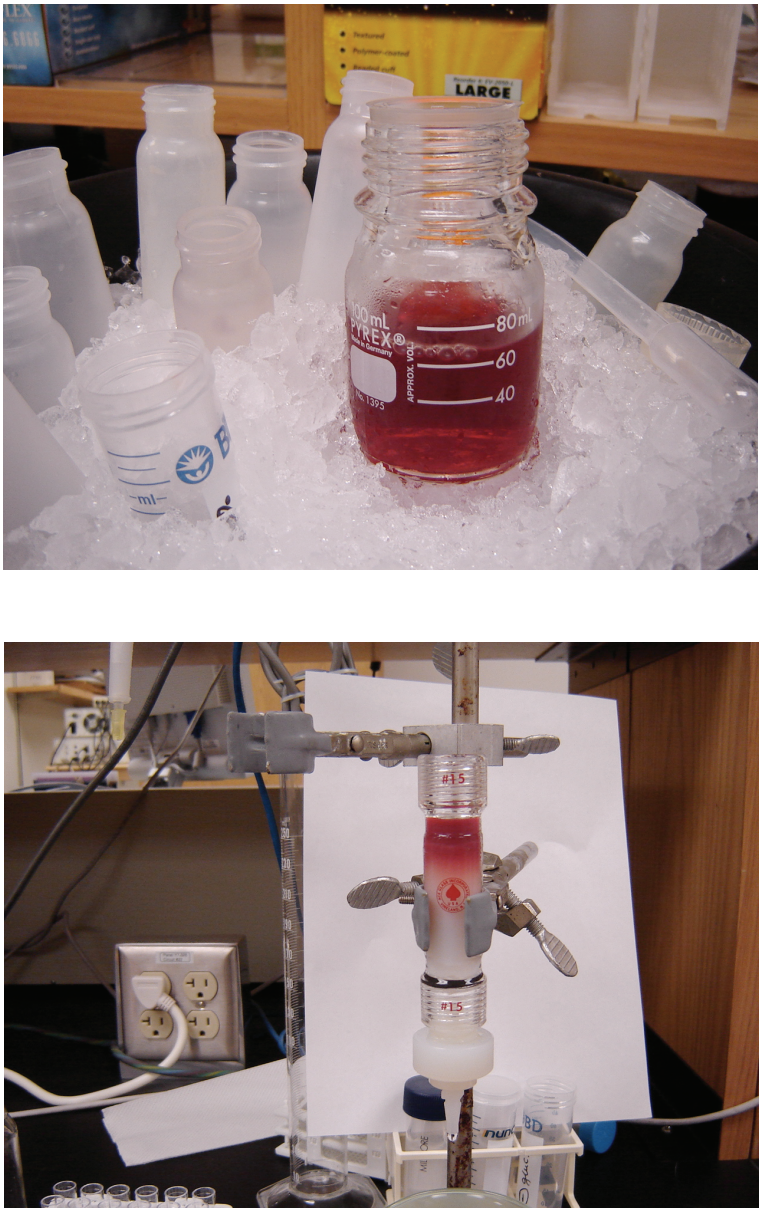

Figure 2.1. **Monitoring hemeprotein purification by its bright red color.** Both photos are from a purification of $DosC_H$. Soluble $DosC_H$, resuspended after fractionation with ammonium sulfate, is shown in the top panel. The bottom panel shows $DosC_H$ binding to an anion exchange column under low salt conditions.

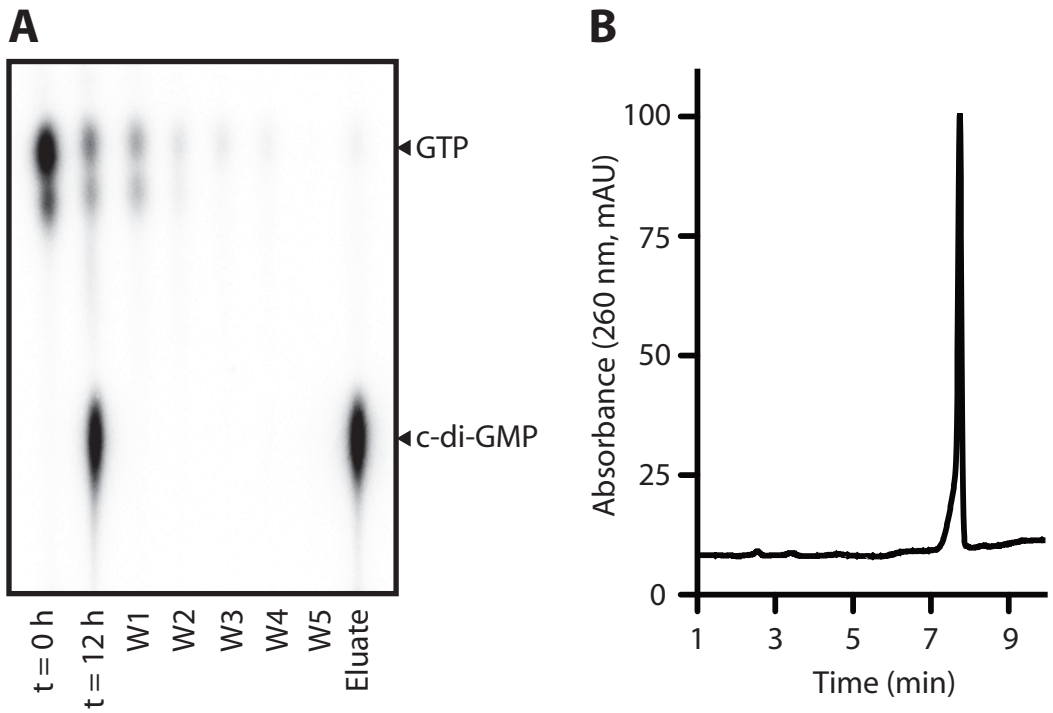

***Figure 2.2*. Synthesis and purification of c-di-GMP. (A)** Radiolabeled c-di-GMP was synthesized from α-[^{32}P]-GTP and purified as described in Materials and Methods (section 2.5). Analysis was on PEI-cellulose TLC plates. **(B)** In addition to its purity on TLC plates, enzymatically synthesized c-di-GMP was found to be pure by HPLC analysis.

CHAPTER THREE

Biochemical Characterization of the *E. coli* Direct Oxygen Sensing Phosphodiesterase DosP

INTRODUCTION

What environmental signals regulate the bacterial diguanylate cyclases and c-di-GMP phosphodiesterases? As mentioned previously, (Section 1.2), the existence of these signals is indicated by the recognizable signaling domains in these proteins that accompany their enzymatic domains (*16, 20, 22, 29, 37*). The first demonstration of coupling of an environmental signal to a DGC or PDE activity was in *G. xylinus*, where c-di-GMP degradation is controlled by the heme-PAS containing phosphodiesterase *Ax* PDE-A1 (*38*). However, nearly a decade elapsed since the initial biochemical characterization of *Ax* PDE-A1, and only two additional environmental signals (light and redox) have been shown to regulate a few DGCs or PDEs (*39, 42, 43*). Simultaneous with the discovery of an O_2-switched PDE activity in *Ax* PDE-A1, a broader role for O_2 in c-di-GMP signal transduction was suggested by the discovery of a heme-PAS domain in a potential *E. coli* PDE (*66*). This

enzyme, initially named *E. coli* Dos (for *E. coli* Direct oxygen sensor, in anticipation of the discovery of an O_2-switched PDE activity), shared 30 % amino acid identity with *Ax* PDE-A1 over its entire length (Figure 1.2).

As a first step toward understanding the initial events in the *Ec* Dos sensing mechanism, a truncation consisting of the isolated heme-PAS domain (*Ec* Dos_H, encompassing residues 1-147) was overproduced and isolated from *E. coli (66, 67)*. Isolated sensory domains are often synthesized to much higher soluble levels in recombinant systems compared to their full-length counterparts. Higher purification yields allow for biochemical analyses that would otherwise be difficult with limiting amounts of protein. For Dos_H, tools such as absorption spectroscopy, ligand binding, and resonance Raman spectroscopy were used to probe the heme environment and its accessibility to ligands.

The most unexpected finiding from the initial biochemical characterization of Dos_H was the discovery of a hexaccordinate heme iron atom in Dos_H independent of the presence of an exogenous ligand, as revealed by absorption spectroscopy (*66*). All hemeproteins contain planar ligation of the heme iron to four nitrogen atoms from the heme porphyrin ring. A fifth axial ligation is usually supplied by the protein, most commonly by an imidazole side chain of a histidine residue that covalently

links the heme to the protein. The two previously identified heme-based O_2 sensors (FixL and *Ax* PDE-A1), as well as many of the most well known hemeproteins (i.e. mammalian Hb and Mb) contain pentacoordinate heme iron atoms. A typical pentacoordinate heme absorption spectrum is shown for deoxy-Mb in Figure 3.1D. The absence of a coordinating ligand at the sixth axial position for deoxy-Mb produces a broad absorption band from 500-600 nm in the deoxy-Mb absorption spectrum. This contrasts with the hexacoordinate hemeproteins, whose deoxy absorption spectra contain two absorption maxima in the 500-600 nm region, with a characteristic strong alpha band around 560 nm. Hexacoordination in the absence of an exogenous ligand is accomplished by the ligation of a protein side chain to the sixth axial position of the heme iron. Later studies using resonance Raman spectroscopy demonstrated a Dos_H heme iron coordinated by His77 on its proximal side and by Met95 on its distal side (Figure 3.1) (*6 7*). Nonetheless, Met95 readily relinquishes its place on the heme iron to exogenous ligands, allowing for stable oxy-heme or carbonmonoxy-heme complexes to form (*66, 67*).

We recently renamed the gene (coding for the *Ec* Dos protein) *dosP*, for direct oxygen sensing phosphodiesterase, to acknowledge this protein's enzymatic activity in addition to its sensing function and to

distinguish it from other potential O_2 sensors in *E. coli* (*68*). The aim of this current study was to purify the full-length enzyme and conduct a biochemical characterization of its ligand-binding and enzymatic properties. Questions we desired to address included: (i) Is full-length DosP hexacoordinate? (ii) With what affinities does full-length DosP bind ligands such as O_2 and CO? (iii) Do ligands switch the DosP PDE activity on or off? (iv) What is the activity profile of DosP in response to sub-saturating levels of ligand? (v) What is the mechanism by which binding of ligand regulates PDE activity?

RESULTS

(3.1) DosP Ligand Binding. From the initial studies of the DosP protein, that had focused on the heme-binding PAS domain ($DosP_{1-147}$, also called $DosP_H$), some surprising results were a His-Met coordination of the heme iron and a similar affinity for O_2 and CO ($K_d \sim 10\ \mu M$) (*66, 67*). Is the same true for full-length DosP? For this study, we purified full-length DosP from *E. coli* as described in Materials and Methods (Section 2.2). We first examined binding of ligands to full-length DosP and compared the properties of the intact enzyme to its domain (Table 3.1). Similar to $DosP_H$, full-length DosP had a hexacoordinate heme iron coordination, as

indicated by the distinctive alpha-band (~ 560 nm) in the deoxy-DosP absorbance spectrum (Figure 3.1B). We directly measured the ligand affinity of DosP by titration with gaseous ligands dissolved in aqueous buffer. From this study, we determined the equilibrium dissociation constant for O_2 binding to be 74 μM and that for CO binding to be 8.0 μM at pH 7.5 and 25 °C (Table 3.1, Figure 3.2). In addition, we discovered a cooperative binding of ligands, with a Hill coefficient *n* of 1.5 for O_2, and 1.2 for CO (Figures 3.2B,D). It was interesting that ligand binding to DosP was different from binding to $DosP_H$ in some important respects. Binding of ligands to $DosP_H$ was noncooperative (*n* of 1.0 for O_2 and CO). The O_2 affinity (K_d of 13 μM) of $DosP_H$ was six-fold higher than that of DosP. This higher O_2 affinity of $DosP_H$ compared to DosP was associated with a slower O_2 off-rate constant (k_{off} ~ 0.8 s^{-1} for DosP compared to 0.03 s^{-1} for $DosP_H$) (Table 3.1). Clearly, regions outside the heme-binding domain could accelerate the dissociation of O_2. Overall, these findings suggested that the enzymatic region of DosP could substantially modulate ligand binding to the heme-PAS domain.

(3.2) DosP is an O_2–Regulated c-di-GMP Phosphodiesterase. In preparation for an analysis of DosP enzymatic activity, a procedure for the

synthesis and purification of the c-di-GMP substrate was developed (see Materials and Methods (Section 2.5)) (Figure 2.2). Figure 3.3 shows representative HPLC traces for the conversion of c-di-GMP (100 μM) to the linear pGpG by deoxy-DosP versus oxy-DosP (1 μM enzyme). Saturation of DosP with O_2 enhanced the phosphodiesterase activity 17-fold over the deoxy-state (50 min^{-1} compared to 3 min^{-1}). We estimate a K_M value of about 4 μM with respect to c-di-GMP for the oxy-state, from numeric fitting of the end of the reaction time course when substrate concentration is low. Both the oxy- and deoxy-DosP phosphodiesterase reactions went to completion, although the latter required about 30 min (Figure 3.3B). We tested whether the activity of DosP might be allosterically enhanced by GTP, as noted for another c-di-GMP phosphodiesterase, but we saw no effect of GTP on the reaction rate *(69).* Carbon monoxide saturation enhanced the activity to the same extent as O_2 saturation. This indicates that ligand polarization upon binding to heme does not contribute significantly to the DosP regulatory mechanism.

(3.3) Ligand-Dose Response of the DosP c-di-GMP Phosphodiesterase. We found the response of DosP to ligand saturation to be highly nonlinear and skewed toward high saturation (Figure 3.4).

There was hardly any effect of O_2 until the protein became 50% saturated with this ligand. In particular, over 80% of the 17-fold enhancement of the activity by ligand occured in the second half of the heme titration ($O_2 > 75$ μM). In other words, a drop in the O_2 saturation of only 20% from full saturation resulted in a loss of over half of the O_2 activation. DosP has been reported to be homo-tetrameric, and as such can have zero, one, two, three, or four bound O_2, with each species having a potentially different phosphodiesterase activity (*70*). The concentration of each species at any O_2 saturation is straightforward to determine from the known O_2 titration curve. Unfortunately, while it is very clear that multiple oxygenations are required for activation, no assignment of activities to each known concentration of liganded species accurately accounts for the observed dose response (Figure 3.4). The dimeric protein kinase FixL achieves a highly nonlinear response to O_2 concentrations via a lag time between the dissociation of O_2 and the completion of the activation process (see Chaper 7) (*71*). Analogous “memory effects” in DosP could potentially result in ten different states, which might completely explain the DosP dose response but would be daunting to model. The DosP dose response, along with other physical limitations, fix the DosP activation in *E. coli* to a relatively narrow range of O_2 concentrations: 75 - 256 μM O_2

(i.e. 30 - 100% saturation with air). On the other hand, the range of CO (> 10 μM) required for activating DosP well exceeds the concentrations that an *E. coli* cell would naturally encounter.

DISCUSSION

Our finding of an O_2-switched PDE in DosP represented only the third demonstration of regulated PDE activity in response to an environmental stimulus, even though the initial recognition that signaling domains are often found associated with the GGDEF/EAL-class enzymes was made nearly a decade ago (*38, 43*). The relative paucity of reports demonstrating signal regulated PDE activity likely indicates the difficulty in conducting biochemical characterizations of these enzymes. The description of DosP ligand binding and ligand dose-response presented here represent the most advanced biochemical study of any signal-regulated DGC or PDE reported to date.

The characterization of DosP described in this chapter yielded a number of unexpected results. That O_2 switches the DosP PDE "on" was unexpected, as the highly similar heme-PAS coupled phosphodiesterase PDE-A1 from *A. xylinum* is switched "off" by O_2. One possible explanation for the differing response to O_2 for PDE-A1 and DosP relates to the nature

of the protein conformational change elicited upon O_2 binding. For PDE-A1, O_2 enters the heme pocket and binds to a pentacoordinate heme iron, converting it from the high-spin deoxy form to the low-spin oxy form (Figure 3.5). For many heme proteins that bind exogenous ligands, the change in spin of the heme iron from high to low is accompanied by movement of the iron atom into the plane of the heme with a concomitant flattening of the heme porphyrin ring. These small conformational changes are thought to be the key initial steps that trigger the sensing mechanism upon ligand binding. For DosP, however, the heme iron is hexacoordinate and low spin whether or not an exogenous ligand is present (*66, 67*). Therefore, a different triggering mechanism likely operates in DosP. One possible triggering step is the movement of Met95, the displaceable distal residue, from the sixth coordinating position of the heme iron to an alternative site after binding an exogenous ligand. The observation that both O_2 and CO activate DosP PDE activity to the same extent, and with a similar ligand-dose response, suggests that movement of Met95 upon exogenous ligand binding is sufficient to trigger the signaling mechanism in this enzyme (Figure 3.4).

A second unexpected result of this study was the highly nonlinear ligand-dose response of DosP. The straightforward expectation that half

saturation of a protein target with an activating ligand would elicit half the maximal enhancement of enzymatic activity clearly does not hold true for DosP. Indeed, at half saturation, DosP has essentially the same activity as DosP in the absence of ligand altogether (Figure 3.4). Why such a nonlinear response of c-di-GMP degradation to O_2 concentration would benefit an individual *E. coli* is still unclear. Possibly, limiting c-di-GMP degradation to a very narrow window of O_2 concentrations (75 – 256 μM) helps to minimize unwanted c-di-GMP removal in response to small and transient rises in O_2 tension during an otherwise well-adapted microaerobic regime.

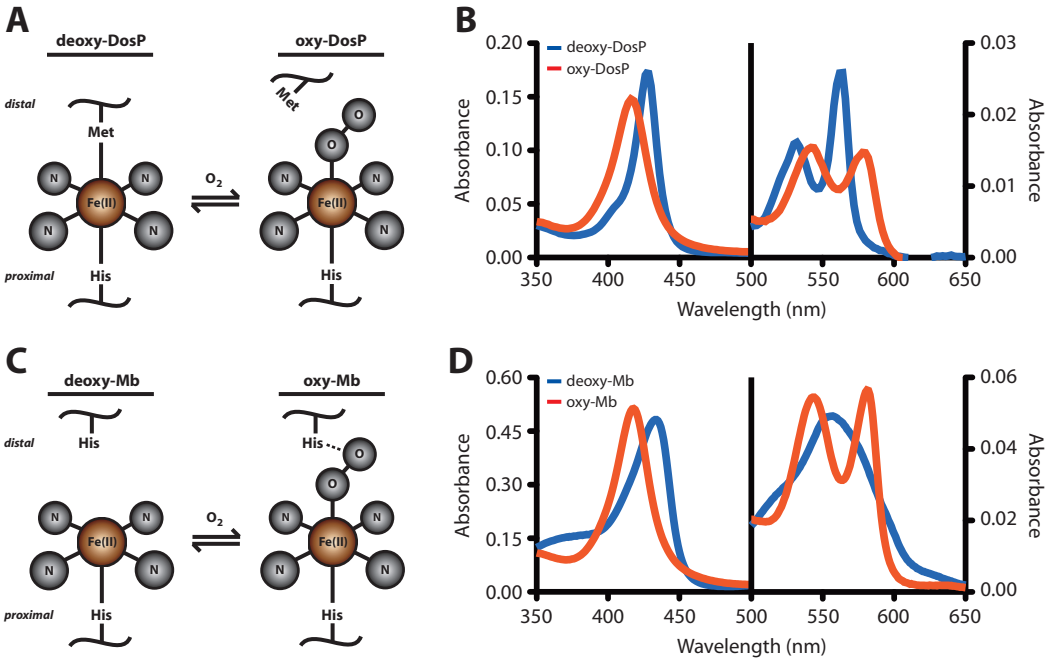

***Figure 3.1*. Hexacoordination of the DosP heme iron. (A)** The heme iron of $DosP_H$, the isolated DosP heme-PAS domain, is hexacoordinate and low spin in the deoxy form, with axial ligation by His77 and Met95. This schematic is derived from data in Delgado-Nixon VM, Gonzalez G, & Gilles-Gonzalez MA. *Biochemistry* (2000) 39: 2685-2691 (*66*); and in Gonzalez G, Dioum EM, Bertolucci CM, Tomita T, Ikeda-Saito M, Cheesman MR, Watmough NJ, & Gilles-Gonzalez MA. *Biochemistry* (2002) 41: 8414-8421 (*67*). **(B)** Full-length DosP is also hexacoordinate, as indicated by the distinctive strong alpha band at ~ 560 nm in the deoxy-DosP (blue) absorbance spectrum. This feature is not observed for pentacoordinate deoxy hemeproteins such as Mb (panels C & D).

Table 3.1. **Ligand binding parameters of oxygen-regulated c-di-GMP phosphodiesterases.**

	O_2			CO			NO
	k_{on} ($\mu M^{-1}s^{-1}$)	k_{off} (s^{-1})	K_d (μM)	k_{on} ($\mu M^{-1}s^{-1}$)	k_{off} (s^{-1})	K_d (μM)	k_{on} ($\mu M^{-1}s^{-1}$)
DosP [a]	0.0092[#]	0.82	74	0.0029[#]	0.023	8.0	
$DosP_H$ [b]	0.0026	0.034[+]	13	0.0011	0.011[+]	10	0.0018
PDE-A1 [c]	6.6	77	12[*]	0.21	0.58	0.28[*]	

[a]This work (*68*); [b]Delgado-Nixon VM *et al.*, (*66*); [c]Chang *et al.*, (*38*). PDE-A1 is from *Gluconacetobacter xylinus* (formerly *Acetobacter xylinum*). K_d values were measured by direct titration except where indicated[*], where they were calculated from k_{off} and k_{on}. [#]Calculated from k_{off} and K_d. [+]Calculated from k_{on} and K_d. Measurements were at pH 7.5 and 25 °C [a], pH 7.0 and 20 °C [b], or pH 8.5 and 25 °C [c].

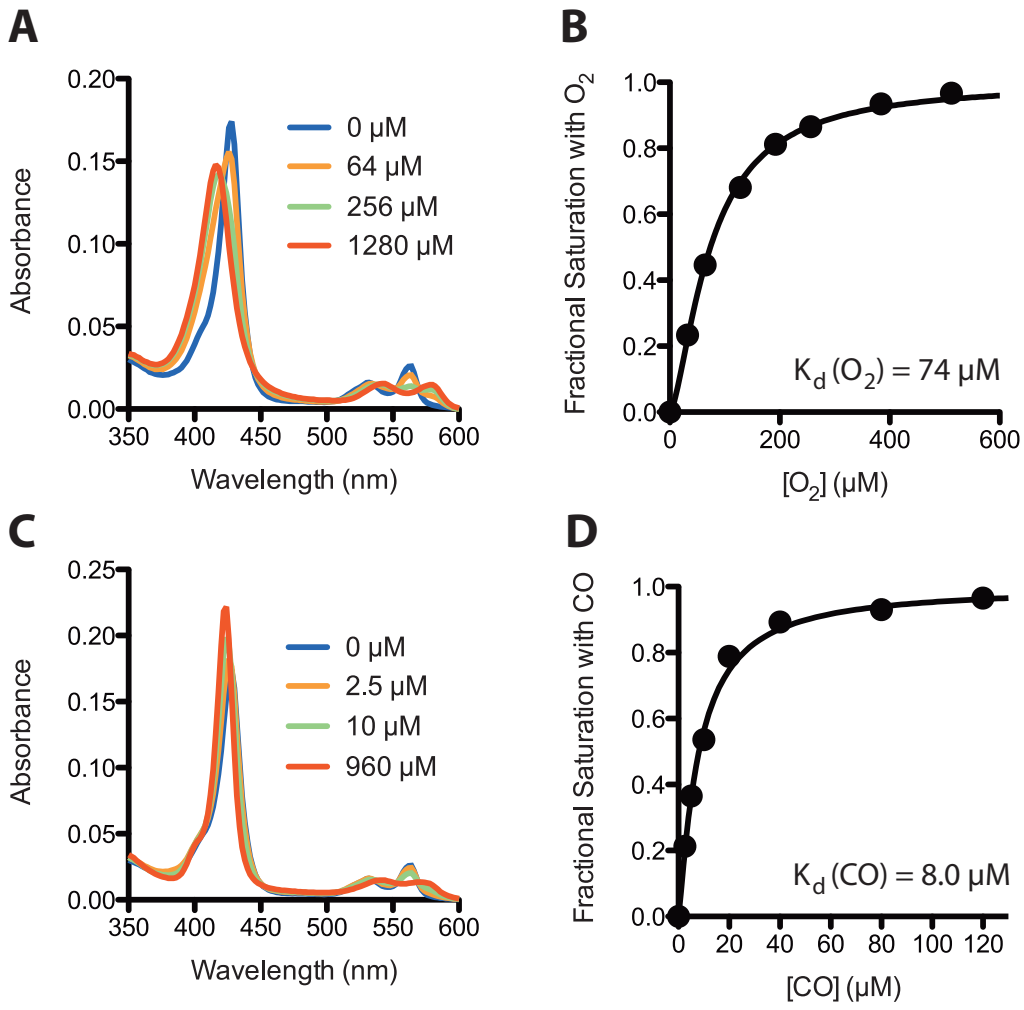

Figure 3.2. **Direct titration of DosP with O_2 and CO. (A, B)** Titration with O_2. **(C, D)** Titration with CO. Data in B and D were fit to the Hill equation. Experimental details are as described in Materials and Methods (Section 2.4). Titrations were at pH 7.5 and 25 °C.

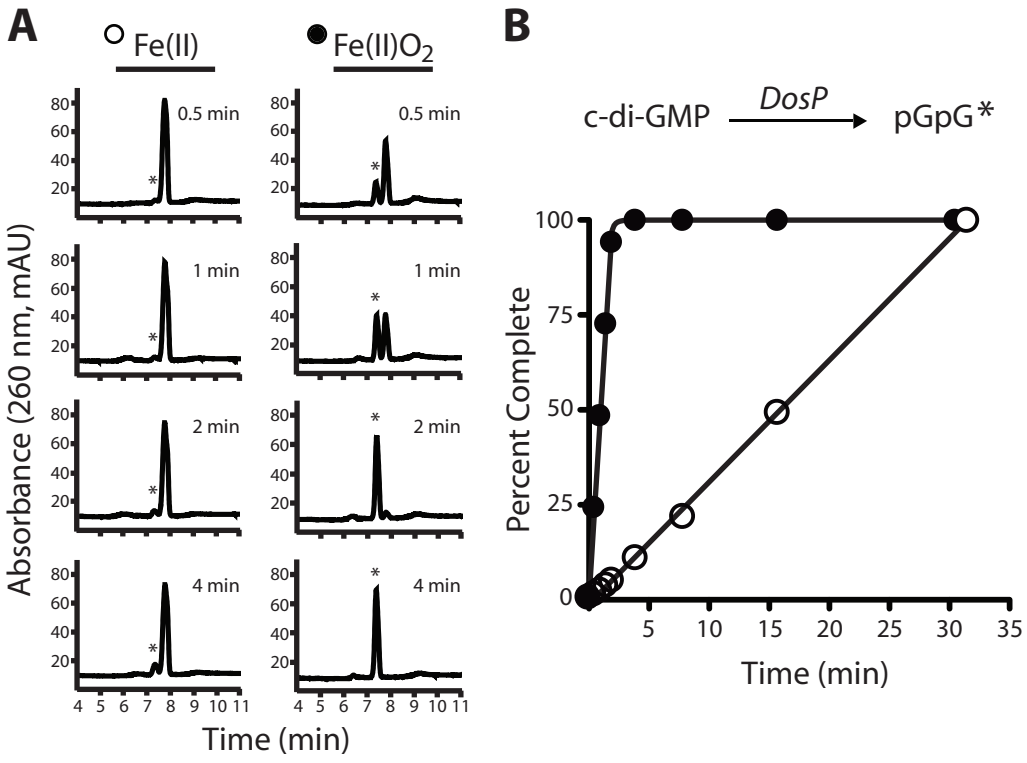

***Figure 3.3*. Oxygen-switching of the c-di-GMP phosphodiesterase in *E. coli* DosP. (A)** Ferrous DosP (1 μM) without ligand (Fe^{II} or deoxy, open circles) or saturated with O_2 ($Fe^{II}O_2$ or oxy, closed circles) was assayed for its ability to catalyze the conversion of c-di-GMP (100 μM) to the linear pGpG at pH 7.5 and 30 C. Representative HPLC traces for stopped time points are shown. The c-di-GMP peak migrates at 7.8 min, and the pGpG peak (indicated by an asterisk) migrates at 7.4 min. **(B)** An analysis of the complete phosphodiesterase data shows that ligation with O_2 enhances the phosphodiesterase activity of DosP more than 16-fold (to 50 min^{-1}) over the activity of the unliganded protein (3 min^{-1}). For both the liganded and the unliganded protein, the reaction velocity is maintained, even in little remaining substrate, until the reaction reaches completion.

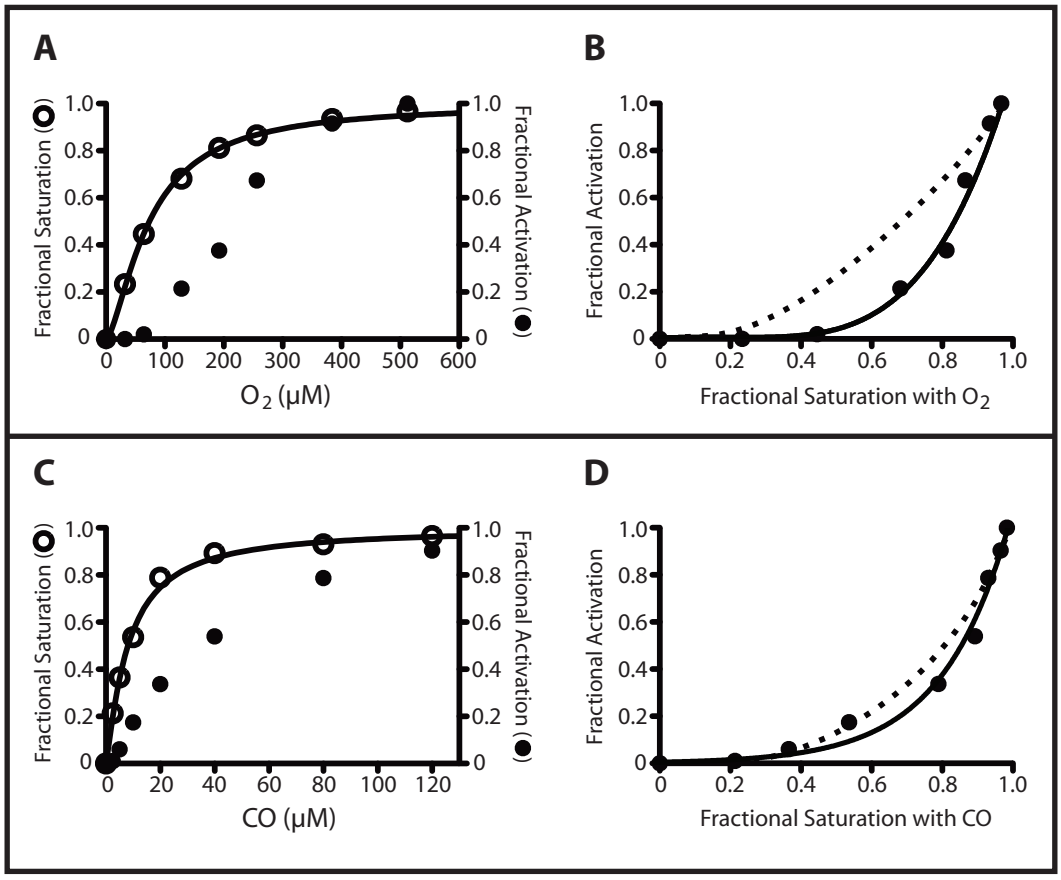

Figure 3.4. **O_2 and CO dose responses of the *E. coli* DosP c-di-GMP phosphodiesterase.** **(A)** Comparison of the effects of increasing oxygen concentrations (0 - 512 μM) on the fractional saturation of the DosP heme (open circles) and on the fractional activation of the DosP phosphodiesterase (closed circles). **(B)** Data from part A, recast as the fractional activation resulting from partially saturating the DosP heme with O_2. Dotted line: fit of the data to a model incorporating positive cooperativity within a tetramer. **(C)** Comparison of the effects of increasing CO concentrations (0 - 120 μM) on the fractional saturation of the DosP heme (open circles) and on the fractional activation of the DosP phosphodiesterase (closed circles). **(D)** Data from part C, recast as the fractional activation resulting from partially saturating the DosP heme with CO. Dotted line: fit of the data to a model incorporating positive cooperativity within a tetramer. All reactions were at pH 7.5 and 30°C.

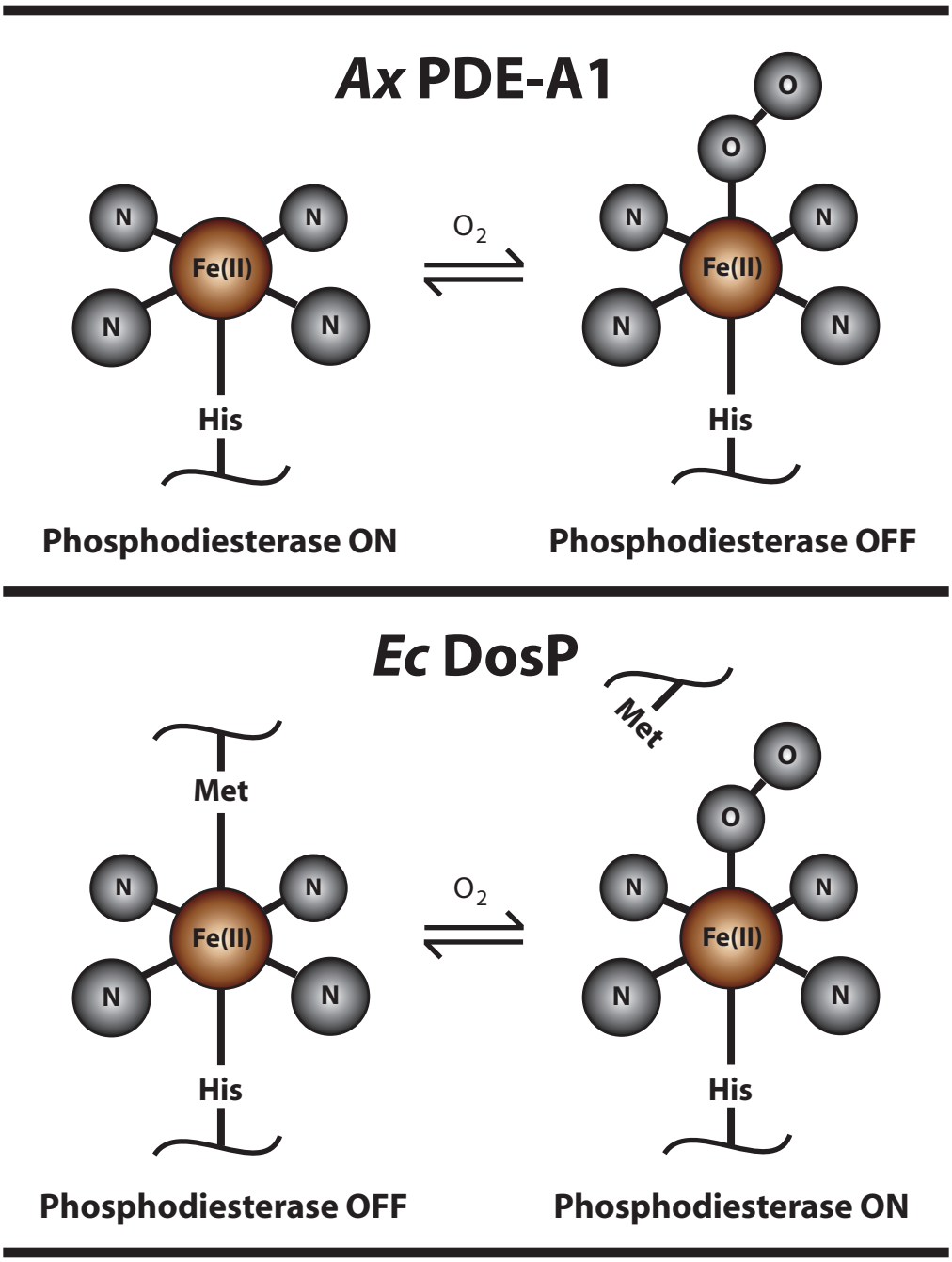

Figure 3.5. **Comparison of the effect of heme-iron ligation on phosphodiesterase activity for *Ax* PDE-A1 and *Ec* DosP.**

CHAPTER FOUR

Biochemical characterization of the globin-coupled diguanylate cyclases *Ec* DosC and *Bpe* GReg

INTRODUCTION

E. coli dosP is found in a two-gene operon. The other member of the operon is an open reading frame that encodes a diguanylate cyclase. This DGC had never before been purified, though the corresponding gene (variously called *yddV*, *yhcK*, and *Ec greg*) had been exploited to complement deletions of GGDEF-domain proteins from several heterologous hosts (*27, 28, 72*). In addition to its C-terminal GGDEF domain (160 amino acids), no other recognizable domain had been noted for YddV, though its overall size (460 amino acids), along with the common finding of signaling domains in GGDEF/EAL-class enzymes, suggested the possibility of an additional sensory module. A more thorough bioinformatic analysis of the N-terminal portion of YddV revealed a probable sensory globin domain. Though similar in overall topology to the classical eight-alpha-helical (helices A → H) vertebrate heme-containing globin domain, the sensory globin domain is distinct in lacking

the typical D-helix and first half of the E-helix. These domains function not as carriers of O_2 or as O_2 storage proteins, but rather as sensors that couple reversible O_2 binding to the regulation of a transmitter within the same polypeptide (*16*). The first sensory globins to be described were the HemAT proteins of *Halobacterium salinarum* and *Bacillus subtilis* (*73*). In these proteins a sensory globin domain is coupled to a methyl-accepting chemotaxis domain (MCPs) for mediating aerotactic responses in these organisms (*73*).

We therefore hypothesized that the *yddV-dosP* region of the *E. coli* genome constitutes a two-gene operon where both of the genes encode heme proteins for O_2-regulated c-di-GMP homeostasis. As such, we renamed the *yddV* ORF to *dosC* (for direct oxygen sensing Cyclase). The promoter for the *dosCP* operon resides upstream of *dosC*, and only the *dosC* stop codon separates this gene from the start of *dosP* (Figure 4.1A). This genetic organization indicated coupling, not only of *dosCP* transcription, but also of DosC and DosP translation. As such, we supposed that, like other bacterial genes that are thus organized, e.g., many histidine-protein kinase and response-regulator couples, the products of the *dosCP* operon might jointly function. As described in Chapter 3, DosP is a c-di-GMP phosphodiesterase with demonstrated O_2-

regulated enzymatic activity has been demonstrated (*66, 68*). By contrast, DosC had never been purified. We therefore undertook a biochemical characterization of this globin-coupled diguanylate cyclase.

RESULTS

(4.1) DosC is a heme-containing diguanylate cyclase. In Figure 4.1C, the DosC N-terminal domain sequence was compared to the sequences of other sensory globins, some of which are of known structure. This comparison showed DosC to be more closely related to the sensory globins (47 % sequence similarity and 18 % identity to HemAT-*Bs*) than to mammalian Mb. Many globins from organisms as diverse as vertebrates, insects, and plants share a general structural fold that allows certain features to be compared. The sensory globins do not share all of these features. For example, the entire D-helix and the first half of the E-helix, including the typical distal (E7) histidine, are absent from HemAT-*Bs*; we expect that this is also true for DosC (*16, 74, 75*). The homology between DosC and mammalian globins is very low. The main globin residues conserved in DosC were the F8-histidine residue of heme attachment and the C2-proline (H98 and P50, respectively). In the alignment, the closest DosC relative was *Bpe*GReg (55 % similarity and 34 % identity overall): a

putative *Bordetella pertussis* diguanylate cyclase with a similar domain organization to full-length DosC. For a further characterization of *Bpe*GReg, see Sections 4.3 and 4.4.

To determine if DosC binds heme in its N-terminal region, we examined two versions of this protein for the presence of heme: the $DosC_H$ fragment, representing only the sensory globin domain (residues 2-160), and a MBP-DosC fusion with the full-length protein (Figure 4.1). Size-exclusion chromatography showed the $DosC_H$ construct to be dimeric (Figure 4.2). Pyridine hemochromogen assays showed that both $DosC_H$ and MBP-DosC contain one heme per monomer (*62*). Absorption spectra of DosC further confirmed its heme protein nature and the capacity of its ferrous state to bind ligands such as O_2 and CO and the ferric state to bind ligands such as CN^- and imidazole (Figure 4.3).

(4.2) Characterization of the DosC heme binding pocket. We examined the nature of the DosC heme binding pocket by a combination of absorption spectroscopy and ligand binding. The met (Fe^{III}, unliganded) form of DosC showed an absorption spectrum typical of a heme with a five-coordinate high-spin iron atom. Specifically, the spectrum showed a Soret absorption band around 391 nm, together with a broad and less

intense band around 500 nm, and a smaller peak around 650 nm (Figure 4.3). Spectra of this sort indicate that water or hydroxide do not coordinate to the heme iron in the ferric state. In two well-established cases where met-spectra similar to that of met-DosC were observed, this was explained by the inability of distal pocket residues to accept a hydrogen bond from bound water or hydroxide (*21, 76-78*). This is in contrast with met-Mb, where distal stabilization allows binding of a water molecule to the ferric heme iron and shifts the Soret absorbance to 409 nm. Additional evidence for an apolar heme pocket comes from the relatively slow kinetics of cyanide binding to met-DosC (Table 4.1). Cyanide enters the heme pocket exclusively as the neutral protonated HCN species, both because this species comprises > 99% of the cyanide at neutral pH and because the charged CN^- species is strongly excluded from the hydrophobic heme pocket (as even the most “polar” ligand-binding heme pocket is far more hydrophobic than aqueous solution). Since HCN is not a heme ligand, the HCN molecule must transfer its proton to a distal-pocket residue before it can bind to the heme iron. The kinetics of cyanide binding in all hemeproteins for which this reaction has been studied is limited by the rate of this deprotonation of neutral HCN inside the heme pocket; for DosC these kinetics suggest that a readily

ionizable residue is not near to the bound ligand (*79*). Consistent with this hypothesis, the alignment in Figure 4.1C suggests that the DosC heme distal pocket is lined with residues F42, Y43, L56, L65, A68, and M69. Compared to SW Mb, the DosC heme iron bound cyanide one hundred times more slowly, yet it bound imidazole thirty times more rapidly. Since the factor limiting the kinetics of binding for ligands as bulky as imidazole is usually steric accessibility, we may conclude that the DosC pocket is much less sterically constrained than that of SW Mb (Table 4.1) (*80*).

DosC binds O_2 about 30-fold less tightly than does the homologous *Bpe*GReg protein (Table 4.2, Figure 4.4). Compared to *Bpe*GReg, the DosC association rate constant for binding of O_2 was 4-fold lower, and the dissociation rate constant was 8-fold higher (Table 4.2). The MBP-DosC and $DosC_H$ constructs showed a similar O_2 affinity ($K_d \sim$ 10-20 μM) (Table 4.2, Figure 4.4). Likewise, the two constructs showed a similar CO affinity ($K_d \sim 1$ μM) (Table 4.2, Figure 4.4). The kinetics for binding of ligands were also alike for the constructs (Table 4.2, Figure 4.5). Overall, DosC is suited to a respond to O_2 in the microaerobic regime (10's of micromolar O_2) (Figure 4.4). In this respect, DosC differs significantly from *Bpe*GReg, which is set to respond to micromolar O_2.

(4.3) Identification of* Bpe*GReg, a sensory globin in B. pertussis. Our *in silico* analysis of microbial genome sequences identified *Bpe*GReg (for *B. pertussis* globin-coupled regulator) from the whooping cough pathogen *B. pertussis* as a potential globin-coupled DGC (Figure 4.1C). As mentioned earlier (Section 4.1), *Bpe*GReg is DosC's closest relative (55 % similarity and 34 % identity). To characterize *Bpe*GReg, we purified recombinant His-tagged *Bpe*GReg by metal-affinity chromatography. The recombinant protein had the expected molecular mass of 53.7 kDa and showed characteristic heme protein absorption spectra in the near UV and visible regions (Figure 4.6). Addition of ligands to the ferrous *Bpe*GReg caused the Soret absorption band to shift from 431 nm (deoxy, unliganded Fe^{II} state) to 416 nm for the O_2-bound, 422 nm for the carbon-monoxide bound, and 420 nm for the nitric-oxide bound states. We further measured the O_2, CO and NO binding affinities and kinetics of *Bpe*GReg (Table 4.2). *Bpe*GReg bound O_2 and CO (K_d = 0.64 and 0.055 μM, respectively) with affinities comparable to those of sperm-whale myoglobin (Table 4.2). The association rate constant for NO binding to *Bpe*GReg was 16 $\mu M^{-1}s^{-1}$, a value similar to that reported for sperm-whale myoglobin (Table 4.2). We concluded that *Bpe*GReg is a heme-binding protein with ligand-binding properties reminiscent of sperm-whale myoglobin.

(4.4) BpeGReg is an O_2 -activated diguanylate cyclase involved in biofilm formation. To test whether *Bpe*GReg functions as a globin-regulated diguanylate cyclase, we measured its conversion of GTP to c-di-GMP by two independent methods: reverse-phase liquid chromatography coupled with mass spectrometry (LC-MS) and a thin layer chromatography (TLC) radioactive assay using [α-^{32}P]-GTP as the substrate. These analyses showed that ferrous *Bpe*GReg readily synthesizes c-di-GMP from GTP (Figure 4.7). We then measured the production of c-di-GMP by various liganded forms of ferrous *Bpe*GReg. The ferrous O_2-bound form of *Bpe*GReg produced the highest amount of c-di-GMP per mole of protein per unit time compared with the unliganded, CO-bound, and NO-bound forms (Figures 4.7B,C). We concluded that *Bpe*GReg is an O_2-switched DGC that cycles between a low-activity unliganded ferrous state and a highly active O_2-bound state.

A *Bpe*GReg homology model predicted that c-di-GMP would bind to inhibitory sites, causing feedback inhibition of the cyclase activity. Such an effect had been noted for the *Caulobacter crescentus* diguanylate cyclase PleD (*46*). To test for possible feedback inhibition of *Bpe*GReg, we coupled the cyclase reaction with a phosphodiesterase (*E. coli* DosP)

that continuously linearized the cyclic nucleotide product to pGpG, and we compared the kinetics of this reaction to those of *Bpe*GReg alone. This comparison of reactions with and without the PDE clearly indicated product inhibition (Figure 4.8A). Without removal of the c-di-GMP product, the reaction quickly slowed and reached equilibrium long before the GTP substrate was exhausted. By contrast, the reaction was linear and proceeded to completion when it was coupled to the PDE (Figure 4.8A). Furthermore, the addition of 20 μM c-di-GMP at the start of a *Bpe*GReg-catalyzed reaction was strongly inhibitory (Figure 4.8B). The adoption of a coupled assay allowed us to measure the reaction rates of the liganded and unliganded forms of *Bpe*GReg without the complications of feedback inhibition. Thus we determined that the O_2-bound *Bpe*GReg produced c-di-GMP at an initial rate (2.5 min^{-1}) 10 times faster than that of the unliganded ferrous form (Figure 4.9). In conclusion, our studies showed that O_2 enhances the DGC activity of *Bpe*Greg, and that this activity may be rapidly quenched by accumulation of the c-di-GMP product.

To examine whether *Bpe*GReg is involved in biofilm formation in its native *B. pertussis* host, our collaborators at the University of Hawaii constructed a *BpeGReg* knockout mutant of *B. pertussis* strain ATCC 9340. A transcriptional fusion suicide vector pFUS2 was used to

inactivate the target *BpeGReg* gene (*81*). Compared with wild-type *B. pertussis* 9340, the knockout strain formed less biofilm (Figure 4.10). The residual biofilm formation could be due to the fact that, besides *Bpe*GReg, the *B. pertussis* genome encodes four other predicted DGCs and four c-di-GMP PDEs (*82*). These proteins likely respond to physiological signals other than O_2 and probably modulate a variety of processes via the second messenger c-di-GMP, including biofilm and virulence factor production. It has been reported that, although *B. pertussis* does not grow anaerobically, this organism can grow in O_2 tensions as low as 6% of atmospheric O_2 (*83*). Thus, the lowest concentration of dissolved O_2 to allow growth, about 78 μM, would be expected to keep *Bpe*GReg (K_d = 0.64 μM) in an O_2-bound active state. Considering that *B. pertussis* colonizes the upper respiratory tract, *Bpe*GReg could serve as a key O_2 sensor for directing *B. pertussis* to colonize or not.

DISCUSSION

Overall, the finding of sensory globin domains in the diguanylate cyclases DosC and *Bpe*GReg from *E. coli* and *B. pertussis*, respectively, highlight the importance of O_2 as an environmental signal for regulating c-di-GMP homeostasis in bacteria. Oxygen appears to influence the

dynamics of c-di-GMP signaling in these two systems quite differently. In *E. coli*, O_2 regulation of c-di-GMP levels is accomplished by opposing synthesis and degradation activities that are both O_2-controlled (*68*). By contrast, in *B. pertussis*, O_2 regulation of c-di-GMP levels is achieved by an O_2-modulated synthesis opposing an O_2-independent degradation (*41*). Clearly, either approach offers the same degree of control over the final equilibrium level of the c-di-GMP, but they differ dramatically in their control of the dynamics of the response. Consider the analogy of the simple laboratory water bath. In these instruments, a heater switches on whenever the temperature drops below the thermometer setpoint, but there is no cooling mechanism. With a sufficiently powerful heater, for example, one can reduce the time necessary to warm up from 30 to 37 ^{o}C to the point where it becomes instantaneous; however, one cannot control the time it takes the bath to cool down from 37 to 30 ^{o}C. If we add to this heater a constant cooling mechanism, we can accelerate the cooling process but at the expense of adding a large constant workload to the heater. By contrast, consider a PCR thermal cycler. The thermoelectric elements in these ingenious devices can either heat or cool, simply by reversing polarity, and they can also be completely switched off. These cyclers not only reach or hold any set temperature, but also approach it

with any desired “ramp”. This analogy may be applied to enzymes that make and degrade a molecule in response to a single environmental cue.

Why would a bacterium want to control c-di-GMP homeostasis via O_2 perception? Cyclic di-GMP is best known for its role in regulating cell surface adhesion and biofilm formation. For most bacteria, production of a biofilm is costly, in terms of both carbon sources and energy. Shutdown of extracellular matrix production when O_2, and therefore energy, is low may be a way of conserving resources. This is likely the case in *G. xylinus*, where the O_2-sensing phosphodiesterase PDE-A1 restricts entry into the biofilm lifestyle to cells living in the most well aerated locations of these cultures (see Section 1.2, Figure 1.6) (*38*). In addition, O_2 perception for bacteria already living within a biofilm is also likely to be important. Stewart and colleagues have beautifully demonstrated the existence of steep O_2 gradients across the thickness of biofilms grown *in vitro* (*84, 85*). Such gradients probably control bacterial metabolism in different layers of the biofilm (*85*). Molecular oxygen might provide important positional information to a bacterium during the biofilm lifestyle. Alternatively, O_2-regulated c-di-GMP signaling could be linked to functional outputs with little or no connection to biofilm formation. In *E. coli*, the *dosCP* operon is under the control of the general stress response and stationary phase

sigma factor σ^S (RpoS), and as such the expression of this operon is induced by the entry of the bacteria into stationary phase (*53, 54*). This suggests that DosC-DosP might serve to integrate information about O_2 availability in response to changes in cell growth. Though the transcriptional control of *dosCP* by RpoS suggests a role for these enzymes in signaling slowed cell growth as typically occurs during biofilm development or maintenance of the biofilm lifestyle, there is as yet no data to support the idea that DosC-DosP directly influence biofilm formation. Clearly, it will take additional study to elucidate the functional output of O_2 perception and c-di-GMP control by DosC-DosP in *E. coli*. Such an examination is described in Chapter Five.

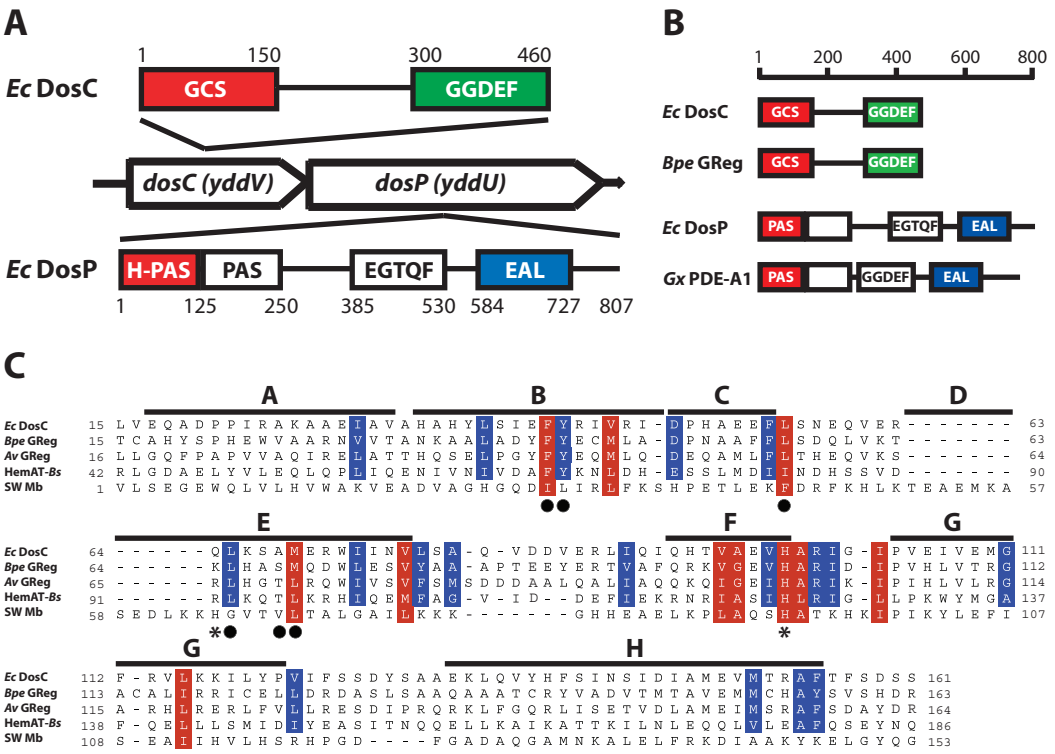

Figure 4.1. **Two heme-based sensors encoded by an operon for c-di-GMP homeostasis. (A)** Genetic organization of the *E. coli dosCP* operon and domain organizations of the corresponding proteins. **(B)** Domain organizations of oxygen-sensing enzymes for c-di-GMP homeostasis. The GGDEF enzymes couple a diguanylate cyclase to an N-terminal modified globin domain. The EAL enzymes couple a c-di-GMP phosphodiesterase to an N-terminal heme-binding PAS domain. **(C)** Amino acid sequence alignment of the sensory region of DosC with that of *Bpe*GReg and *Av*GReg (a sensory globin from *Azotobacter vinelandii*), and structural alignments of HemAT-*Bs* with sperm whale myoglobin (SW Mb). The lines above the sequences indicate the A- through H-helices of SW Mb. The residues highlighted in red are conserved in the sensory globins and SW Mb; those highlighted in blue are similar in the globin-coupled sensors but different from corresponding positions in SW Mb. The asterisks denote the SW Mb proximal (F8) histidine of heme attachment and distal (E7) histidine; the filled circles indicate HemAT-*Bs* residues lining the ligand-binding heme distal pocket.

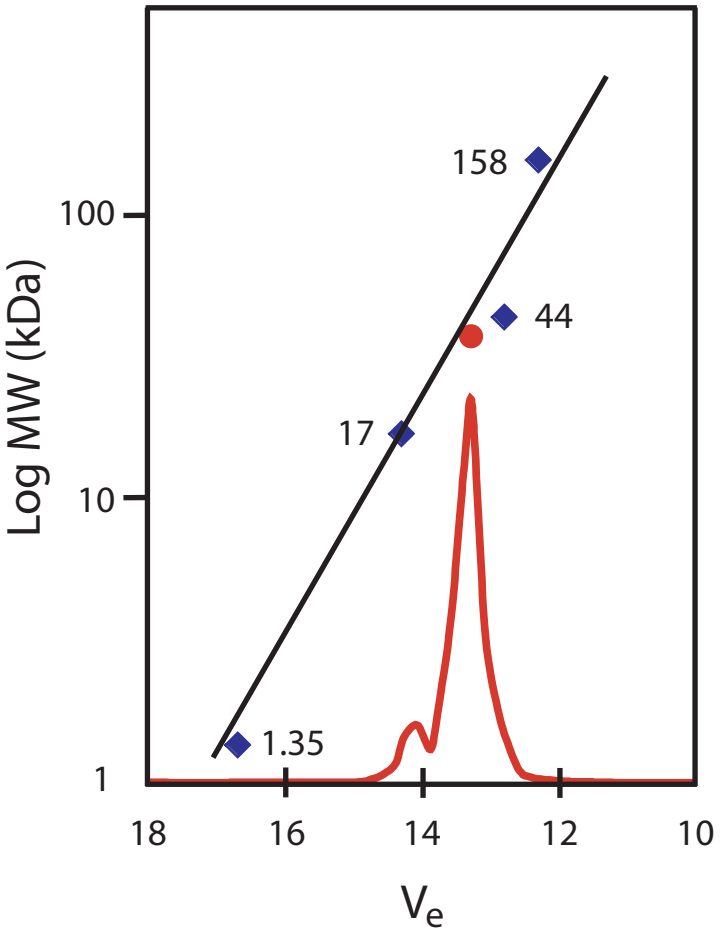

Figure 4.2. **The isolated sensory globin in DosC is dimeric.** Molecular weight determination of the DosC sensory globin domain by FPLC. The predicted monomer mass is 18.7 kDa.

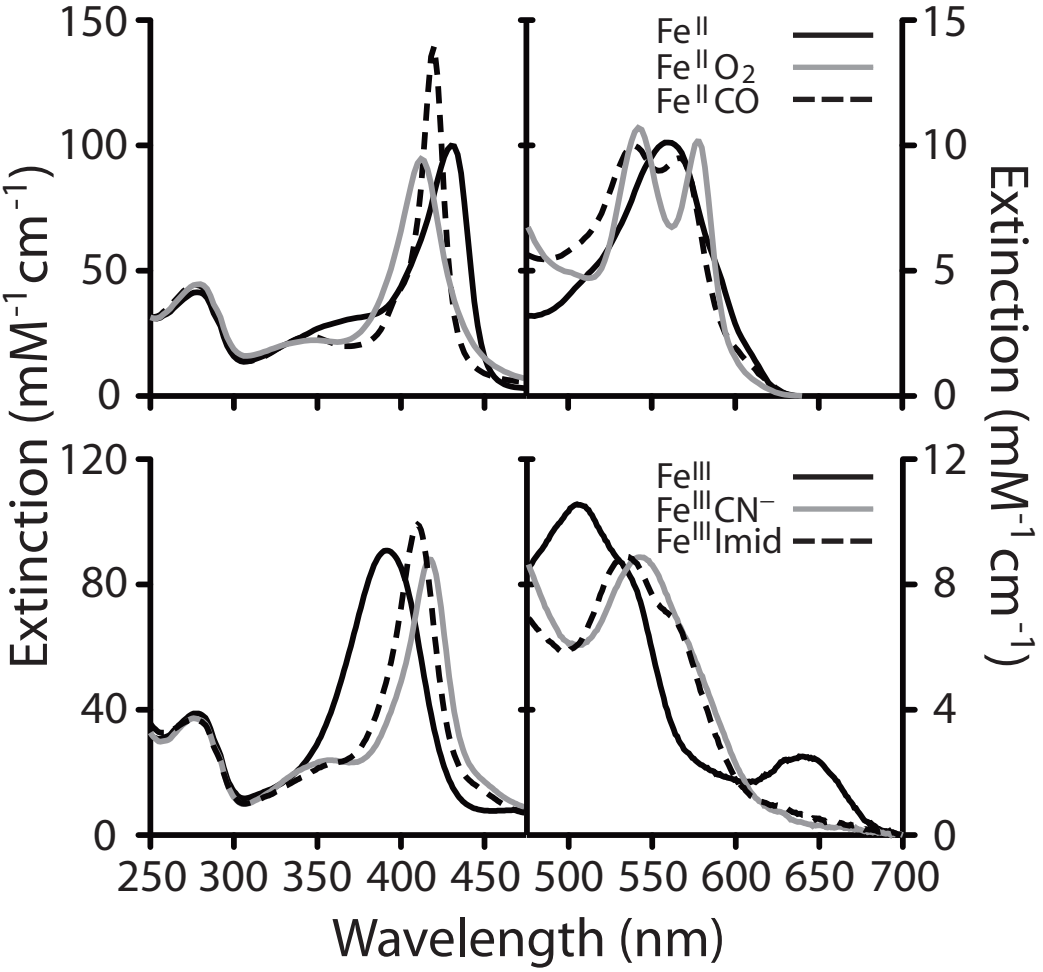

Figure 4.3. ***E. coli*** **DosC contains a sensory globin domain.** Absorption spectra of DosC. The top panel shows ferrous species: deoxy (Fe^{II}, black), oxy ($Fe^{II}O_2$, gray), and carbonmonoxy ($Fe^{II}CO$, broken line). The bottom panel shows ferric species: met (Fe^{III}, black), cyanomet ($Fe^{III}CN^-$, gray), and imidazolemet (Fe^{III}Imid, broken line).

Table 4.1. **Autoxidation parameters of selected heme proteins and binding of ligands of ferric heme.**

	CN^-			Imidazole			
	k_{on} ($mM^{-1}s^{-1}$)	k_{off} (s^{-1})	K_d (μM)	k_{on} ($mM^{-1}s^{-1}$)	K_d (mM)	Met λ max(nm)	k_{ox} (h^{-1})
$DosC_H$ [a]	0.0028	0.000017	6.1[b]	5.0	0.075[c]	391	2.4
$FixL_H$	0.027	0.0001	4.6	50	2	395	2.3
SW Mb	0.32	0.0004	1.3	0.16	22	409	0.06

Hemeproteins were selected to demonstrate a wide range of ferric ligand-binding parameters. [a]This work (*68*); [b]calculated from k_{off} and k_{on}; [c]measured by direct titration. Measurements on $DosC_H$ were at pH 7.5 and 25 °C. Measurements on *Sinorhizobium meliloti* $FixL_H$ are from Gilles-Gonzalez *et al*., (*14*), and Winkler *et al*., (*86*). Measurements on SW Mb are from Quillin *et al*., (*87*); Dou *et al*., (*79*); Mansy *et al*., (*80*); and Brantley *et al*., (*88*).

Table 4.2. **Ligand binding parameters of the oxygen-regulated diguanylate cyclases DosC and *Bpe*GReg.**

	O_2			CO			NO
	k_{on} ($\mu M^{-1}s^{-1}$)	k_{off} (s^{-1})	K_d (μM)	k_{on} ($\mu M^{-1}s^{-1}$)	k_{off} (s^{-1})	K_d (μM)	k_{on} ($\mu M^{-1}s^{-1}$)
MBP-DosC[a]	1.8	36	21	0.13	0.13	0.98	
$DosC_H$ [a]	3.2	18	9.7	0.13	0.080	0.64	7.9
*Bpe*GReg [a]	7.1	4.5	0.63*	1.0	0.57	0.057*	16
				0.13		0.44*	

[a] This work (*41, 68*). K_d values were measured by direct titration except where indicated*, where they were calculated from k_{off} and k_{on}. Measurements were at pH 7.5 and 25 °C.

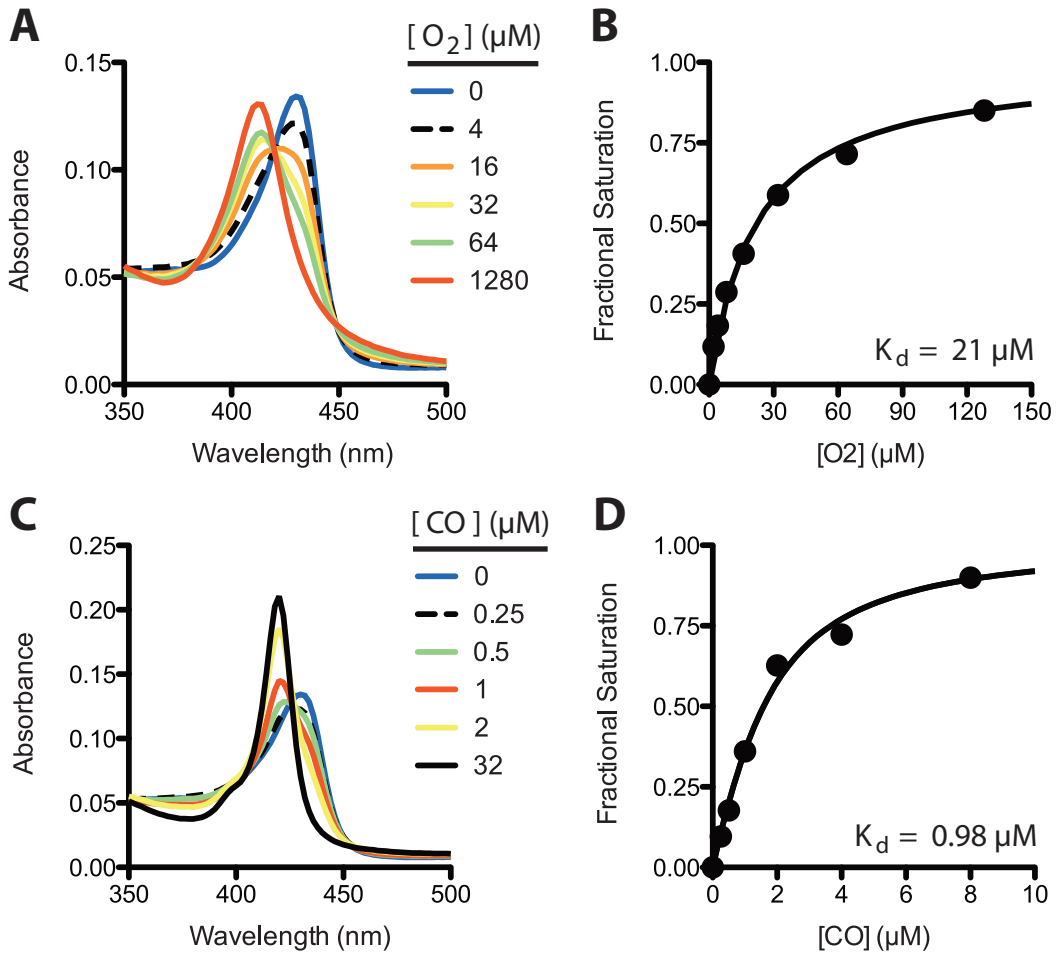

Figure 4.4. **Binding of O_2 and CO to DosC.** **(A)** Absorption changes observed for the transition of deoxy-MBP-DosC (blue, 0 μM O_2) to oxy-MBP-DosC (red, 1280 μM O_2) with intermediate saturations with ligand. **(B)** Determination of the DosC O_2 affinity (K_d (O_2)) via deconvolution of the spectra in panel A and fitting the data to the Hill equation. **(C)** Absorption changes observed for the transition of deoxy-MBP-DosC (blue, 0 μM CO) to carbonmonoxy-MBP-DosC (black, 32 μM CO) with intermediate saturations with ligand. **(D)** Determination of the DosC CO affinity (K_d(CO)) via deconvolution of the spectra in panel C and fitting the data to the Hill equation. Measurements were at pH 7.5 and 25 °C.

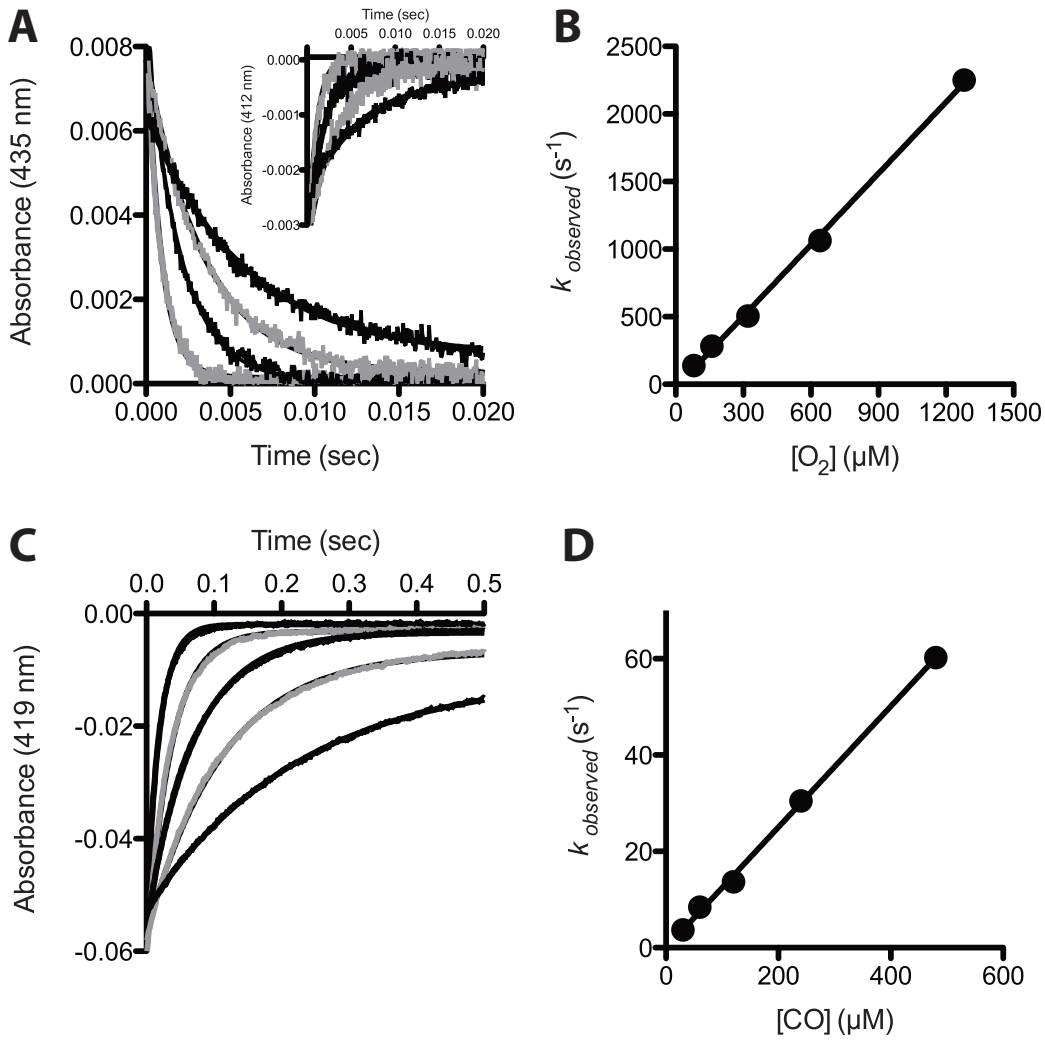

Figure 4.5. **DosC O_2 and CO association rate measurements. (A)** Representative kinetic traces showing the rates of O_2 association to MBP-DosC at pH 7.5 and 25°C. The main panel shows the accelerating rates as the DosC binds 80, 160, 320, and 640 μM O_2, as monitored at 435 nm from the disappearance of the deoxy state; the inset shows the same process monitored at 412 nm from the appearance of the oxy state. **(B)** Determination of the DosC oxygen association rate constant ($k_{on}(O_2)$). **(C)** Representative kinetic traces showing the rates of CO association (30, 60, 120, 240, and 480 μM) to MBP-DosC at pH 7.5 and 25°C, as monitored at 419 nm from the appearance of the carbonmonoxy state. **(D)** Determination of the DosC CO association rate constant (k_{on}(CO)). Rates of both O_2 and CO binding were measured by laser-flash photolysis. Similar results were obtained for CO binding to $DosC_H$.

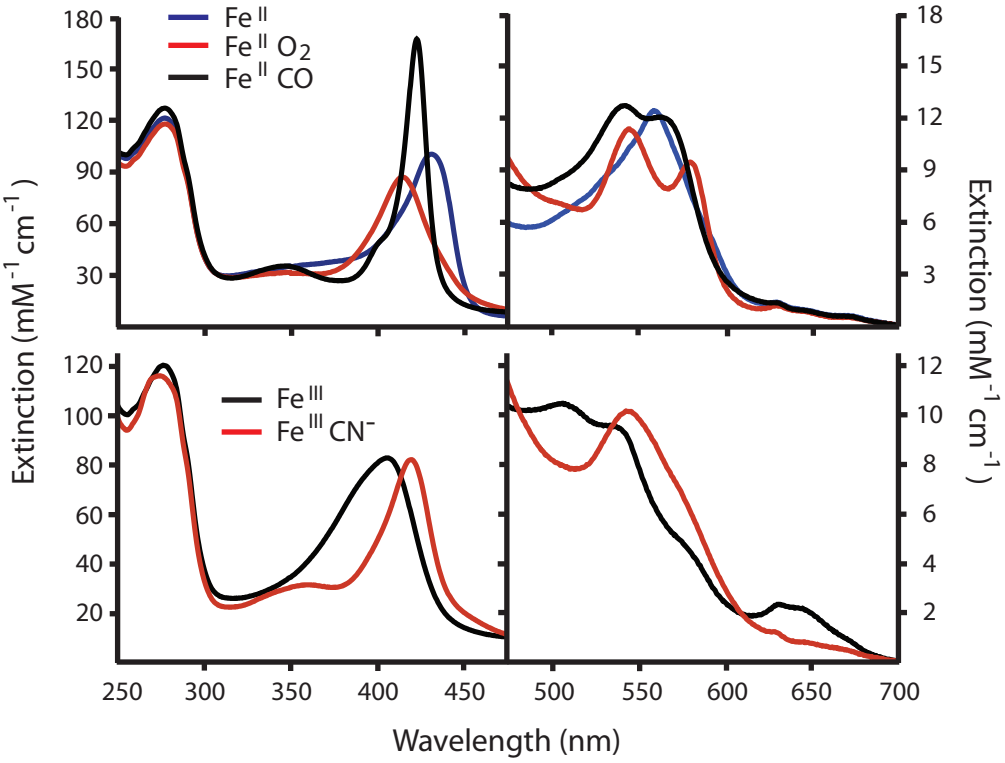

Figure 4.6. **A sensory globin in *Bpe*GReg.** Absorption spectra for ferrous *Bpe*GReg species (top panel) and for ferric *Bpe*GReg species (bottom panel). All spectra were at pH 7.5 and 25°C in 100 mM sodium phosphate.

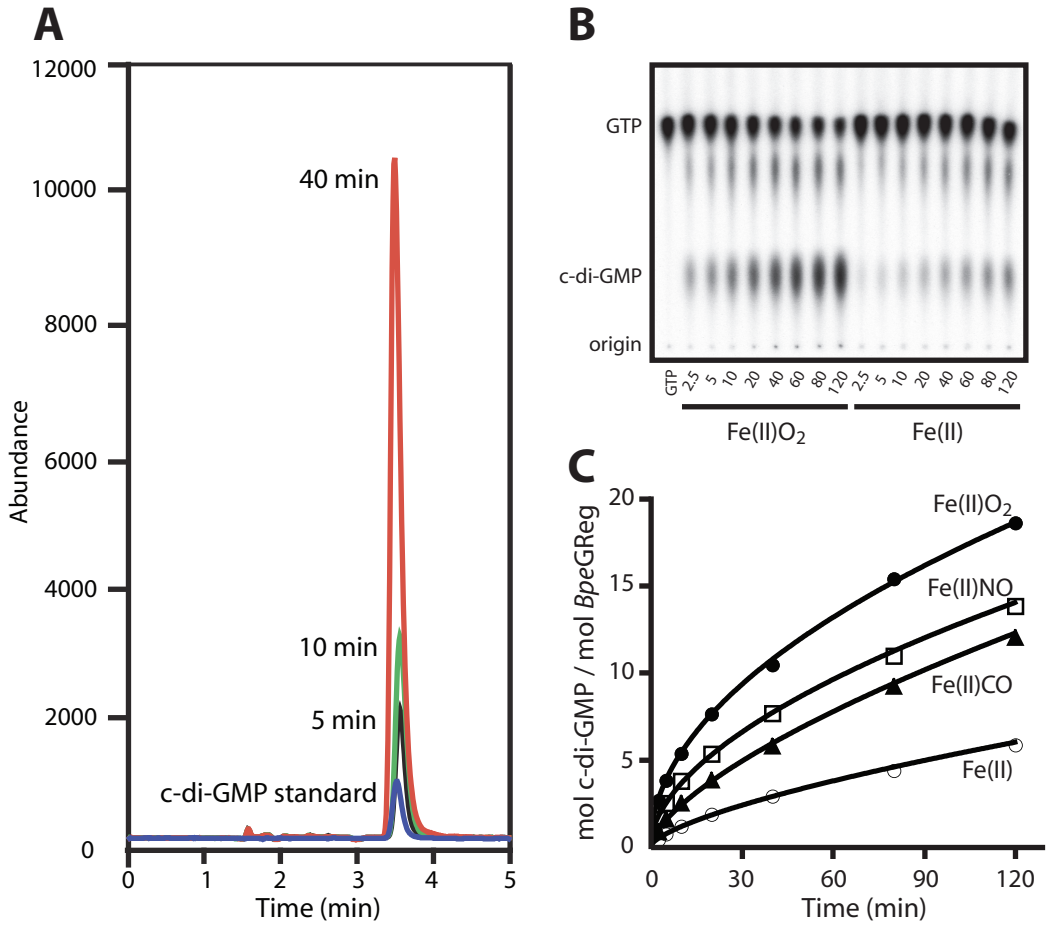

Figure 4.7. **Ferrous *Bpe*GReg synthesizes c-di-GMP. (A)** Diguanylate cyclase activity of *Bpe*GReg at 5 min (black), 10 min (green), and 40 min (red), as assayed by mass spectra of HPLC eluted reaction products. The c-di-GMP was detected in negative single-ion mode at *m/z* of 689. **(B)** Influence of O_2 on *Bpe*GReg activity; levels of c-di-GMP were measured by TLC for reactions stopped at 2.5, 5, 10, 20, 40, 80, and 120 min. **(C)** Influence of ferrous heme ligands on *Bpe*GReg activity. All reactions were at pH 7.5 and 30 °C.

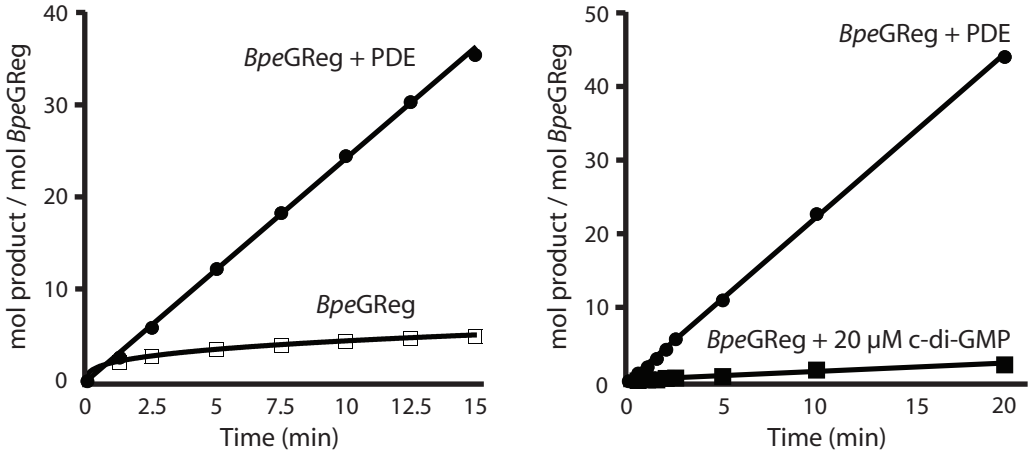

Figure 4.8. **Feedback inhibition of *Bpe*GReg by c-di-GMP.** Rates of conversion of 500 µM GTP to c-di-GMP were followed either by measuring c-di-GMP directly or by measuring formation of pGpG from a PDE-coupled reaction. **(A)** Activity of 5 µM oxy-*Bpe*GReg without coupling to a PDE (open squares) or with coupling to a PDE (closed circles). **(B)** Activity of 1 µM oxy-*Bpe*GReg in a reaction started in the presence of 20 µM c-di-GMP or coupled to a PDE. All reactions were at pH 7.5 and 30 °C.

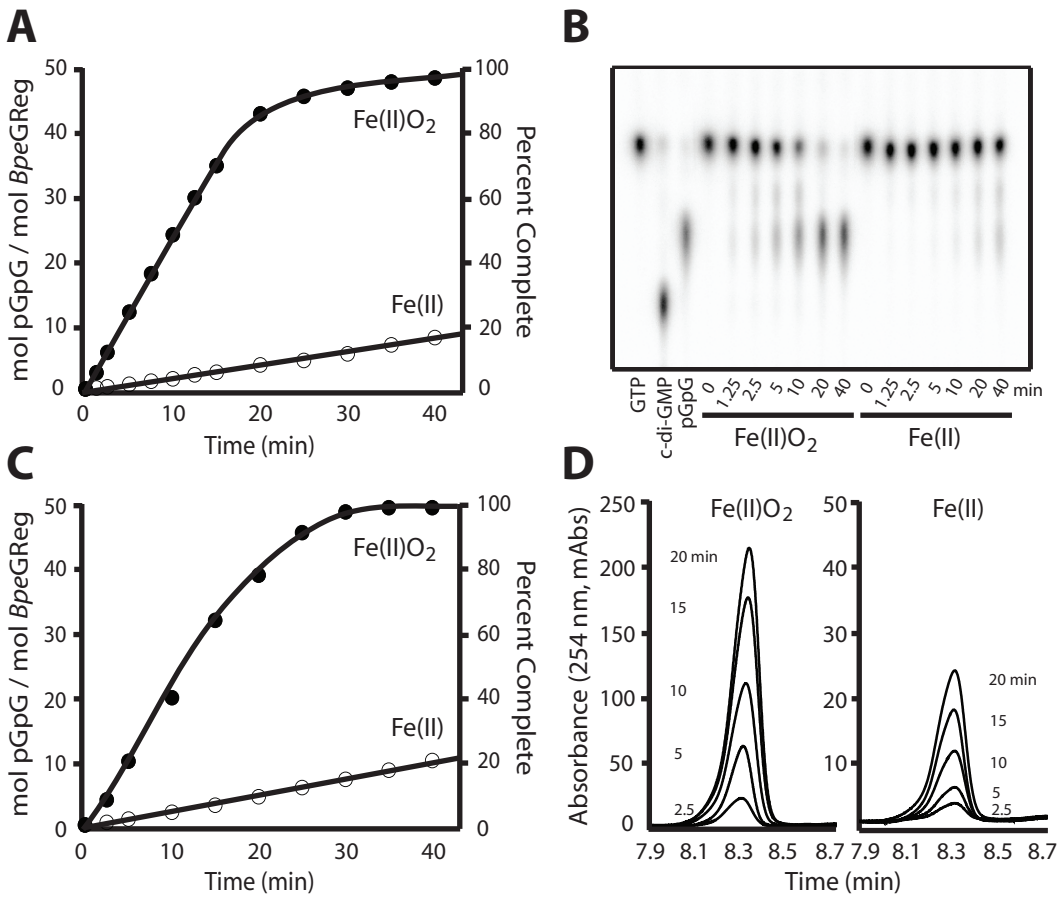

Figure 4.9. ***Bpe*GReg is an O_2-activated diguanylate cyclase.** Rates of conversion of 500 μM GTP to c-di-GMP by *Bpe*GReg were followed by measuring the formation of pGpG in a PDE-coupled reaction. **(A)** DGC activity of 5 μM *Bpe*GReg in air [Fe(II)O_2] or under anaerobic conditions. Note the 13-fold drop in activity in the absence of O_2, and note that the reaction is essentially complete within 30 min in air. **(B)** TLC showing representative time points from the reactions in panel A. The first three lanes are shown as references, with the *R* values being 0.58 for GTP, 0.18 for c-di-GMP, and 0.34 for pGpG. **(C)** Repeat of the reaction shown in panel A for analysis by HPLC. **(D)** HPLC traces of representative pGpG peaks from the reactions shown in panel C; the peaks are from the 2.5, 5.0, 10, 15, and 20 min time points. All reactions were at pH 7.5 and 30 °C.

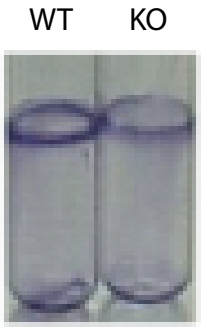

Figure 4.10. **Reduced biofilm formation in a *Bpe*GReg knockout strain.** Biofilm assay of wild-type (WT) *B. pertussis* and the *Bpe*GReg knockout (KO) strain after 7 days of growth in static cultures at 37 ^{o}C. Adherent cells were stained with crystal violet.

CHAPTER FIVE

Functional importance of DosC-DosP

INTRODUCTION

What are the functions of the globin-coupled diguanylate cyclases in *B. pertussis* and *E. coli*? The deficiency of the *B. pertussis BpeGReg* knockout strain to form a normal biofilm clearly indicates the importance of *Bpe*GReg in this process, although the exact mechanistic details connecting second-messenger synthesis and extracellular matrix production are not yet elucidated (*41*). On the other hand, the influence of *dosCP* on *E. coli* biofilm production remains unknown. We expect that the results of a *dosCP* knockout will be more difficult to interpret because of the more complex O_2 regulation resulting from these proteins. For example, effects of *dosCP* deletion on biofilm formation would likely be observed only under a specific set of O_2 tensions. In addition, the possibility remains that DosC-DosP do not directly control aspects of *E. coli* biofilm formation, in which case the attempted observation of a biofilm phenotype with *dosCP* deletion mutants would be noninformative. The background numbers of GGDEF/EAL-class enzymes in *E. coli* (12

GGDEF, 10 EAL, 7 GGDEF + EAL) pose yet another problem, as the mutation of a single GGDEF or EAL in *E. coli* might be more easily complemented by another resident DGC/PDE than is possible in *B. pertussis*, which contains only 4 PDEs and 4 DGCs in addition to *Bpe*GReg. Due to the possible difficulties in interpreting *dosCP* mutations, we sought to gain insights into the *in vivo* function of DosC-DosP by conducting a biochemical analysis of this O_2-sensing DGC-PDE couple.

RESULTS

(5.1) A poly(A)-polymerizing activity copurifies with DosC-DosP as part of a larger complex. A moderate overexpression of *dosCP* in *E. coli* resulted in the production of DosC and DosP as a complex (Figure 5.1) (*68*). *In vitro* this complex actively converted [α-^{32}P]-GTP to pGpG, due to coupling of a modest c-di-GMP synthesis by DosC to a robust c-di-GMP hydrolysis by DosP (Figures 5.1B, 5.2A). When we presented [α-^{32}P]-ATP to the same enzyme complex, a wholly unexpected radiolabeled product appeared at the origin of the polyethyleneimine thin-layer chromatographic plate, where large anionic molecules, such as nucleic acids or some proteins, would be expected (Figure 5.2A). SYBR Gold nucleic-acid staining of this product, following its electrophoresis, revealed it to be

poly(A) RNA, with a well-defined length, slightly longer than 1000-bases (Figure 5.2B). *E. coli* proteins with such a poly(A) polymerizing activity include two enzymes involved in post-transcriptional modification of RNAs: poly(A) polymerase (PAP1) and polynucleotide phosphorylase (PNPase). The polymerizing activity was identified as issuing from PNPase based on a more robust poly(A) polymerization with ADP, a known substrate of PNPase but not PAP1, and based on the diminished polymerase activity of anti-PNPase-treated reactions (Figure 5.3).

To rule out the possibility of an adventitious PNPase association with the DosC-DosP couple, we expressed the *dosCP* operon by three alternative schemes for purification of the corresponding proteins. The first scheme produced wild-type DosC and DosP, which co-purified during hydrophobic interaction (phenyl sepharose) and size-exclusion (Sephacryl-S300) chromatographies (Figure 5.1) (*68*). The second scheme produced a 6His-tag-DosC that co-purified with DosP by Ni-NTA-affinity and size-exclusion chromatographies. The third scheme produced a MBP-DosC fusion that co-purified with DosP by amylose-affinity chromatography (Figure 5.4A). In each case the presence of PNPase in the DosC-DosP complex was confirmed by its activity and by immunodection of this enzyme in western blots (Figures 5.4B,C). As a

control, we purified MBP by the same procedure used to isolate the MBP-DosC-DosP complex and were unable to detect PNPase in the eluate of the MBP alone purification (Figures 5.4B,C). Overall, these results suggest that DosC-DosP copurify out of *E. coli* as part of a stable complex that contains PNPase.

(5.2) An oxygen sensing RNA degradosome. Since *E. coli* RNA degradosomes contain PNPase as a core component, we hypothesized that this enzyme's association with the DosC-DosP couple might be indicating a c-di-GMP responsive degradosome and set out to explore this possibility. To this end, we purified MBP-DosC and DosP from *E. coli* expressing *malE:dosCP* by a gentle one-step amylose-affinity purification, and we compared all the assays of the MBP-DosC-DosP complex to assays of MBP recovered by a similar procedure from *E. coli* expressing *malE*. From Figure 5.4A, it is clear that the MBP-DosC-DosP associated stably with a group of proteins that did not interact with MBP alone. These proteins were found to associate with DosC-DosP as part of a large (~ 1.3 MDa) complex, as indicated by their migration on gel filtration (Figure 5.4D). *E. coli* RNA degradosomes typically consist of four core proteins: the endoribonuclease RNase E, the exoribonuclease PNPase, the DEAD-

box family RNA helicase RhlB, the glycolytic enzyme enolase, plus additional proteins that vary in their association with this core (*89-94*). A determination of enolase activity by a colorimetric assay of the conversion of 2-phosphoglycerate to phosphoenol pyruvate also revealed the presence of this enzyme in the DosC-DosP associated complex (Figure 5.5) (*95*).

A more comprehensive analysis of the proteins in the complex by mass spectrometry (MS/MS) confirmed the presence of PNPase and additionally identified RNase E, the heat shock proteins DNaJ, DNaK, and GroEL, and the RNA terminator protein Rho as being among its components (Table 5.1). Although the complex clearly possessed enolase activity (Figure 5.5), enolase and RNA helicase were not identifiable by mass spectrometry, possibly because of a lower stoichiometry of these components. The role of enolase in degradosomes is unclear, as is that of the heat-shock proteins; however they have all been proposed to belong to degradosomes because of their frequent association with RNase E (*90, 92*). Though the association of Rho with RNA degradosomes is reported here for the first time for *E. coli*, Rho is a known degradosome component in *Rhodobacter capsulatus* (*96*). In addition to degradosome proteins, the DosC-DosP complex also included

RNAs, based on its content of RNase-sensitive ethidium bromide staining macromolecules (Figure 5.6A). One RNA whose presence we suspected was OxyS, a small non-coding RNA known to target some mRNAs to *E. coli* degradosomes as part of an oxygen response. We tested for OxyS by RT-PCR and indeed found this RNA to associate with DosC-DosP (Figure 5.6B). Overall, these results led us to suppose that there exist specialized oxygen-sensitive degradosomes in *E. coli* that respond to local c-di-GMP levels established by DosC and DosP.

(5.3) PNPase is a direct high-affinity target for c-di-GMP. Given the consistent co-purification of the DosC-DosP complex with PNPase, we asked whether this degradosome component is a target for c-di-GMP. To address this question, we obtained pure PNPase by the methods of Jones and colleagues from *E. coli* overexpressing the corresponding gene (Figure 5.7A) (*63*). Titration of this purified PNPase with c-di-GMP showed a saturable binding of nucleotide, with $K_d \sim 3\ \mu M$ (Figure 5.7B). Importantly, c-di-GMP was not utilized as a substrate by PNPase (Figure 5.8). We then asked whether c-di-GMP serves as an allosteric effector of PNPase activity. We began by examining a phosphoryl-exchange activity well-established for PNPase (Figures 5.9, 5.10A,B) (*64*). We compared

the effect of adding 10 μM c-di-GMP to the reaction versus omitting this dinucleotide and found the phosphoryl-exchange activity to be accelerated 10-fold by the c-di-GMP addition (Figures 5.10A,B). We additionally developed a sensitive assay of the real-time production of poly(A) from ADP and further examined the PNPase response to c-di-GMP by this approach. An enhancement of the PNPase activity could be detected in c-di-GMP concentrations as low as 0.1 μM (Figure 5.10C). This was due to a pre-steady-state effect of the c-di-GMP on the reaction giving a nearly four-fold enhancement in rate per micromolar c-di-GMP (Figures 5.10D,E). Alternative cyclic nucleotides, such as cGMP and cAMP, showed no effect on either the phosphoryl-exchange or poly(A)-synthesis reactions of PNPase. We therefore deduced that PNPase is a direct high-affinity target of c-di-GMP. This result, coupled with the finding that PNPase copurifes with a pair of O_2-regulated c-di-GMP metabolizing enzymes, strongly suggest that these specialized degradosomes are able to respond to information about cellular oxygenation via a localized c-di-GMP signaling circuit.

DISCUSSION

A new role for c-di-GMP: post-transcriptional RNA processing.

Overall, the results of this study advanced our understanding of two crucial questions in the elucidation of c-di-GMP signaling mechanisms. (i) What are the molecular targets of c-di-GMP? The allosteric activation of PNPase by c-di-GMP provides an unexpected answer to this question. As a second messenger, c-di-GMP is closely associated with cellular adaptations from a vegetative to a biofilm lifestyle. Possibly, the control of RNA stability represents a major route to this adaptation. Alternatively, the RNAs regulated by the DosC-DosP degradosome might play little or no role in biofilm formation whatever and instead regulate processes not yet appreciated as being under c-di-GMP control. Regardless of the pathways involved, our results expand the influence of c-di-GMP regulation to include the control of post-transcriptional RNA processing, an entirely new mode of physiologic control for this important bacterial second messenger.

C-di-GMP signaling complexes.

(ii) Does c-di-GMP occur in bacterial cells as a freely diffusible pool or in precise subcellular localizations? The examples of an O_2-sensing *G.*

xylinus cellulose synthase complex, together with the current finding of a c-di-GMP regulated *E. coli* degradosome complex, strongly suggest that localized c-di-GMP signaling does occur *in vivo* (Figure 5.11). We suspect that signaling complexes may become increasingly appreciated as ways to compartmentalize c-di-GMP signaling circuits within individual bacterial cells. These local c-di-GMP circuits, coupled with the control of DGCs and PDEs by specific environmental stimuli, also helps to explain the great multiplicity of GGDEF/EAL-class enzymes in bacteria.

Specialized RNA degradosomes.

To date there have been no reports of DosC-DosP association with degradosome preparations despite intensive efforts to characterize the protein components of degradosome complexes (*89-92*). This can be explained in two ways: (i) the *dosCP* operon is expressed in stationary phase, while most investigations of RNaseE-associated degradosome components have involved isolating these complexes from log-phase cells. (ii) The DosC-DosP degradosomes likely represent only a small subpopulation of total *E. coli* RNA degradosomes, even for cells in stationary phase. Recent reports suggest that the composition of *E. coli* degradosomes can vary dynamically in response to environmental stimuli,

though the signaling mechanisms underlying these variations remains unclear (*93, 97-99*). The DosC-DosP degradosomes likely work to modify only a specific subset of *E. coli* RNAs in response to changing cellular O_2 levels. Our results have led us to propose a model for O_2-regulated RNA processing, where DosC and DosP serve as O_2 sensing components of a specialized RNA degradosome complex (Figure 5.12). Signal transduction is done through the second messenger c-di-GMP, whose target, PNPase, resides near the sensory components of the complex. PNPase is allosterically activated by c-di-GMP to process specific RNA transcripts, where the specificity of RNAs recruited to the oxygen-sensing degradosome is provided by a small number of non-coding RNAs present within the complex.

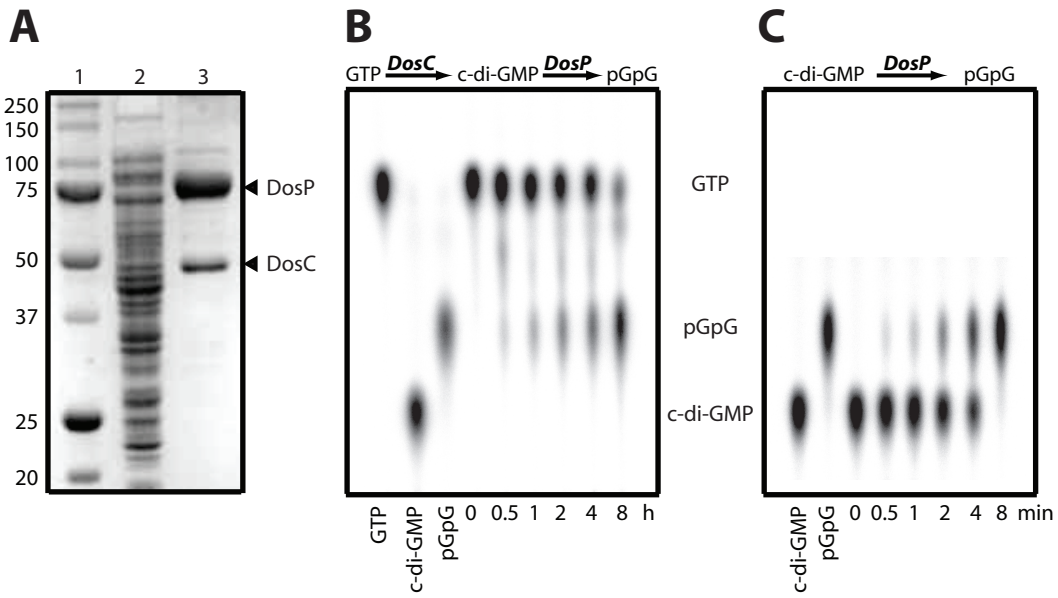

Figure 5.1. **The DosC and DosP proteins copurify from *E. coli*.** **(A)** Purification of DosC and DosP from *E. coli* moderately overexpressing the wild-type *dosCP* operon. A crude cell lysate (lane 2) from the *dosCP*-expressing cells is compared by Coomassie-stained SDS-PAGE to molecular weight markers (lane 1) and the copurified proteins (lane 3) after phenyl-Sepharose and gel-filtration chromatographies. **(B)** Presence of diguanylate cyclase activity in the DosC-DosP complex, as measured from the conversion of an [α-^{32}P]-GTP substrate to ^{32}P-labeled linear pGpG, in a coupled assay. **(C)** Presence of c-di-GMP-specific phosphodiesterase activity in the DosC-DosP complex, as measured from the conversion of a ^{32}P-labeled c-di-GMP substrate to linear pGpG.

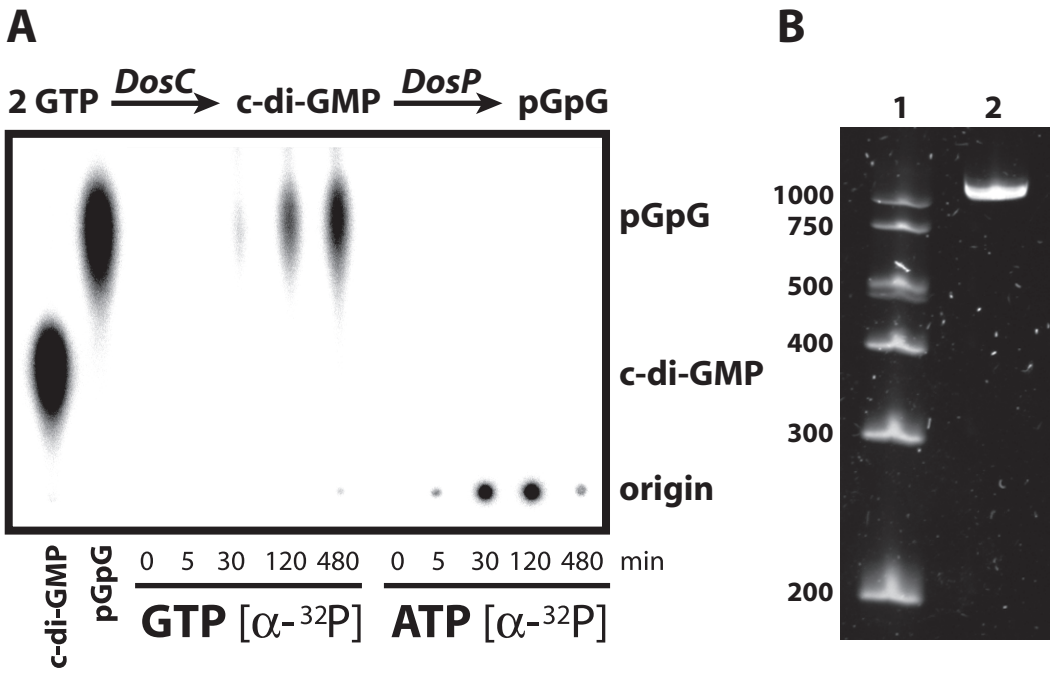

Figure 5.2. **A poly(A) polymerizing activity co-purifies with DosC-DosP. (A)** Accumulation of radiolabel at the origin of polyethyleneimine thin-layer chromatography (PEI-TLC) plates for the DosC-DosP complex with [α- ^{32}P]-ATP as substrate. **(B)** SYBR-Gold stained urea acrylamide gel (6 %) of the 120 min time point from the ATP reaction in panel A.

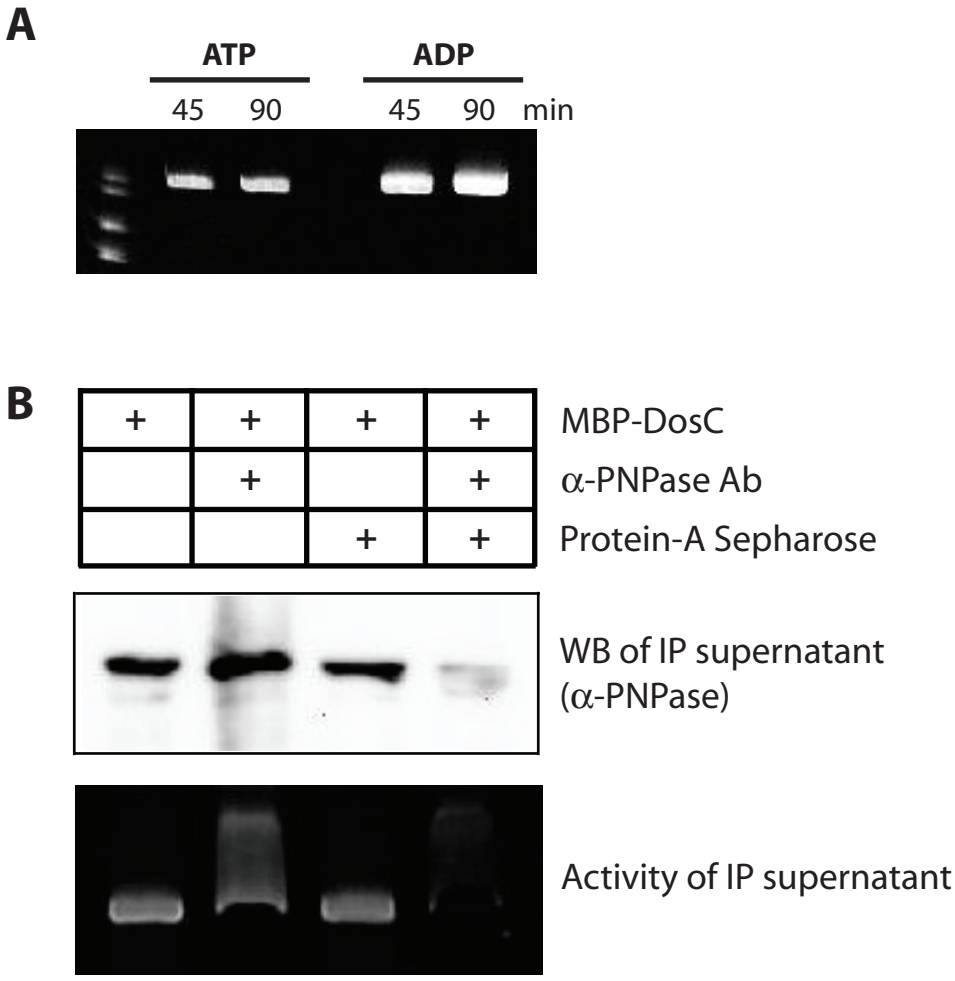

Figure 5.3. **Initial identification of PNPase as a DosC-copurifying enzyme.** **(A)** DosC preparations contain a poly(A) polymerizing activity with substrate preference for ADP. **(B)** Supernatants from DosC samples immunodepleted of PNPase have diminished poly(A) polymerizing activities.

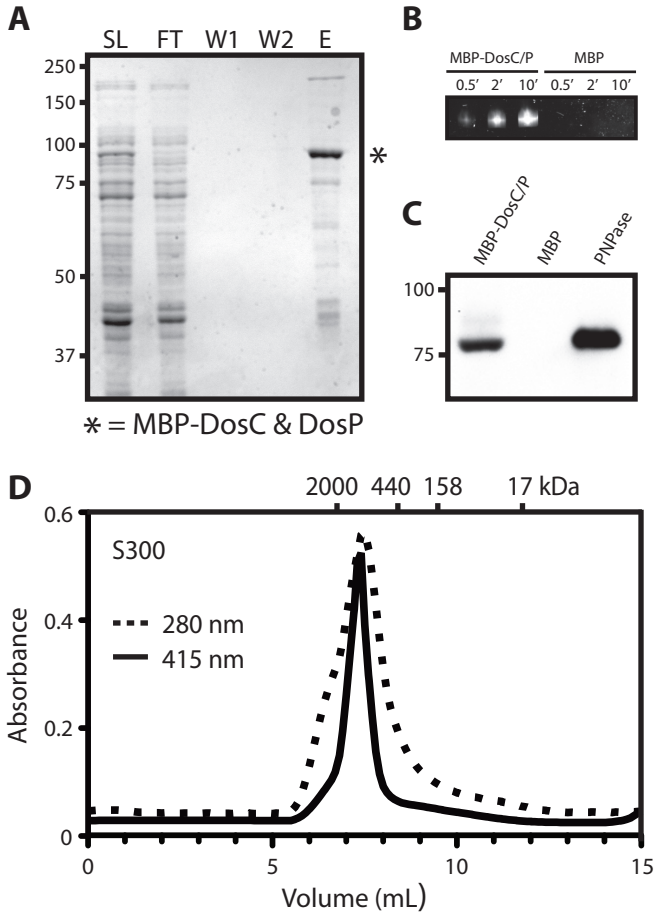

Figure 5.4. **Purification of DosC-DosP as part of a larger complex. (A)** Overexpression of a *malE:dosCP* fusion in *E. coli*, followed by purification of the corresponding proteins via amylose affinity, recovers MBP-DosC, DosP, and a number of additional copurifying proteins, as determined by Coomassie-stained SDS-PAGE. SL, soluble lysate; FT, flow-thru from the amylose column; W1-2, washes from the amylose column; E, amylose column eluate. **(B)** Presence of PNPase activity in the MBP-DosC eluate, as determined by SYBR-Gold staining of a urea acrylamide gel from reactions of eluates (MBP-DosC or MBP alone) with ADP. **(C)** Presence of PNPase in the MBP-DosC eluate, as determined by Western blotting with PNPase antisera. **(D)** Size exclusion chromatographic analysis (Sephacryl 300) of the MBP-DosC eluate indicates DosC copurifying proteins associate with DosC as part of a larger complex. Solid line, heme absorbance at 415 nm; dotted line, protein absorbance at 280 nm. Positions of standards [blue dextran (2000), ferritin (440), aldolase (158), and myoglobin (17)] are shown.

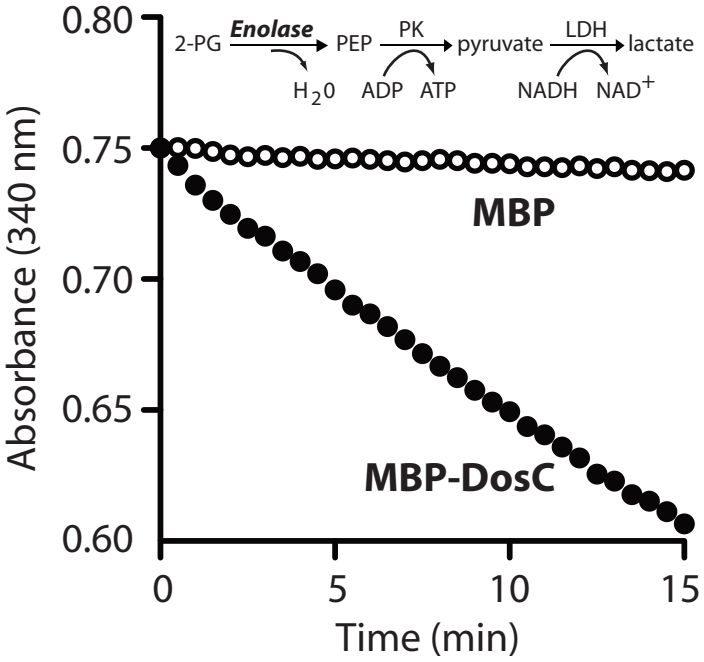

Figure 5.5. **Presence of enolase in the DosC-DosP complex.** A colorimetric assay of enolase activity (pH 7.5 and 23°C) indicated the presence of enolase in the DosC-DosP complex.

***Table 5.1*. MS/MS protein identification of *E. coli* RNA degradosome components with DosC and DosP.**

Protein	GI number	Percentage of RNaseE [a]	MW (Da)
DosC	218700119	3384	53,147
DosP	188491677	944	91,146
Rho	15804373	178	46,967
DnaK (HSP 70)	15799694	170	69,072
RNase E	16129047	100	118,125
GroEL (HSP 60)	38491464	64	57,268
DnaJ (HSP 40)	16128009	56	41,074
PNPase	170682265	28	77,067

[a] MS/MS protein ID values were initially obtained as MASCOT scores, which were normalized to the MASCOT score for RNase E (MASCOT score = 730).

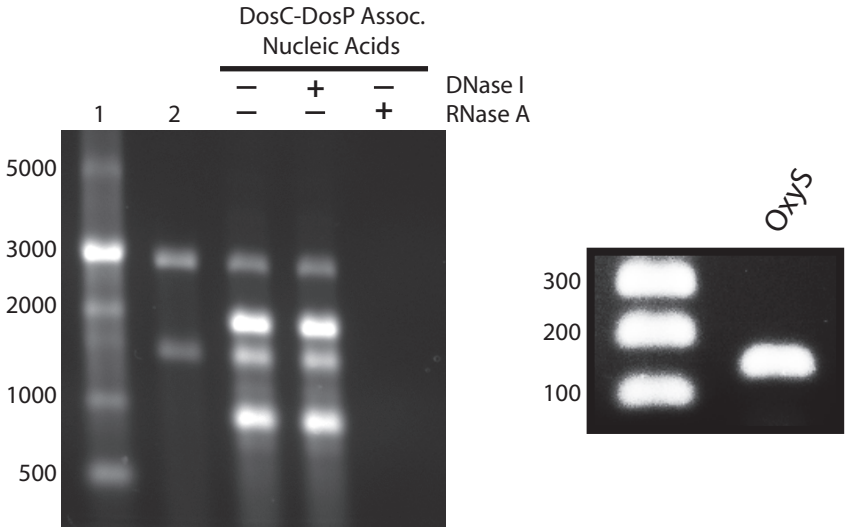

Figure 5.6. **Presence of RNAs in the DosC-DosP complex.** **(A)** Nucleic acids extracted from the DosC-DosP complex are RNAs, as determined by their stability to DNase and sensitivity to RNase A. Lane 1, ssRNA Ladder (New England Biolabs); Lane 2, total *E. coli* MC1061 RNA; Lane 3, total nucleic acids extracted from the DosC-DosP complex. Samples were electrophoresed on a 1% TBE agarose gel and stained with ethidium bromide. **(B)** The snRNA OxyS is a component of the DosC-DosP complex, as determined by RT-PCR. cDNAs were prepared by priming a reverse transcriptase reaction with random hexamers, where total DosC-DosP associated RNAs served as the template. This cDNA (40 ng) served as the PCR template for OxyS amplification.

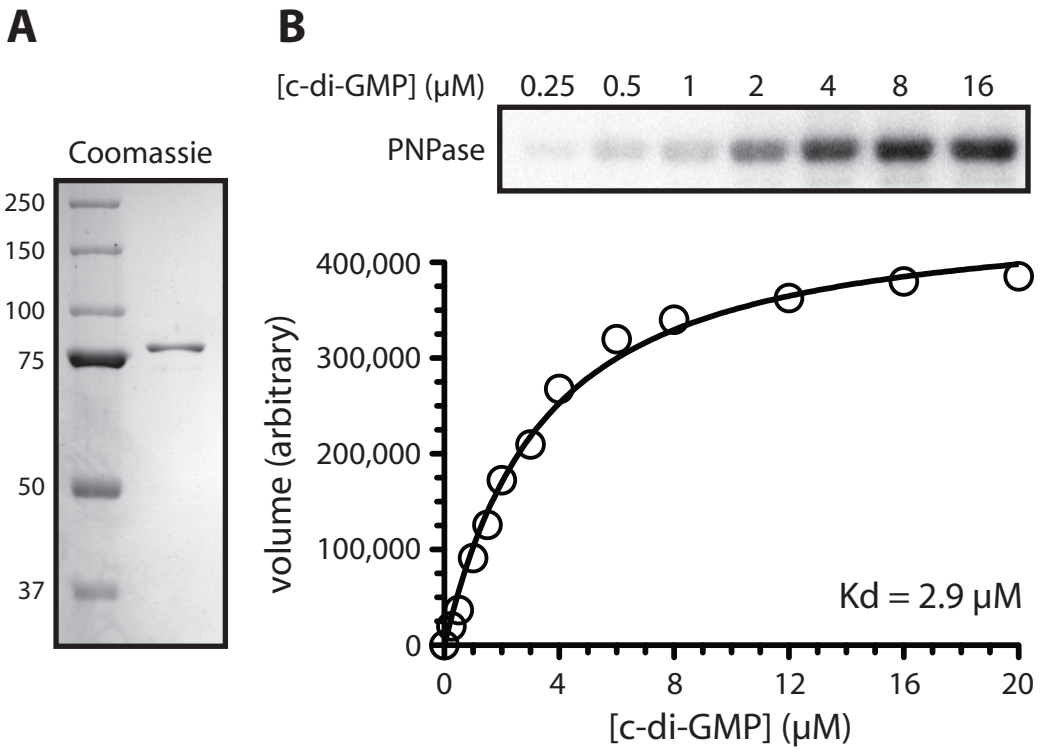

***Figure 5.7*. Purified PNPase binds c-di-GMP. (A)** Purified *E. coli* PNPase was obtained by the method of Jones and colleagues (Jones GH *et al., Prot Exp Purific.* (2003) 32: 202-209). **(B)** Saturable binding of UV-crosslinked [^{32}P]-c-di-GMP to purified PNPase at pH 8.0 and 23 ^{o}C.

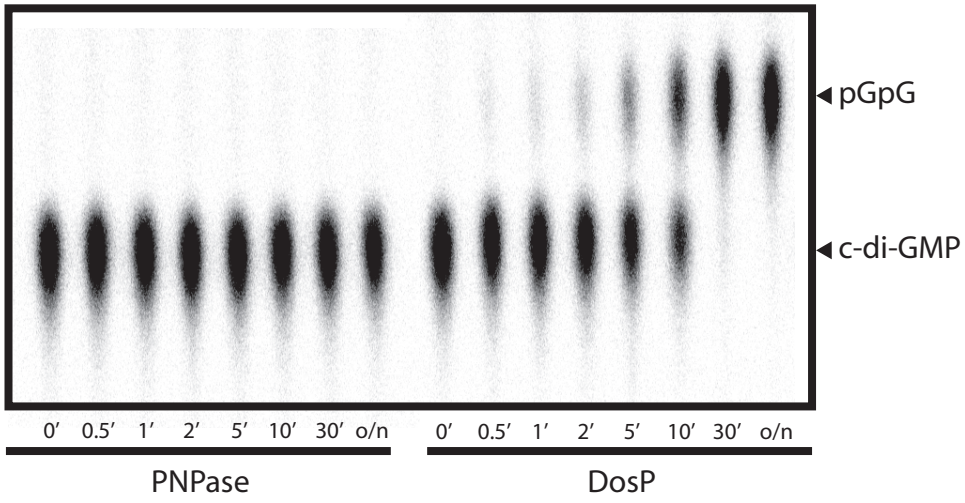

Figure 5.8. **PNPase does not utilize c-di-GMP as a substrate.** Stability of c-di-GMP toward PNPase (5 μM) or DosP (0.1 μM, oxy) at pH 8.0 and 30 °C. Reactions were stopped at the times indicated and analyzed by TLC.

Reactions catalyzed by *Ec*PNPase:

1. Phosphorolysis and Polymerization

$$(p^{5'}N^{3'}OH)_x + Pi \rightleftharpoons (p^{5'}N^{3'}OH)_{x-1} + pp^{5'}N$$

2. Nucleoside Diphosphate - Pi Exchange

$$pp^{5'}N + {}^{*}Pi \rightleftharpoons {}^{*}pp^{5'}N + Pi$$

Figure 5.9. **Reactions catalyzed by *E. coli* PNPase.**

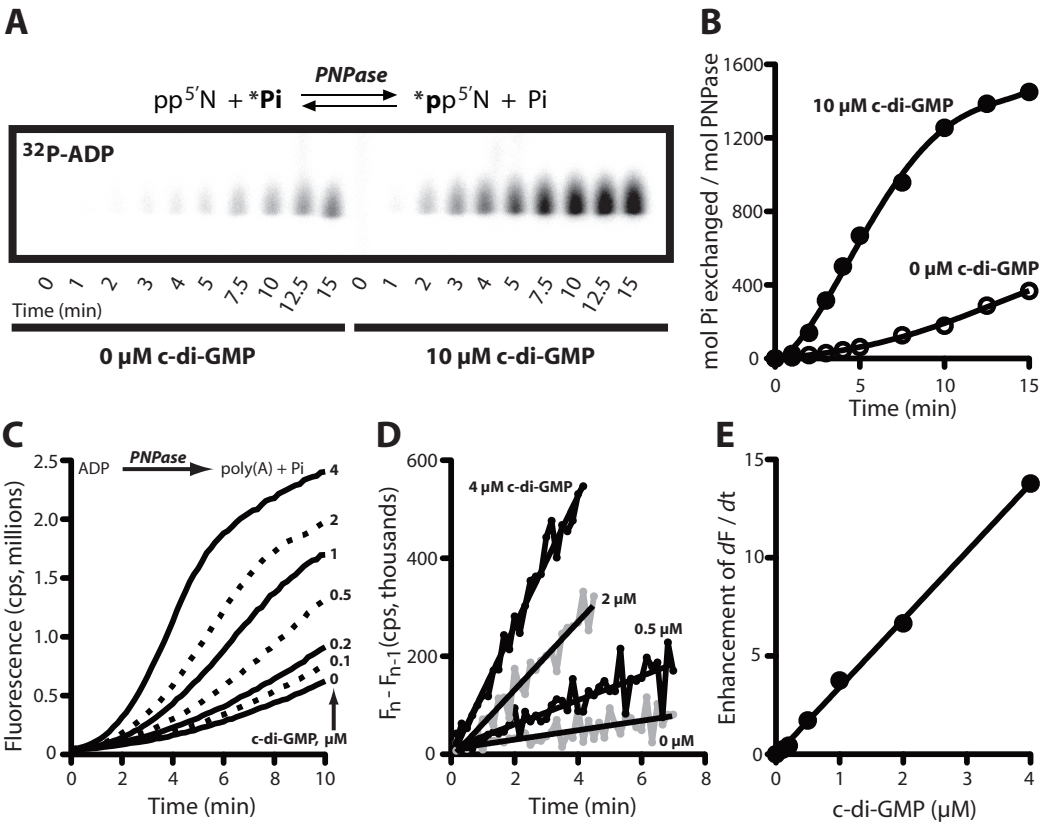

Figure 5.10. **PNPase is a high-affinity target for c-di-GMP.** **(A)** C-di-GMP enhances a PNPase-catalyzed phosphoryl-exchange between ADP and Pi. **(B)** Quantification of the data in panel A. **(C)** A PNPase-catalyzed poly(A) polymerizing activity from ADP is enhanced by c-di-GMP in a dose-dependent manner, as determined by real-time fluorescence measurements of poly(A). **(D)** C-di-GMP enhances the pre-steady state kinetics of the PNPase poly(A) polymerizing activity, as indicated by the linearity of the first derivatives ($F_n - F_{n-1}$) from reactions in panel C. **(E)** The enhancement of pre-steady state kinetics on the PNPase poly(A) polymerizing reaction is directly proportional to the c-di-GMP concentration, such that a nearly four-fold enhancement in rate is achieved per micromolar c-di-GMP. All reactions were at pH 8.0 and 23 ^{o}C as described in Materials and Methods (Section 2.11).

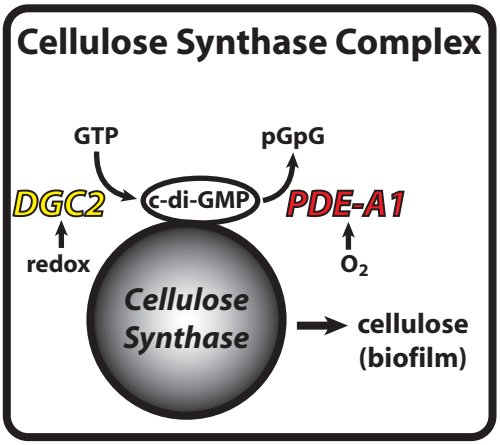

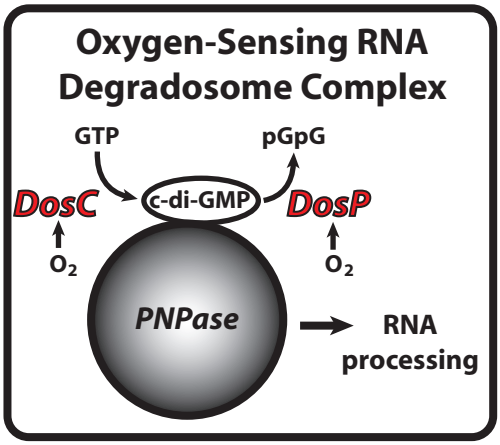

PDE-A1 Chang AL, Tuckerman JR, Gonzalez G, Mayer R, Weinhouse H, Volman G, Amikam D, Benziman M & Gilles-Gonzalez MA. *Biochemistry* (2001) 40:3420-3426 (*38*).

DGC2 Qui Y, Rao F, Luo Z, & Liang ZX. *Biochemistry* (2009) 48:10275-10285 (*42*).

Tuckerman JR, Gonzalez G, Sousa EH, Wan X, Saito JA, Alam M, & Gilles-Gonzalez MA. *Biochemistry* (2009) 48:9764-74.

Tuckerman JR, Gonzalez G, & Gilles-Gonzalez MA. (*Under review*).

Figure 5.11. **Signaling complexes serve to segregate c-di-GMP circuits in bacteria.** Comparison of O_2-controlled c-di-GMP signaling complexes in *G. xylinus* and *E. coli*.

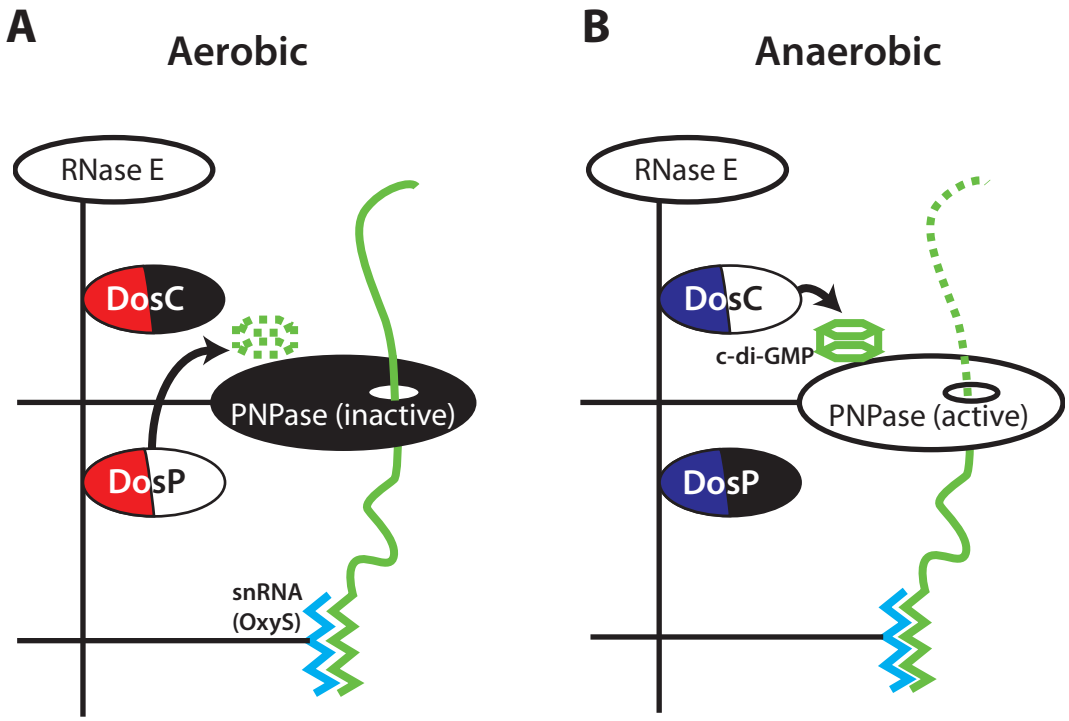

Figure 5.12. **Model for O_2 -regulated RNA processing in *E. coli*.** **(A)** Under aerobic conditions, binding of O_2 to DosC and DosP leads to a net deficit of c-di-GMP due to the enhanced DosP phosphodiesterase activity. The absence of c-di-GMP leaves PNPase in an inactive state. **(B)** Transition to anaerobic conditions leads to dissociation of O_2 from DosC and DosP. Here, a net production of c-di-GMP is observed, which activates PNPase either to degrade or to 3′-tail an existing RNA. The specificity of RNAs recruited to this specialized degradosome is provided by the the presence of small noncoding RNAs, one of which is OxyS. Thus a small subset of *E. coli* RNAs are either degraded or stabilized in an O_2-dependent and c-di-GMP mediated manner.

PART TWO: STUDIES ON O_2-REGULATED TWO-COMPONENT SYSTEMS

CHAPTER SIX

Introduction and Literature Review

(6.1) Two component signaling systems.

Two-component regulators are a large family of signal-transducing protein pairs. In a "classic" two-component regulator, the components are a sensor kinase and its cognate response regulator (*100, 101*). Each component contains a characteristic domain, easily identified from its amino acid sequence: a histidine kinase or "transmitter" domain in the sensor-kinase protein and a "receiver" domain in the response-regulator partner (Figure 1.3). These defining domains impart a similar strategy of phosphoryl transfer. They are combined with other more unique domains to detect and respond correctly to specific environmental signals. A common scenario is as follows. Detection of a signal molecule by an imput domain modulates transfer of a gamma phosphoryl group from ATP through residues in both conserved domains, specifically a conserved

histidine on the kinase domain then a conserved aspartate on the receiver domain. The phosphorylation status of the receiver domain modulates the DNA affinity of a helix-turn-helix region coupled to that receiver. Binding of DNA triggers or suppresses gene expression appropriate to adapt to the environmental signal sensed. Finally, this system is reset by hydrolysis of the phosphoryl group from the response regulator.

(6.2) The FixL-FixJ System in Rhizobia.

In *Sinorhizobium meliloti*, the two-component regulatory system consisting of the FixL and FixJ proteins functions to ensure that that induction of nitrogen fixation (*nif*, *fix*) genes begins only after these symbiotic bacteria in a developing root nodule experience an internal O_2 concentration of ≤ 50 μM (Figures 1.3, 1.4) (*20, 102*). This O_2 level may be sufficiently low for nitrogenase in bacteroids to remain functional, though transiently inactive (*103*). Full nitrogenase activity is manifested in the mature nodule, which contains < 10 nM free O_2 (*104, 105*). In FixL, a sensory heme-binding PAS domain directly preceeds the C-terminal histidine kinase domain (Figures 1.2, 1.3) (*19, 20*). The kinase domain in FixL belongs to the large family of two-component regulatory system histidine kinases (*101, 106*). Deoxy-FixL (unliganded, Fe^{2+}) catalyzes

transfer of a phosphoryl group from ATP to a conserved aspartate residue on FixJ (*19, 107*). Reversible binding of O_2 (K_d ~ 50 μM for *S. meliloti* FixL) to the FixL sensory domain inhibits this reaction (*14, 19, 107*). Phosphorylation of FixJ enables this DNA-binding protein to dimerize and induce the expression of the *nifA* and *fixK* genes, both of which encode transcription factors (*108-110*). In *S. meliloti*, the end result is a cascade of expression of more than 20 *nif* and *fix* genes (Figure 1.3) (*111*).

(6.3) The M. tuberculosis hypoxic response.

Transcriptional regulation in response to environmental stimuli encountered during infection is a common theme in bacterial pathogenesis. Such regulation is often accomplished by sensory kinases and their cognate response regulators that comprise classical two-component signaling systems. One environmental signal of particular importance to pathogenic bacteria is O_2, as the availability of O_2 often changes dramatically from the primary site of infection to the location in the host where the bacteria must persist. Nowhere is this typified more than for *Mycobacterium tuberculosis*, an obligate aerobe. A typical *M. tuberculosis* infection begins with the bacterium gaining entry into the host via the richly aerated lungs, but engulfment by a macrophage and

sequestration into either a phagosome, or ultimately into the context of a granuloma, leads to a much lower level of O_2 than was first available to it (*112-116*).

In *M. tuberculosis*, the response regulator DosR (for dormancy survival regulator; also DevR) governs the genetic response to O_2 limitation (*117-120*). As such, signaling through DevR has been postulated as a major determinant of *M. tuberculosis* survival during the nonreplicating persistent phase of human infection, a period of time that can range from months to the entire lifetime of the infected individual (*119, 121-126*). Nearly 2 billion people worldwide are infected with *M. tuberculosis*, making our understanding of processes involved in survival of the bacterium in the human host of primary importance (*127*).

The *devR* gene (*Rv3133c*) is found together with *devS* (*Rv3132*), a gene encoding a histidine protein kinase, plus a gene of unknown function (*Rv3134c*) in a three-gene operon in *M. tuberculosis* (Figure 6.1). Recent studies suggest that DevR-DevS comprise a prototypical sensor kinase—response regulator two-component system (*123, 124*). In addition, *M. tuberculosis* contains DosT, a kinase 62.5 % identical to DevS over its entire length (Figures 1.2, 6.1) (*125*). Various N-terminal truncations of DosT have been shown to phosphorylate DevR *in vitro*

(*124, 126*). Both DevS and DosT contain tandem N-terminal GAF (for cyclic GMP (cGMP)-regulated cyclic nucleotide phosphodiesterases, adenylate cyclases, and bacterial transcriptional regulator FhlA) domains (Figures 1.2, 6.1). These domains are ubiquitous modules present in a large number of signaling proteins (*37*). Mutational analysis of DevS and DosT suggest that both enzymes are needed to achieve maximal induction of DevR target gene transcription under hypoxic conditions (*124*). Nonetheless, prior to our studies, the mechanism by which DevS and DosT exert their O_2-dependent regulatory activity upon DevR was not known.

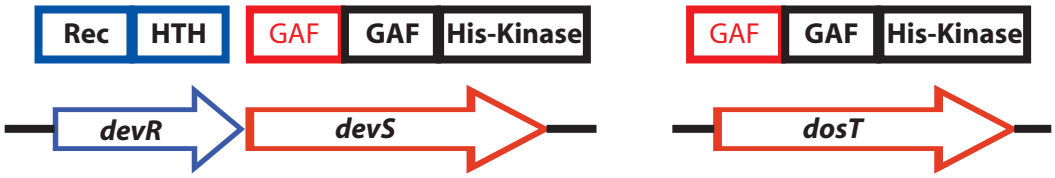

Figure 6.1. **Genetic organization and gene products governing the *M. tuberculosis* hypoxic response.** Hypoxia leads to increased activity of the two component response regulator DosR (DevR) at DevR target promoter elements. The hypoxic activation of DevR is mediated by the combined activities of the sensor kinases DevS and DosT.

CHAPTER SEVEN

A memory effect explains the hysteretic FixL oxygen-dose response

INTRODUCTION

As a sensory kinase, FixL is unusual in having a well-known regulatory ligand, well-established kinetic and equilibrium parameters (k_{on}, k_{off}, and K_d) for ligand binding, and a measurable kinase response to ligand regulation. The K_d values of 140 μM measured for binding of O_2 to *Bradyrhizobium japonicum* FixL and 50 μM for binding to *Sinorhizobium meliloti* FixL are consistent with the O_2 tensions at which these two proteins switch on the genes they control in these organisms (*14*). On the other hand, the noncooperative binding of O_2 to FixL proteins should cause a very gradual decrease in saturation with lowering O_2 tensions, and this has been inconsistent with the reported sharp physiological responses caused by these proteins (Figure 7.1) (*102, 128*). In air, *Bj*FixL would be expected to retain over one-third of its activity if the kinase activity were simply proportional to the deoxy fraction of the protein. The maximum possible allosteric effect would result if a single O_2 molecule would switch off a FixL dimer, such that "oxy-deoxy" as well as "oxy-oxy" dimers would be inactive. However, even if the only active species in any

FixL population were the “deoxy-deoxy” dimers, then *Bj*FixL in air (~ 250 μM O_2) would possess 13 % of its full anaerobic activity. By contrast to these predictions from ligand binding, *in vivo* a very low basal activity is noted for FixL target promoters in air, and a sharp, greater than 30-fold rise in the expression of these genes is observed as the O_2 tensions drop to near the K_d value for binding of O_2 (Figure 7.1) (*102, 128*).

Measurement of an accurate *in vitro* dose response had not been possible for FixL until recently for two main reasons. First, on exposure to O_2, the ferrous FixL (Fe^{2+}) is oxidized rapidly to the ferric (Fe^{3+}) state, and this oxidation accelerates at low saturations with O_2 (*14, 129*). Second, FixL, like other sensory histidine kinases, naturally possesses a rather low enzymatic activity. The purpose of a metabolic kinase, *e.g.*, phosphofructokinase, is maximal turnover of a substrate, whereas that of a signaling kinase such as FixL is to phosphorylate relatively few molecules of a transcription factor at precisely controlled rates. This feature presented a challenge to measuring the activities of inhibited states of the enzyme. We set out to examine of the O_2 dose response of FixL in a well-defined biochemical system *in vitro*. To this end, we developed the methods for protecting FixL from oxidation and for optimizing the enzymatic activity that enabled those measurements. This

study resulted in the formulation of a simple model that explains the FixL dose response based on measurable characteristics of FixL and only one fitted parameter.

MATERIALS AND METHODS

Preparation of deoxy-FixL. Homogeneous deoxy-FixL was prepared by reducing a degassed and concentrated stock of the protein with 10 mM DTT for more than 10 min inside an anaerobic chamber (Coy Laboratory Products, Inc.) while monitoring the 350 – 700 nm absorption with a UV-vis spectrophotometer (Cary 4000, Varian). Subsequent assays of the deoxy state were done in the anaerobic chamber.

Preparation of carbonmonoxy-FixL and measurement of CO affinity. To prepare carbonmonoxy-FixL, the deoxy protein described above was diluted 10-fold with CO-saturated TKE buffer [50 mM Tris-HCl, 50 mM KCl, 5 % (v/v) ethylene glycol, pH 8.0] inside an anaerobic chamber, and the 350 – 700 nm absorption was monitored. For determinations of affinity, the deoxy-FixL in a stoppered cuvette was titrated with 0, 1.2, 2.4,

4.8, 9.5, and 32 μM CO in TKE buffer, at 25 °C inside the anaerobic chamber. The K_d value for binding of CO under phosphorylation assay conditions was determined from saturation changes calculated by multiple linear regression analysis of whole spectra.

Stable 12 % to 64 % O_2 saturation of ferrous FixL. Binding of CO to ferrous FixL protects the heme center from oxidation and has little effect on the FixL kinase activity. Taking advantage of these desirable properties of CO, we prepared our fractionally saturated oxy-FixL in O_2/CO mixtures. Specifically, ferrous FixL was mixed with 24 μM CO in TKE buffer containing 1.0 mM DTT. Oxygen-saturated TKE buffer was added to this mixture to yield final O_2 concentrations of 200, 600, and 940 μM, which corresponded to 12 %, 28 %, and 38 % saturation with O_2, respectively, with the balance consisting principally of carbonmonoxy-FixL. The saturation of FixL with O_2 and CO in these mixtures, verified by multiple linear regression analysis of whole 350 – 700 nm absorption spectra, agreed with the calculations of the K_d (CO) under assay conditions. An example of such an analysis is shown in Figure 7.2. No oxidation was detected for over 45 min. As a validation of our use of O_2/CO mixtures, we compared the activities of 64 % O_2-saturated *Bj*FixL

in air to 64 % O_2-saturated *Bj*FixL prepared in a background of CO. A slightly slower turnover in the O_2/CO mixture compared to air (O_2/N_2) could be entirely attributed, within the experimental error, to the slightly lower activity of carbonmonoxy-*Bj*FixL compared to the deoxy form (see Results).

Stable equilibration of ferrous FixL with 1 atmosphere of O_2. Deoxy-FixL in TKE buffer containing 10 mM DTT was gently and continuously mixed with pure O_2. During the phosphorylations in 1 atm of O_2, a stream of pure O_2 was maintained perpendicularly over the reaction mixture inside a container. From the 350 – 700 nm absorption spectra routinely collected throughout the reaction, oxidation was insignificant for over 30 min.

Assays of phosphorylation. These assays determined the rates of conversion of *Bj*FixJ to phospho- *Bj*FixJ by deoxy-, oxy-, or carbonmonoxy-*Bj*FixL, or mixtures of these species. Before and after every assay, the heme state was verified from the 350 – 700 nm absorption spectra of the reaction mixtures to ensure that it was unchanged. The reactions were at 23 °C and contained 1 μM FixL, 25 μM FixJ, and 1 mM ATP/$MgCl_2$ in "phosphorylation buffer" [unlabeled ATP

from Sigma and γ-(^{32}P)-ATP from Amersham Pharmacia Biotech, of specific activity 0.42 Ci/mmol, in 50 mM Tris-HCl, 50 mM KCl, 5 % (v/v) ethylene glycol, 50 μM $MnCl_2$, pH 8.0]. Under these conditions, where FixL is complexed with FixJ, the FixL is dimeric in unliganded as well as liganded states. Reactions were begun by introducing the ATP and stopped at 1.0, 2.5, 5.0, 10, 20, and 30 min by mixing 10 μL aliquots of the reaction mixtures with one-third volume of "stop buffer" [40 mM EDTA, 4 % (w/v) SDS, 0.5 M Tris-HCl, 0.2 M NaCl, 50 % (v/v) glycerol, and 2 % (v/v) β-mercaptoethanol, pH 6.8]. The products were electrophoresed on 15 % (w/v) polyacrylamide gels (*61*). The levels of phosphorylated protein in the dried gels were quantified with a phosphorimager (Bio-Rad Personal Molecular Imager FX).

RESULTS

(7.1) Controlling the O_2 saturation during activity measurements. We used two approaches to circumvent the oxidation of FixL during exposure to O_2. At or above air saturation, a continuous reservoir of gas was supplied to the reaction, together with a mild reducing agent (10 mM DTT), to prevent changes in the heme-iron saturation and oxidation state

(Figure 7.3). At O_2 tensions below the air saturation, for which the reactions required sealed atmospheres, oxidation was prevented by substituting carbonmonoxy-FixL for deoxy-FixL as the active protein fraction. Although CO does slightly inhibit FixL, the kinase activity of the ferrous FixL in CO solutions is linear with respect to the saturation with CO. The turnover rate (k_{cat}) is 1.1 min^{-1} for the carbonmonoxy fraction (70 % of the activity of the deoxy form) regardless of the varying saturations of the preparations (Figure 7.4A). Our analysis of FixL in O_2/CO mixtures therefore treated the carbonmonoxy-FixL as a slightly less active deoxy species.

(7.2) Verifying a stable O_2 saturation throughout a reaction. The heme-state stability was routinely verified by recording an absorption spectrum at the start of each reaction, “zeroing” the spectrophotometer on this mixture, and collecting difference spectra over the reaction time course (~ 30 min for low-activity states). For example, the absence of anything but noise from the insterts to Figure 7.3 shows that, for FixL exposed to air or pure O_2, no change occurred during at least 30 min in the O_2 concentration, in the O_2 affinity due to reactants or products, or in the oxidation state. Deconvolution of the spectra of *Bj*FixL in the

phosphorylation assay mixtures showed this protein to be 64 % saturated with O_2 while in air and 88 % saturated when in 1 atm of O_2. These are the saturations expected from the published K_d value for binding of *Bj*FixL to O_2 (*14*). Although this current study treated *Bj*FixL, an examination of *Rm*FixL found its affinity for O_2 to be likewise unaffected by the phosphorylation reaction components and products (see Discussion).

To ensure that the proportion of oxy-*Bj*FixL remained constant during the reaction time courses done in mixtures of O_2 and CO, absorption spectra were collected for the assay mixtures at the start and end of the experiments and compared, as above. The proportions of oxy- and carbonmonoxy-protein in the assay mixtures were quantified by multiple linear regression analyses of whole spectra, as shown in the example in Figure 7.2. The CO affinity (K_d = 2.1 μM) of *Bj*FixL under the enzymatic assay conditions was entirely consistent with the proportions of oxy- and carbonmonoxy-protein directly observed in defined concentrations of O_2 and CO (Figure 7.4B).

(7.3) A quantitative measure of FixL regulation. The phosphorylation activities of all FixL species are described here as their turnover rates, or

k_{cat}. To our knowledge, very few sensor kinases have been assayed under conditions that allow their activities to be reported as k_{cat} values.

$$\text{Turnover:} \quad \text{FixJ} + \text{ATP} \xrightarrow{\text{FixL}} \text{P-FixJ} + \text{ADP}$$

The turnover rates (or k_{cat}) for the FixL/FixJ reactions, represent the number of FixJ molecules that one molecule of FixL can convert to phospho-FixJ per minute, while the FixL is saturated with both of its substrates, FixJ and ATP. Such an analysis of reaction kinetics required a large excess of both substrates (25-fold excess of FixJ and 500-fold excess of ATP were supplied), so that the saturation of the enzyme-substrate complex would not change during the part of the reaction time course on which rates were based. All turnover rates were determined at steady state, i.e., when the rate of FixJ phosphorylation matched the rate at which the phospho-FixL intermediate was replenished. For inhibited states of FixL, there can be a lag while the enzyme intermediates are building up. For the most active species, there can be a relatively early deceleration of the reaction rate due to rapid depletion of substrate. Therefore it was essential to collect complete time courses and to base

the rates only on the portion of each time course where product was accumulating at a constant rate.

(7.4) Quantitative enzymatic phosphorylation of FixJ. Under our present assay conditions a k_{cat} of 1.5 min^{-1} was determined for deoxy-*Bj*FixL and a k_{cat} of 1.1 min^{-1} for the carbonmonoxy form (Figure 7.5A). In a previous study of the activities of different *Bj*FixL states, the k_{cat} values were reported as 0.43 min^{-1} (26 h^{-1}) for the deoxy state and 0.10 min^{-1} (8.2 h^{-1}) for the carbonmonoxy state (*130*). The difference was due principally to the use of a *Bj*FixJ substrate in the current work and a *Rm*FixJ substrate in the previous study. An additional improvement was achieved by supplying Mg^{2+} at physiological levels together with the Mn^{2+} used previously. The use of Mg^{2+} alone would not substitute for Mn^{2+}, and interestingly, the ideal combination of divalent cations for the reaction mimicked the reported concentrations of these cations in symbiotic root nodules (*131*). These conditions allowed the reaction to proceed until all the FixJ was phosphorylated (Figure 7.5A, closed circles). To our knowledge, this represented the first instance of the quantitative enzymatic phosphorylation of a response regulator of the two-component class by its cognate kinase. As shown in Figure 7.5A, equilibrium was

reached when the molar ratio of radiolabeled phosphate to FixJ was about 1:2. This resembled the level of phosphorylation achieved by reacting FixJ with acetyl phosphate and indicated that only one monomer is phosphorylated in the resulting FixJ dimers (*132*). The phospho-FixJ formed under these reaction conditions was quite stable, and there were no side reactions, such as the generation of free phosphate (*133*).

(7.5) An inhibition that is robust and disproportionate to the oxygen saturation. Figure 7.6 shows the relative activity of FixL as a function of the O_2 saturation, with 100 % activity being defined as the k_{cat} measured for 100 % deoxy-FixL. The enzymatic data (red circles) did not fit to models that show a relative activity proportional to the fraction of deoxy-protein (gray line), or a relative activity proportional to the fraction of "deoxy-deoxy" dimers (dashed curve). Instead, the data fit a simple hysteretic "memory effect model" (solid black curve); importantly they also agreed with the published *in vivo* O_2 response of *B. japonicum* FixL/FixJ (black squares). We therefore concluded that: (i) a simple *in vitro* system containing only FixL and its FixJ and ATP substrates could recapitulate the highly nonlinear response of FixL-dependent gene expression in living

rhizobia; (ii) of the models considered, a simple memory-effect model best fit the actual O_2 response of FixL (see Discussion).

DISCUSSION

A sharp in vitro oxygen-dose response. The proportion of *Bj*FixL remaining in the deoxy state in air is 36 %, and in pure O_2 is 12 %. If the enzymatic inhibition of *Bj*FixL were to follow its corresponding saturation profile, then in air *Bj*FixL should manifest about one-third of its anaerobic activity, whereas in pure O_2 it should retain about one-tenth of its anaerobic activity (assuming that an oxy-FixL subunit is 100 % inhibited). Such a model clearly fails to explain why the observed turnover rates of *Bj*FixL in air and in 1 atm of O_2 are only 2 % and 0.08 % of the anaerobic activity, respectively (Figure 7.5).

As FixL is dimeric, an alternative model worth considering was one in which the ligation of O_2 to a single subunit sufficed to inactivate a dimer. Even this scenario, where the only active species are “deoxy:deoxy” dimers, would allow about 13 % of the activity to persist in air. Given the observation that FixL is only 2 % active in air, these results would indicate that, in preparations of FixL exposed to O_2, the O_2 inhibits not only the

"oxy:oxy" and "oxy:deoxy" dimers to which it is bound, *but also most of the "deoxy:deoxy" dimers to which it is <u>not</u> bound*. A desire to understand the origin of the *<u>inactive</u> deoxy-FixL* in aerobic solution led us to map the drop that occurs in the enzymatic activity for increasing saturations with O_2.

Memory effect: an elegant strategy for nonlinear regulation by a ligand. When O_2 binds to FixL, the heme-binding domain undergoes a conformational change. This change is subsequently recognized by the kinase, which undergoes some change of its own toward an enzymatically inactive conformation. When O_2 dissociates from FixL, the heme-binding domain returns to its activating (deoxy) conformation, and this is followed by a relaxation of the enzymatic domain back to its active conformation. Importantly, the response of the kinase domain to the oxygenation or deoxygenation of the heme differs from the process of O_2 binding or dissociation. Ligand binding is quite local to the heme-containing domain; it has its own kinetics, distinct from those of the kinase activation or deactivation, and it must be complete for any change to occur in the kinase. Suppose the kinase switches off immediately upon detecting that the FixL heme is in the oxy state, but the kinase relaxes back to its active state relatively slowly after the FixL heme dissociates O_2. It is easy to

imagine activation-energy barriers in the coupling mechanism between the heme-binding domain and the kinase that would cause such a lag in propagating the “deoxygenation” message but not the “oxygenation” message. The following mathematical analysis shows that meeting this simple condition can account for the observed dose response of FixL.

Mathematical analysis of the memory effect. If we assume that there are three FixL species at any intermediate O_2 saturation: (i) A = active deoxy-FixL, (ii) I = inactive deoxy-FixL, and (iii) IO_2 = oxy-FixL. The fractional amounts of each of these species (Y) is equal to their individual amounts divided by the total amount of FixL, such that:

$Y_A = A/[FixL]$; $Y_I = I/[FixL]$; $Y_{IO2} = IO_2/[FixL]$

$Y_A + Y_I + Y_{IO2} = [FixL] = \text{total FixL}$

For hemeproteins that bind O_2 non-cooperatively (Hill coefficient $n = 1$), the fractional saturation with O_2 (Y) is equal to $([O_2]/([O_2] + K_d))$ and can be easily calculated for any O_2 concentration if the $K_d(O_2)$ is known. As such, the fractional *un*saturation is equal to (1 – Y). Let us therefore further define a few additional parameters:

$D = (1 - Y) = Y_I + Y_A$ = fraction of FixL not bound to O_2

K_d = equilibrium dissociation constant for binding of $O_2 = k_{off} / k_{on}$

k_{IA} = rate of conversion from inactive to active

At equilibrium, the concentrations of all species will be constant, therefore:

$d[A]/dt = 0 = k_{IA}[I] - k_{on}[O_2][A] \Rightarrow [A] = (k_{IA}[I] / k_{on}[O_2])$

$d[I]/dt = 0 = -(k_{on}[O_2] + k_{IA})[I] + k_{off}[IO_2] \Rightarrow [IO_2] = ((k_{on}[O_2] + k_{IA})[I] / k_{off})$

$Y_A = [A] / ([I] + [A] + [IO_2])$

$Y_A = (k_{IA}[I] / k_{on}[O_2]) / ([I] + (k_{IA}[I] / k_{on}[O_2]) + ((k_{on}[O_2] + k_{IA})[I] / k_{off}))$

$Y_A = k_{IA} / (k_{on}[O_2] + k_{IA} + (k_{on}[O_2] + k_{IA})(k_{on}[O_2] / k_{off}))$

$Y_A = (1 / (1 + ([O_2] / K_d))((k_{IA} / k_{on}[O_2]) / (1 + (k_{IA} / k_{on}[O_2])))$

Again, for any hemeprotein that binds O_2 noncooperatively, $1/(1 + ([O_2] / K_d))$ is simply the fraction of deoxygenated protein, D.

$Y_A = (D)((k_{IA} / k_{on}[O_2]) / (1 + (k_{IA} / k_{on}[O_2])))$ ***Equation 1***

A relevant property for the current model is the relative population of oxy-state molecules ($[IO_2]$) in the reaction mixtures; this can be

measured directly by deconvoluting the UV-visible spectra of the mixtures into their pure components. Errors in measuring the O_2 *concentrations* were avoided by eliminating the O_2 concentration from Equation 1 and deriving an expression for activity purely as a function of the O_2 *saturation*, which could be precisely measured. If we substitute (k_{off} (1 – Y) / Y) for $k_{on}[O_2]$ in Equation 1, we obtain:

$$Y_A = D\ (k_{IA} Y / (k_{off}\ D + k_{IA}\ Y)) \qquad \textbf{\textit{Equation 2}}$$

This is the equation that is fit to the data in Figure 7.6B (solid black curve). One possible way to get an intuitive sense for the memory effect model is to recast this model in terms of the fraction of an average molecule's time that is spent in each of the available states. Although every *individual* FixL cycles through all of the available states (oxy, inactive-deoxy, and then active-deoxy) every few seconds, the total number of molecules in each state within a *population* will remain constant as long as the O_2 concentration is stable. The average time for the recovery of activity after O_2 dissociates, T_{rec} (a kinase property, independent of the heme), is the reciprocal of the reactivation rate, i.e., (1 / k_{IA}). Similarly, (1 / $k_{on}[O_2]$) gives T_{deoxy} (a heme property, independent of the kinase), the average lifetime

of a deoxy state (either inactive-deoxy or active-deoxy) before rebinding O_2 at a particular concentration. Therefore, an alternative form of Equation 1 in terms of state lifetimes rather than rates is:

$$Y_A = D ((T_{deoxy} / T_{rec}) / (1 + (T_{deoxy} / T_{rec}))) \qquad \textbf{\textit{Equation 1a}}$$

The recovery time (T_{rec}) is a property of the kinase and is *independent* of the O_2 saturation, whereas the T_{deoxy} will shorten as the O_2 concentration increases. Therefore the T_{deoxy} / T_{rec} ratio depends on both the saturation and binding characteristics of a particular ligand.

Carbon monoxide binds slowly to *Bj*FixL (k_{on} = 0.005 $\mu M^{-1}s^{-1}$), which becomes half-saturated in 2 μM CO (Figure 7.4). When the heme is half-saturated, the lifetime of a deoxy state equals the lifetime of a carbonmonoxy state. For CO, this lifetime is 100 s (i.e., 1 / (0.005 $\mu M^{-1}s^{-1}$ x 2 μM)). This is about 50-fold longer than the estimated T_{rec} of 1.9 sec. Therefore there should essentially be no deoxy molecules in the process of recovery. If, for a wide range of ligand saturations, T_{rec} is short compared to the lifetime of a deoxy state ($T_{rec} << T_{deoxy}$), then $Y_A \sim D$ in Equation 1a, and the activity simply becomes proportional to the protein fraction in the deoxy state. This is why the modest inhibition caused by

CO binding is linear with respect to the CO saturation and shows no sign of a memory effect (Figure 7.4A).

Oxygen binds to *Bj*FixL at a rate of 0.14 $\mu M^{-1}s^{-1}$, and the protein becomes half-saturated in 140 μM O_2 (*14*). Therefore, at half-saturation, the T_{deoxy} is only 0.051 s (i.e., 1 / (0.14 $\mu M^{-1}s^{-1}$ x 140 μM)) and about 37 times *shorter* than T_{rec}. Therefore very few deoxy-FixL molecules manage to regain activity before rebinding O_2. Since $T_{deoxy} < T_{rec}$ for most O_2 saturations, very little of the time that a FixL molecule spends in the deoxy state will be spent as a productive kinase if even a small amount of O_2 is present. In air, out of any 100 *Bj*FixL, 64 will be oxy. Of the remaining 36 deoxy, 34 will be recovering and only 2 will be active, resulting in only 2 % of the maximum activity. Equation 1 predicts a rapid drop in Y_A with a rise in the O_2 concentration, and this matches the observed FixL dose response *in vitro* and *in vivo* (Figure 7.6). Note that when FixL is returned to anaerobic conditions, all the deoxy-FixL molecules will relax back to the active state within seconds, and 100 % activity will be restored.

Biochemical implications of the memory effect. During the mid-1960s, Brian R. Rabin proposed that slow conformational transitions occurring during enzyme reactions might cause apparent cooperative behavior,

even in a monomer (*134*). Soon thereafter, Carl Frieden called this behavior an “enzyme hysteresis” and defined it as a slow response of the enzyme activity to fast changes in ligand concentration (*135*). Many important metabolic enzymes fit the category of hysteretic enzymes, with the conversion times from one kinetic form to another ranging from seconds to minutes (*136*). Variations in enzyme hysteresis deriving from an assortment of changes result in many fascinating behaviors (*135, 136*). The slow response might be a conformational change induced by a substrate, product, or noncompetitive inhibitor; it might be an isomerization; it might be the displacement of a tightly bound ligand by another that differently affects the activity; or it might be a change in the kinetics of substrate binding and the affinity for substrate. The memory-effect model predicts that FixL would remain inactive several seconds after a large instantaneous drop in the O_2 concentration, and therefore FixL represents a special case of a hysteretic enzyme. The general equations governing hysteresis are quite complex. For FixL, however, it is straightforward to measure relevant equilibrium and kinetic parameters and to show that many of the considerations that can greatly complicate hysteretic models do not apply. For example, the single-exponential binding of O_2 to full-length *Bj*FixL and a *Bj*FixL$_H$ truncation lacking the

enzymatic domain justify the assumption that $k_{on}(O_2)$ is the same for both active and inactive deoxy. The deoxy and oxy forms of FixL bind ATP and FixJ equally well (*137*). Indeed, FixL may be the most comprehensible and accessible hysteretic enzyme for systematic study. To our knowledge, FixL provides the first example of a hysteretic sensory enzyme.

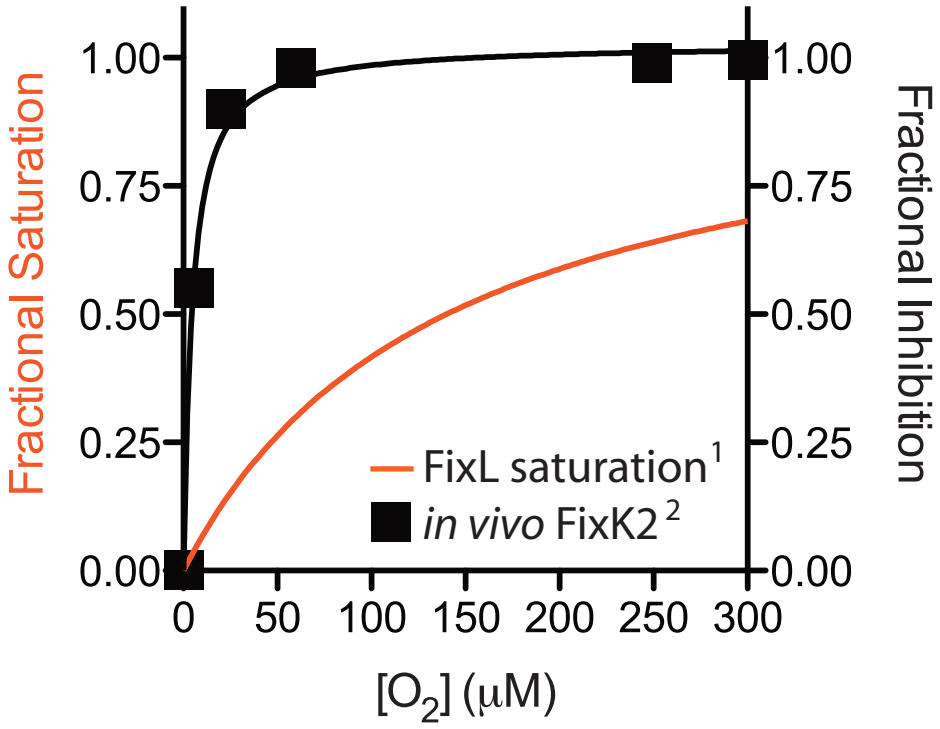

[1] Gilles-Gonzalez MA *et al.*, *Biochemistry* (1994) 33: 8067-8073 (*14*).
[2] Sciotti MA *et al.*, *J Bacteriol.* (2003) 185: 5639-5642 (*128*).

Figure 7.1. **Discrepancy between FixL O_2 saturation and hypoxic regulation of FixLJ target genes.** Data shown are for the *in vivo* repression of FixLJ target genes with exposure of *Bradyrhizobium japonicum* to increasing O_2 levels. These data are compared to the *in vitro* O_2 saturation profile of *Bj*FixL.

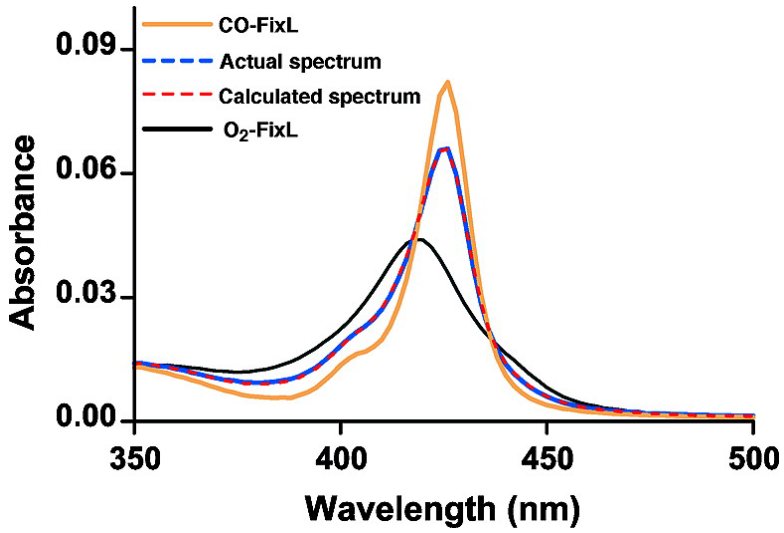

Figure 7.2. **Determination of FixL saturation with O_2 in defined mixtures of O_2 and CO at pH 8.0 and 25 °C.** Example of the analysis of oxy- and carbonmonoxy-*Bj*FixL mixtures that result from adding O_2 and CO to ferrous *Bj*FixL. Here, a mixture of 1.2 mM O_2 and 21 μM CO results in 58 % carbonmonoxy-*Bj*FixL and 42 % oxy-*Bj*FixL (true spectrum, blue), as determined from a linear combination of the absorption spectra (calculated spectrum, red) of pure carbonmonoxy-FixL (orange) and pure oxy-FixL (black).

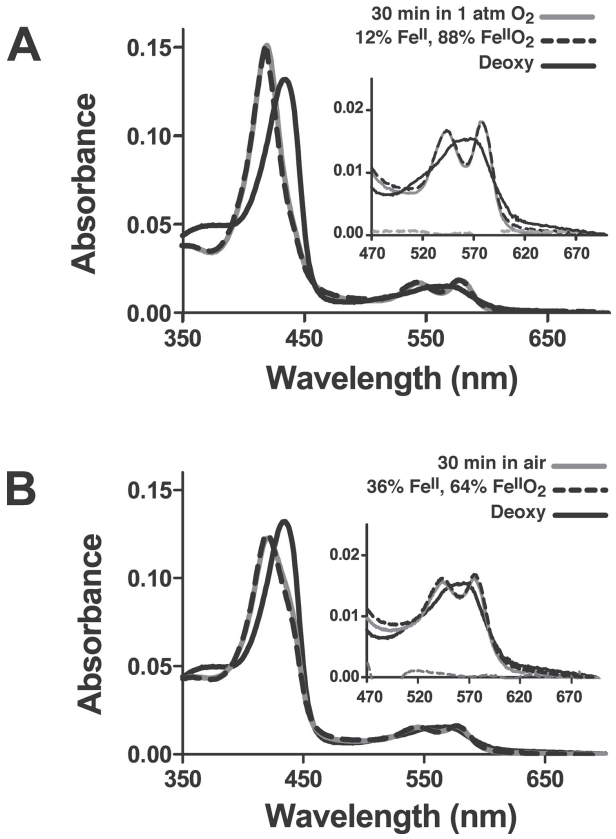

Figure 7.3. **Stable saturation of FixL with O_2 in air or pure O_2 under reaction conditions.** Panel A shows the absorption spectra of 1.2 μM *Bj*FixL before (solid black curve) and 30 min after (solid gray curve) mixing the deoxy form with an O_2 -saturated buffer having all the reaction components at pH 8.0 and 25°C; a synthetic spectrum of 12 % deoxy- and 88 % oxy-FixL is also shown (dashed black curve). Panel B shows the absorption spectra of 1.2 μM *Bj*FixL before (solid black curve) and after (solid gray curve) mixing the deoxy form with an air-saturated buffer containing the same reaction components; a synthetic spectrum of 36 % deoxy- and 64 % oxy-FixL is also shown (dashed black curve). The insets show a 6-fold expansion of the 470-700 nm region and the difference obtained on subtracting spectra of O_2 -exposed *Bj*FixL recorded at a 30 min interval (dashed gray curve). The reaction mixtures were in phosphorylation buffer (see Materials and Methods, Chapter 7) in vessels open to a continuous reservoir of O_2 in panel A, or air in panel B.

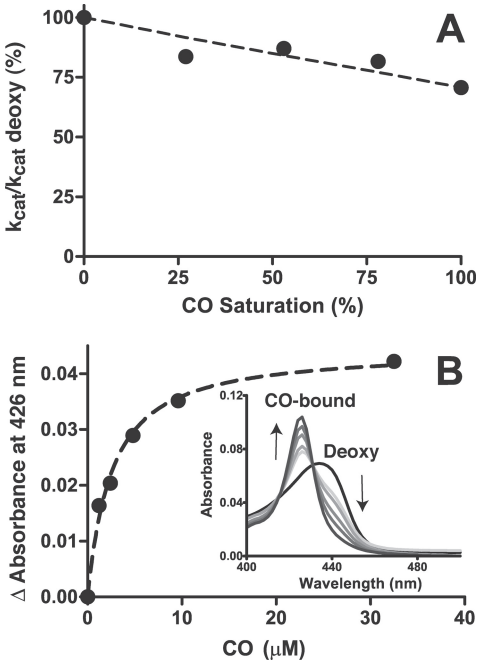

***Figure 7.4*. Binding of CO to FixL under assay conditions and influence of CO on kinase activity.** Panel A shows the turnover of *Bj*FixJ (25 μM) to phospho-*Bj*FixJ by 0 %, 27 %, 53 %, 78 %, and 100 % CO-saturated *Bj*FixL (1 μM) at pH 8.0 and 23°C. Initial rates were obtained by fitting to single exponential phosphorylation curves having 0, 1.0, 2.5, 5.0, 10, 20, and 30 min time points. The reported [(k_{cat}) / (k_{cat} deoxy)] percent (or relative turnover percent) represents these initial rates of turnover divided by the value measured for the deoxy form. Note the linear trend and relatively poor inhibition by CO, with 70% activity remaining for the fully saturated protein. Panel B shows the titration of *Bj*FixL (0.5 μM) with 0, 1.2, 2.4, 4.8, 9.5, and 32 μM CO at pH 8.0 and 25 C. The dashed line shows a fit to a quadratic single binding site equation; the inset shows the 400 - 500 nm absorbance changes on coversion of the deoxy form to the carbonmonoxy form.

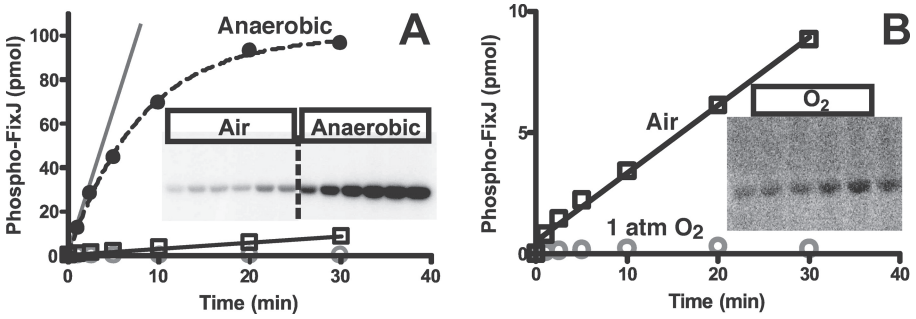

Figure 7.5. **Comparison of the activities of FixL under nitrogen, air, and oxygen at pH 8.0 and 23°C.** Reactions of 1 μM *Bj*FixL with 25 μM *Bj*FixJ and 1-mM gamma-[^{32}P]-ATP were carried out at 23°C in a chamber with an atmosphere of pure nitrogen (panel A, closed circles), in air (panels A and B, squares), or in a container supplied with a continuously flowing atmosphere of pure O_2 (panels A and B open circles, and labeled O_2 in panel B). The anaerobic activity was calculated by fitting the whole curve to a first-order kinetics equation and taking the initial rate to be the initial linear phase of the reaction (panel A, gray line). For a closer inspection of the results in air and pure O_2, a 10-fold expansion of the ordinate is provided together with the autoradiograph of a time course under O_2 (panel B). Note that the reactions contained 200 pmol of *Bj*FixJ, one-half of which was phosphorylated at equilibrium (panel A, closed circles). The higher background in the gel of reactions done under pure oxygen (panel B) results from the requirement of a longer exposure to show the linear phase of the reaction for the ~ 1000-fold less active protein.

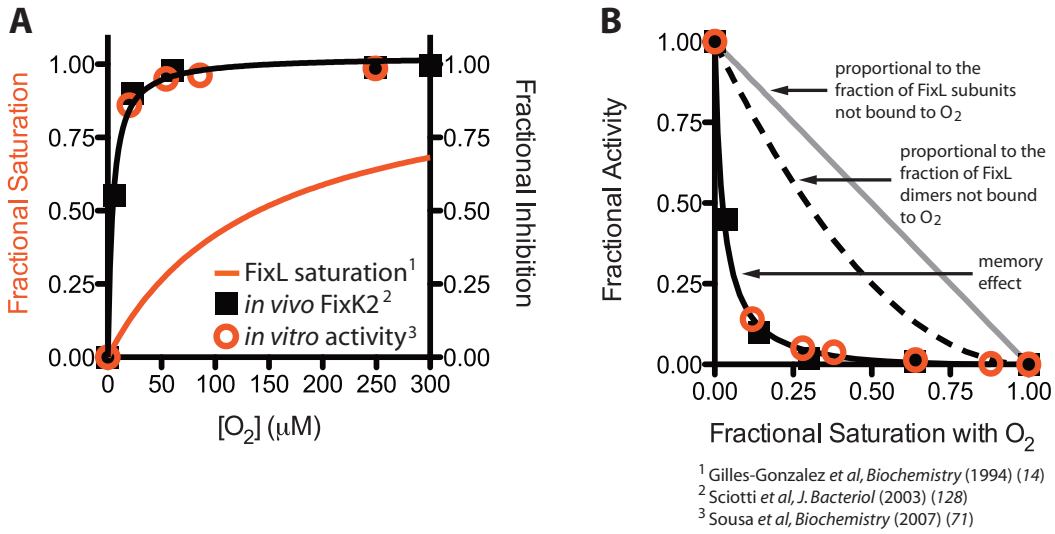

Figure 7.6. **Correspondence of the FixL O_2 regulation *in vitro* to FixLJ target gene expression *in vivo*.** The relative turnovers of *Bj*FixJ at *Bj*FixL saturations of 0 %, 12 %, 28 %, 38 %, 64 %, and 88 % with O_2 are shown as open red circles in panels A and B. These data recapitulate the induction of FixLJ target gene expression seen in *Bradyrhizobium japonicum* with decreasing O_2 (black squares). The FixL O_2 dose response is highly nonlinear and fits a "memory effect" model with $k_{IA} \sim 0.53\ s^{-1}$ ($T_{rec} \sim 1.9$ s) (panel B, solid black curve; see Equations 1 and 1a). This contrasts to the fits expected if the FixL activity were proportional to the fraction of FixL subunits not bound to O_2 (panel B, gray line), or if the activity were proportional to the fraction of FixL dimers not bound to O_2 (panel B, dashed line).

CHAPTER EIGHT

DosT and DevS are oxygen-switched kinases in *M. tuberculosis*

INTRODUCTION

Bioinformatics studies suggest that many symbiotic and pathogenic bacterial species possess heme-based sensors. It is logical that this should be so, since the availability of O_2 often drops dramatically as the bacteria move from the primary site of attachment on the host to the location inside it where they can best persist. For example, in the obligate aerobe *Mycobacterium tuberculosis*, infection begins with entry into the host via the richly aerated lungs; a macrophage then engulfs this bacterium and confines it into a phagosome, or ultimately a granuloma (*112-114*). While information on the O_2 concentration in tuberculous human lesions is limited, measurements of O_2 levels in granulomas from other mammals have shown them to be hypoxic, and there is clear evidence that O_2 is depleted from blocked human cavities to a sufficient degree that conditions corresponding to those seen in the Wayne *in vitro* model of *M. tuberculosis* non-replicative persistence are attained (*112, 115, 117, 138*). The transcription factor DevR governs nearly all genetic

responses of *M. tuberculosis* to O_2 limitation (*119, 121-126, 139-149*). About two billion people worldwide are infected with *M. tuberculosis*, and this reservoir is a major challenge in eradicating the disease (*127*). It is therefore urgently important to understand processes that are thought to assist the survival of *M. tuberculosis* in its human host. Among these are the adaptive responses of this pathogen to hypoxia (*112, 117*).

Rhizobia also experience a large drop in the O_2 concentration as they move from their initial site of attachment on a root hair to the site of chronic persistence in a newly-formed symbiotic root nodule (*150-152*). In these bacteria, *in vitro* O_2 limitation initiates gene-expression cascades similar to those induced during symbiosis (*150-152*). This leads to the expression of nitrogen-fixation genes as well as genes essential for surviving O_2 deprivation, such as those encoding alternative terminal oxidases for respiration in low O_2 (*150-152*).

The biochemical mechanisms of hypoxic induction are well described for *Sinorhizobium meliloti* and *Bradyrhizobium japonicum*. In both cases, a classical prokaryotic two-component regulatory system made up of the FixL and FixJ proteins governs a direct response to O_2 (*111, 128*). In FixL, a protein-histidine kinase activity is coupled to a neighboring heme-binding domain such that O_2 switches off the kinase,

and hypoxia switches it on (*15, 19*). Under hypoxic conditions, FixL catalyzes the transfer of a γ-phosphoryl group from ATP to FixJ, a response-regulating transcription factor that functions as FixL's regulatory partner (*107, 130, 153*). The phosphorylation of FixJ causes it to dimerize and bind to target sites in DNA (*132*).

For *M. tuberculosis*, the importance of the DevR transcription factor was initially appreciated from genetic experiments, which suggested that DevR is essential for survival of the pathogen during hypoxia *in vitro* (*119, 122-124, 140-143, 145, 146, 149, 154*). Two closely related protein-histidine kinases, DosT and DevS (62.5% sequence identity) were thought to activate DevR, and the DevS protein was found to contain heme (*123, 124, 126, 155, 156*). The domain organization of DevS is reminiscent of that in FixL, with one notable difference being that FixL binds its heme within a PAS rather than a GAF domain (Figure 1.2) (*78*). Until our work, only versions of DosT and DevS lacking heme, either because of deletion of their N-terminal region or treatment with denaturants, had been shown to phosphorylate DevR *in vitro* (*123, 124, 126*). We asked whether the DosT protein contains heme, and if so, if the heme-GAF domains in DosT or DevS direct a response to gaseous ligands. To answer these

questions, we isolated full-length DosT and DevS, each with its full complement of heme, and examined switching in these sensors.

MATERIALS AND METHODS

***Genetic Manipulations*.** The full-length *dosT* and *devS* genes, formerly called *Rv2027c* and *Rv3132c*, respectively, were amplified by PCR with *M. tuberculosis H37Rv* genomic DNA as the template. The oligonucleotide primers for the amplifications were designed to add a *NdeI* site before the 5' end and an *HindIII* site after the 3' end of each gene. Fragments encoding the first GAF domain of each protein and consisting of codons 1-208 for *dosT* and 1-210 for *devS* were similarly amplified. Template DNA was a gift from Dr. David Russell (Veterinary Medical Center, Cornell University), and primers were based on the *M. tuberculosis H37Rv* genome database (*157*). The amplified products were inserted as *NdeI-HindIII* fragments into a pUC19-derived *E. coli* vector. The resulting expression vectors conferred ampicillin resistance and maintained the relevant genes (full-length *dosT*, $dosT_{1\text{-}208}$, full-length *devS*, or $devS_{1\text{-}210}$) under *tac*-promoter regulation.

Gene expression and protein purification. The *M. tuberculosis dosT* and *devS* genes, as well as the $dosT_H$ and $devS_H$ truncations, were overexpressed in *E.* coli strain MC1061 in a 4-L Bioflow 3000 fermentor at 37 °C, 200-500 rpm, and 20 % of atmospheric O_2. The specific details of this fermentor are described above for the overexpression of the *dosCP* operon. When the culture reached an A_{600} ~ 0.5, expression of the recombinant protein was induced with 1 mM IPTG. The cells were harvested 12-24 h post-induction by centrifugation in a continuous flow centrifuge.

The full-length DosT and DevS proteins were purified as follows: harvested cells were lysed by sonication, and the lysate was cleared by centrifugation at 70,000 rpm (Ti 70 rotor, Beckman). The corresponding cleared lysate was equilibrated with 30 % saturation with ammonium sulfate, centrifuged at 12,000 rpm, 10 min, 4 °C, and the red precipitate was recovered. This pellet was redissolved in 10 % saturated ammonium sulfate and desalted on a size-exclusion column (Sephadex G-25) pre-equilibrated with 50 mM Tris-HCl, 50 mM NaCl, 5 % (v/v) glycerol, and 10 mM β-mercaptoethanol (pH 7.5). The desalted sample was applied to an anion-exchange column (15 mL, DEAE-Sephacel, Amersham Pharmacia) pre-equilibrated in 50 mM Tris-HCl, 100 mM NaCl, 5 % (v/v) glycerol, and

10 mM β-mercaptoethanol (pH 7.5). The column was washed extensively with the above buffer and eluted with buffer containing 200 mM NaCl. Eluted fractions were concentrated and further purified by gel filtration (Superdex S-200, GE Healthcare). Protein purity and concentration was determined from their spectra, from Bradford protein assays (Bio-Rad), and from Coomassie-stained SDS-PAGE gels (*61*). The heme content of purified proteins was quantified by a pyridine hemochromagen assay, with hemin as the standard (*62*). Purified proteins were stored at –80 °C.

The $DosT_H$ and $DevS_H$ truncations were purified by the same series of fractionation steps, with the following variations: A 30-60 % cut of saturated ammonium sulfate was initially used to recover the hemeprotein from the cleared *E. coli* lysate, and the anion-exchange fractionation used loading and elution buffers containing 75 mM NaCl and 150 mM NaCl, respectively, in 50 mM Tris-HCl, 5 % (v/v) glycerol, and 10 mM β-mercaptoethanol (pH 7.5).

Absorption spectra. All spectra were measured on a Cary 4000 UV-Visible Spectrophotometer (Varian) for proteins in 50 mM Tris-HCl, 50 mM KCl and 5 % (v/v) ethylene glycol at pH 8.0 and 23 ^{o}C, unless otherwise stated. Deoxy-DosT or DevS was prepared inside an anaerobic chamber

(Coy Laboratory Products, Inc.) by adding dithionite and immediately removing this reducing agent with a desalting column (Sephadex G25). Oxy-DosT or DevS was prepared by mixing the deoxy proteins with O_2- or air-saturated buffer. Carbonmonoxy-DosT or DevS was prepared by mixing the proteins with CO-saturated buffer.

Heme ligand binding assays. All measurements of kinetics used 2-5 μM of DosT in 50 mM Tris-HCl, 50 mM KCl, 5% (v/v) ethylene glycol at pH 8.0 and 25 ^{o}C. Ligands were prepared in the same buffer. The measurements were done with a LKS-60 Stopped-flow/flash photolysis spectrometer fitted with a Pi-star stopped-flow drive unit (Applied Photophysics Ltd, Leatherhead, UK). For sample excitation, the LKS.60 spectrometer was coupled to a Quantel Brilliant B Nd:YAG laser with second-harmonic generation. Data acquisition was provided by an Agilent 54830B digital oscilloscope for fast measurements or a 12-bit ADC card within the instrument workstation for slow measurements. To determine the rates of O_2 or CO association, a quartz cuvette was filled in an anaerobic chamber with deoxy-DosT or DevS, and an aliquot of a saturated O_2 or CO solution was added to bring the sample to the desired final concentration of ligand (60 – 1024 μM for O_2, and 30-480 μM for CO).

The cuvette was immediately stoppered and brought to the LKS-60 for measurement. Rebinding of ligand after flash photolysis was followed from the change in the absorbance at 435 nm for O_2 at 420 nm for CO. At least five kinetic traces were averaged at each ligand concentration. All the association kinetics fit a single exponential process, i.e. each with one k_{obs} value. The reported association rate constants were determined from the slope of k_{obs} (s^{-1}) versus ligand concentration (μM), determined by linear regression ($R^2 \geq 0.99$). The entire determinations of the O_2 and CO on-rate constants were repeated at least three times, with several different protein samples.

Rates of CO dissociation from carbonmonoxy-DosT or DevS were followed at 423 nm after mixing a solution of ferrous protein equilibrated with a low CO concentration with a solution supplying a large excess of O_2 in a stopped-flow apparatus. For carbonmonoxy-DosT, equilibration was with 20 μM CO, and 256 – 1280 μM O_2 were added. For DevS, equilibration was with 0.5 μM CO, and 640 μM O_2 was added.

The rate of O_2 dissociation from oxy-DevS was followed at 423 nm after mixing a solution of ferrous DevS equilibrated with 40 μM O_2 with a solution supplying a large excess of sodium dithionite (1.25 mM), in a stopped-flow apparatus.

The equilibrium dissociation constant for binding of O_2 was directly measured by mixing deoxy-DosT or DevS with buffer [50 mM Tris-HCl, 50 mM KCl, 5% (v/v) glycerol, pH 8.0] containing 0.80 – 1200 μM O_2. The basis spectra for the deoxy and oxy states were used to determine the saturation at varying O_2 concentrations by multiple linear combination of whole spectra. A plot of the saturation versus ligand concentration was fitted ($R^2 > 0.99$) to a non-linear Hill Plot equation using GraphPad Prism software version 4.03. The equilibrium dissociation constant for binding of CO to deoxy-DosT was similarly determined by directly titrating the protein with buffer [50 mM Tris-HCl, 50 mM KCl, 5% (v/v) glycerol, pH 8.0] containing 0.30 – 940 μM CO. To estimate the equilibrium dissociation constant for binding of NO, ferrous DosT or DevS was equilibrated with CO and competitively titrated with NO. For DosT, equilibration was in 240 μM CO [in 50 mM Tris-HCl, 50 mM KCl, 5% (v/v) glycerol, pH 8.0] and the competitive titration was with 0.5 to 9.0 μM NO. For DevS, equilibration was in 10 μM CO in the same buffer, and the competitive titration was with 0.50 to 28 μM NO.

DevS and DosT autophosphorylation assays. Deoxy-DosT was prepared inside an anaerobic chamber by incubating the purified protein

for more than 15 min with 10 mM DTT. Oxy-DosT was prepared by adding pure O_2 to the deoxy protein and maintaining a continuous atmosphere of pure O_2 during the phosphorylation reaction. Carbonmonoxy-DosT was prepared by adding CO-saturated buffer to a final concentration of 100 μM CO in the reaction mixture. Nitrosyl-DosT was prepared by adding NO-saturated buffer to a final NO concentration of 40 μM NO. Deoxy-DevS was prepared by reducing this protein with dithionite inside an anaerobic chamber and promptly removing this reducing agent with a gel-filtration column (Sephadex-G25). Conversion to the oxy-, carbonmonoxy or nitrosyl forms was as described for DosT. Ferric DevS was prepared by exposing the protein to an equimolar level of ferricyanide and removing this oxidizing agent with a bio-spin column (Bio-Rad). Cyanomet-DevS was made by adding 20 mM KCN to ferric DevS.

All DosT and DevS species were verified before and after each reaction from the absorption spectra. Assays were done with 4-5 μM DosT or DevS and 0.5-1.0 mM ATP/$MgCl_2$ [unlabeled ATP from Sigma and γ-^{32}P-ATP from Amersham Pharmacia Biotech, specific activity 0.21 Ci/mmol, in 50 mM Tris-HCl, 50 mM KCl, 5.0 % (v/v) ethylene glycol, pH 8.0], unless otherwise specified. Reactions were begun by introducing the ATP; they were stopped at timed intervals (0.5, 1.0, 2.0, 4.0, 8.0, 10 and

14 min for DosT; 0.5, 1.0, 1.5, 3.0, 6.0, 12, 24, and 48 min for DevS) by mixing 10-μL aliquots of the reaction mixtures with one-third volume of "stop buffer" [40 mM EDTA, 2 % (w/v) sodium dodecyl sulfate, 0.40 M Tris-HCl, 50% (v/v) glycerol, and 2% (v/v) ß-mercaptoethanol, pH 6.8]. The products were electrophoresed on 11% (w/v) polyacrylamide gels (*61*). To verify the stability of the phosphorylations, aliquots of the stopped reaction mixture (1 μL) were fractionated on polyethyleneimine-cellulose thin-layer chromatographic (TLC) plates developed with 0.75 M NaH_2PO_4, pH 3.5. Levels of phosphorylated protein in the dried gels and of low-molecular weight species on the TLC plates were quantified with a phosphorimager (Bio-Rad Personal Molecular Imager FX).

RESULTS

(8.1) Isolation of holo-DosT. Expression of the *dosT* gene in modest levels in *E. coli*, and purification of the corresponding protein by relatively gentle methods, showed that the full-length protein is soluble in its native form. A distinctive red color was evident in the harvested cell pellet and became more intense in the cleared lysated and with every subsequent purification step. The purified DosT protein was recovered in the oxy-state with a UV/Soret absorption ratio (A_{280nm}/A_{415nm}) of 0.6 (Figure 8.1A). The

extent of heme contained in the purified DosT was determined using pyridine hemochromogen assays according to the procedure of Appleby (Materials and Methods, Section 2.3) (*62*). Using this analysis, we determined that our isolated DosT contained 1.1 b-type heme per DosT monomer. For DevS, heme binding was reported for a truncated form of the protein consisting of only the N-terminal GAF domain (*156*). To determine if heme is similarly situated in DosT, we prepared a similar truncation of DosT ($DosT_{1-208}$). As isolated, $DosT_{1-208}$ contains characteristic hemeprotein absorptions spectra (Figure 8.1A inset). Pyridine hemochromogen assays showed that this truncation binds 1 heme per monomer of $DosT_{1-208}$. We therefore conclude that DosT is a heme-containing kinase, where heme binding is confined to the DosT N-terminal GAF domain.

The absorption maxima for ferrous DosT in the deoxy state, or bound to O_2, CO, or NO, resembled those of FixL (Table 8.1). The spectra of deoxy-DosT indicated a pentacoordinate high-spin heme iron (Figure 8.1A, Table 8.1). Previously, a $DosT_{380-573}$ fragment consisting of only the C-terminal kinase region was purified as a solubilized protein initially obtained from inclusion bodies (*126*). This protein showed no sign of heme binding because it lacked the first GAF domain. A full-length S-

tagged DosT had also been reported (*124*). In that case, the solubilization of the protein from inclusion bodies by detergents and high pH had removed the heme, yielding the apoprotein (*124*). Our discovery of heme in DosT is consistent with this protein's suspected involvement in the hypoxic response of *M. tuberculosis* and with the strong resemblance of DosT to DevS (Figures 1.2, 6.1) (*124, 126, 156*).

(8.2) Isolation of holo-DevS. A modest overexpression of the *devS* gene in *E. coli* also yielded—for the first time—the soluble full-length holo-enzyme (Figure 8.1B). DevS was recovered using non-denaturing conditions from soluble cell extracts, even though this protein was predicted to contain transmembrane regions (*123*). The heme content of the full-length DevS was 1.0 heme per subunit, in agreement with previous reports of heme binding by the DevS N-terminal GAF domain (*155, 156*). Absorption spectra of ferrous DevS were similar to those of DosT and FixL (Figure 8.1B, Table 8.1).

(8.3) Inertness of DosT to Oxidation. An unusual characteristic of DosT was the extraordinary stability of the ferrous state to O_2 exposure. The DosT oxidation rate in air at 37 ^{o}C was too slow to measure (Figure 8.2).

Based on multiple-linear-regression analysis of whole spectra, less than 6% oxidation to the met form (Fe^{3+}) was detectable after 16 hours of monitoring. We estimated that the half-life of ferrous DosT in air exceeds 60 hours. For comparison, the half life of ferrous sperm-whale myoglobin in air is about 11 hours, and that of ferrous FixL is only 15 minutes (*87, 129*). Addition of electron shuttlers such as methyl viologen (5 μM) accelerated the reaction to about 17% oxidation after 16 hours in air (Figure 8.2). DosT was relatively stable toward oxidizing reagents, such as ferricyanide, that are routinely used in stoichiometic amounts with heme proteins to generate the ferric forms instantaneously. Reaction with even a four-fold excess of ferricyanide took several minutes. The strong resistance of DosT to oxidation rules out any possibility that this protein could serve as a sensor of redox potential. This inertness likely indicates a built-in protection for DosT against the highly oxidative and nitrosative environments encountered by *M. tuberculosis* in macrophage phagosomes (*113, 114*). Compared to DosT, the oxidation rate of DevS was at least 10-fold faster ($t_{1/2} \sim 4$ h at 37 ^{o}C) (Table 8.2). Understanding the basis of the DosT heme stability toward oxidation will likely be of great value, as one of the problems that currenty complicates the development

of heme-based blood substitutes involves overcoming the tendency of these molecules to oxidize prematurely.

(8.4) DosT and DevS ligand binding. From direct titrations of the sensors with ligands, we found O_2 to bind without cooperativity (Hill coefficient n = 1.0) and with an equilibrium dissociation constant (K_d) of 26 μM for DosT and 3 μM for DevS (Figure 8.3; Table 8.2). Oxygen affinities in this range are common in heme-based sensors, and likely reflect the O_2 concentrations at which hypoxic adaptation becomes necessary for the host organisms (*15*). The association-rate constant for binding of O_2 to DosT was 0.79 $\mu M^{-1}s^{-1}$, about 5-fold higher than for *Bj*FixL, but around 20-fold lower than for sperm-whale myoglobin (Figure 8.3C, Table 8.2). For DevS, the O_2 on-rate constant (k_{on} = 8.8 $\mu M^{-1}s^{-1}$) resembled that of sperm-whale myoglobin and was 11-fold higher than for DosT (Figure 8.3D, Table 8.2). By contrast to the association rate constants, the values for the O_2 off-rate constants were similar for the two *M. tuberculosis* sensors (DosT $k_{off} \sim 20\ s^{-1}$, and DevS $k_{off} \sim 12\ s^{-1}$) (Table 8.2).

Carbon monoxide also bound to DosT without cooperativity (Hill coefficient n = 1.0); the K_d value measured by titration with CO was 0.94 μM (Figure 8.4A, Table 8.2). For DevS, the CO affinity was too high to be

measured by direct titration. Instead, the K_d value for CO binding was estimated at 36 nM, as determined from the on- and off-rate constants (Table 8.2). Whereas DevS was myoglobin-like in its rate of association with CO (k_{on} = 1.8 $\mu M^{-1}s^{-1}$), for DosT the CO on-rate constant was about 40-fold lower (k_{on} = 0.05 $\mu M^{-1}s^{-1}$) (Table 8.2). The directly measured CO off-rate constant for both DosT and DevS was 0.06 s^{-1}, a value typical for many CO-binding hemeproteins (Table 8.2).

The K_d values for binding of NO were found to be about 5 nM for DosT and 10 nM for DevS, as determined by competition against CO (Figures 8.4B,C). These values are one- to four-thousand-fold lower than for sperm-whale myoglobin (Table 8.2) (*158*). As NO affinities have been reported for very few heme proteins, it is currently unknown how the K_d(NO) values measured here for DosT and DevS compare with “typical” heme proteins.

(8.5) Oxygen-switched kinase activity in DosT and DevS. We investigated whether ligands such as O_2, CO, and NO could regulate the DosT or DevS autophosphorylation with ATP. The autophosphorylation reactions in Figure 8.5 show for the first time that the *M. tuberculosis* DosT and DevS proteins are heme-based sensors, whose kinase activity is

switched off by O_2. The K_m values for the autophosphorylation reactions of deoxy-DosT and deoxy-DevS with respect to ATP for were 39 μM and 73 μM, respectively; a range similar to the K_M(ATP) measured for the FixLs. Deoxy-DosT reacted with 500 μM ATP/Mg^{2+} at an initial rate of 3.0% min^{-1} (Figure 8.5A). This was about 6 times faster than a previously reported phosphorylation of the $DosT_{380-573}$ kinase fragment (*126*). The deoxy-DosT autophosphorylation was also about 6 times faster than that of FixL (*130, 153*). Oxy-DosT had an activity of only 0.062% min^{-1}, i.e. about 50 times lower than that of the deoxy-protein (Figure 8.5A). For deoxy-DevS, the initial rate of autophosphorylation was 0.25% min^{-1} (Figure 8.5B). Binding of O_2 slowed the autophosphorylation rate of DevS about 6-fold (0.041% min^{-1}) and to an "inhibited" rate similar to that measured for oxy-DosT (0.062% min^{-1}) (Figure 8.5B).

(8.6) Nitric oxide and carbon monoxide fail to switch off DosT or DevS. By contrast to the strongly inhibited oxy-form of DosT, the fully saturated carbomonoxy- and nitrosyl-forms of the proteins were completely active (Figure 8.5A). For DevS, the results were qualitatively similar and also showed inhibition for the O_2-bound form only (Figure 8.5B). These results demonstrate that DosT and DevS are designed to

sense O_2 and to discriminate against regulation by CO or NO (Figure 8.5C). As such, CO and NO are best seen as antagonists of DosT and DevS signaling, as low concentrations of either ligand could block the inhibitory action of O_2 under aerobic conditions.

DISCUSSION

This discovery of O_2 switching of DosT and DevS represented the first identification of a signal ligand for a *M. tuberculosis* kinase (Figure 8.5). This work also provided the first evidence of a direct O_2 effect on a component of the *M. tuberculosis* proteome. DosT and DevS are heme-based O_2 sensors with K_d values of 26 μM and 3 μM, respectively, for binding of O_2 (Figure 8.3, Table 8.2). As such, these two proteins will be switched on at the various low O_2 concentrations that have been reported for the physiological observations of hypoxic responses by *M. tuberculosis*. In each case, the deoxy-form is the active kinase, and conversion to the oxy-form switches off the activity by preventing an initial autophosphorylation of the sensor with the γ-phosphoryl group from ATP (Figure 8.6). This is entirely analogous to the way the deoxy-FixL kinase activity is switched off by O_2 (*107*). In contrast to FixL, which is slightly

inhibited by CO or NO, no regulation was detectable for DosT or DevS saturated with either of these ligands (Figure 8.5) (*130, 153*).

Why feature two sensors for modifying a single response regulator? One explanation is that the sensors might simply be redundant. Alternatively, the sensors could belong to different physiological states, with DosT being the DevR kinase most likely to survive oxidative assault from the host immune system. Yet another possibility is that the pathogen might require an O_2 dose response achievable only with two sensors of different affinities and kinetics (Table 8.2).

Numerous workers have noted that exposure of *M. tuberculosis* to NO donors under aerobic conditions causes the DevR transcription factor, i.e. a known target of DosT and DevS activation, to induce a similar set of genes as during hypoxia (*118, 148, 160-165*). This observation has, in some cases, been taken to imply that the hypoxic responses of *M. tuberculosis* are somehow mediated by NO. It is important not to interpret a failure to sense O_2 as sensing of NO. The results are more simply explained by NO's avid binding ($K_{d(O2)}/ K_{d(NO)} \sim 5000$) to DosT, coupled with its incapacity to regulate the kinase. Even at the low (micromolar) levels of NO generated by the NO donors used in *in vivo* experiments, to achieve concentrations of dissolved O_2 sufficient to displace a significant

fraction of the NO and inhibit DosT, at least five atmospheres of pure O_2 would be required. Likewise, the ligation of CO to aerobic DosT or DevS will cause these sensors to behave as if hypoxically activated. As mentioned earlier, CO and NO are best understood as antagonists of DosT and DevS signaling, where low concentrations of either antagonistic ligand can block the true inhibitory action of O_2 under aerobic conditions. Such a scenario would effectively "blind" the sensor from properly sensing the presence of O_2.

The results in Figure 8.5 show that O_2 is the true signal for DosT. As the course of a primary mycobacterial infection involves an initial transition from the O_2-rich lungs prior to macrophage engulfment to a situation of markedly reduced O_2 in the granuloma, hypoxia likely acts as a primary stimulus for adaptation to the latent regime. The simplest way to detect hypoxia is by directly sensing O_2. We propose that the DosT and DevS proteins serve as triggers of the *M. tuberculosis* latency response by directly sensing O_2 (Figure 8.6).

This study of DosT and DevS was inspired in great part by observations on FixL (*15*). Although the interaction of *M. tuberculosis* with humans is obviously not symbiotic, striking parallels exist between the infections by these mycobacteria in humans and the formation of

symbiotic root nodules by rhizobia in their leguminous hosts. In both cases, bacteria are switching to a hypoxic lifestyle inside of a eukaryotic cell. FixL proteins trigger cascades of bacterial gene expression in response to hypoxia that eventually lead to a state in which replication is virtually, if not completely, stopped (*150-152*). DosT has been proposed to play a similar role (*124, 126*). The morphology of the non-replicating cells bear some similarities, including an accumulation of cytoplasmic lipid droplets, as observed for *M. tuberculosis*, *M. bovis BCG*, and *Rhizobium etli* (*140, 166-168*). In these respects, the latency of *M. tuberculosis* resembles a symbiosis. For example, leguminous plants typically initiate root nodule formation with symbiotic bacteria when their soil is nitrogen poor, i.e. when resources are scarce. Might a host immune response that would normally completely clear the mycobacteria instead try to contain them into granulomas when some aspects of immune function are compromised? After controlling the bacteria into a granuloma, the relationship would confer protection to both microbe and host: to the microbe, because persistence in a granuloma prevents the host from clearing the infection, and to the host, because the granuloma prevents the massive tissue damage seen in active cases of clinical tuberculosis. Others have also noted a potential for a sort of symbiosis between *M.*

tuberculosis and their human host, though arguing from a different set of observations. For example, it has been suggested that the strong T-cell response to an initial *M. tuberculosis* infection, with subsequent granuloma formation, is beneficial to the host for control of the infection and to the pathogen as a means to increase its efficacy of transmission once reactivated from its protracted latency (*169*). Such a scenario clearly does not represent a true symbiosis, but rather a forced compromise struck during inopportune circumstances.

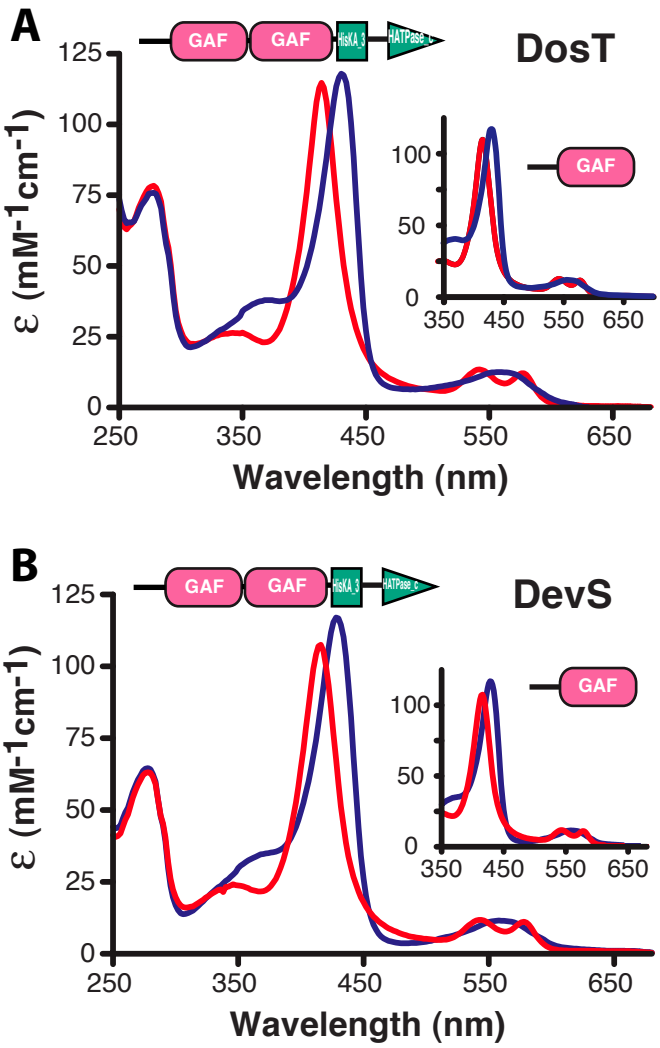

Figure 8.1. **DosT and DevS are heme-containing kinases in *M. tuberculosis.*** **(A)** Absorption spectrum of full-length ferrous DosT in air (red) and under anaerobic conditions (blue). The heme is in the DosT N-terminal GAF domain, as indicated by the absorption spectrum of this isolated domain, shown in the inset. **(B)** Absorption spectrum of full-length ferrous DevS in air (red) and under anaerobic conditions (blue). Similarly to DosT, DevS contains a single heme per monomer, and the heme is in the N-terminal GAF domain, as indicated by the absorption spectrum of this isolated domain, shown in the insert.

***Table 8.1*. Absorption maxima of ferrous-DosT and DevS species.**

	Fe^{2+}		$Fe^{2+}O_2$			$Fe^{2+}CO$			$Fe^{2+}NO$		
	γ	α/β	γ	β	α	γ	β	α	γ	β	α
DosT [a]	430	554	415	542	578	422	542	568	420	546	576
DevS [a]	430	558	416	542	578	422	542	568	420	546	575
*Bj*FixL [b]	437	556	419	545	562	427	548	560			

[a] This work (*17*); [b] Gilles-Gonzalez *et al.,* (*14*).

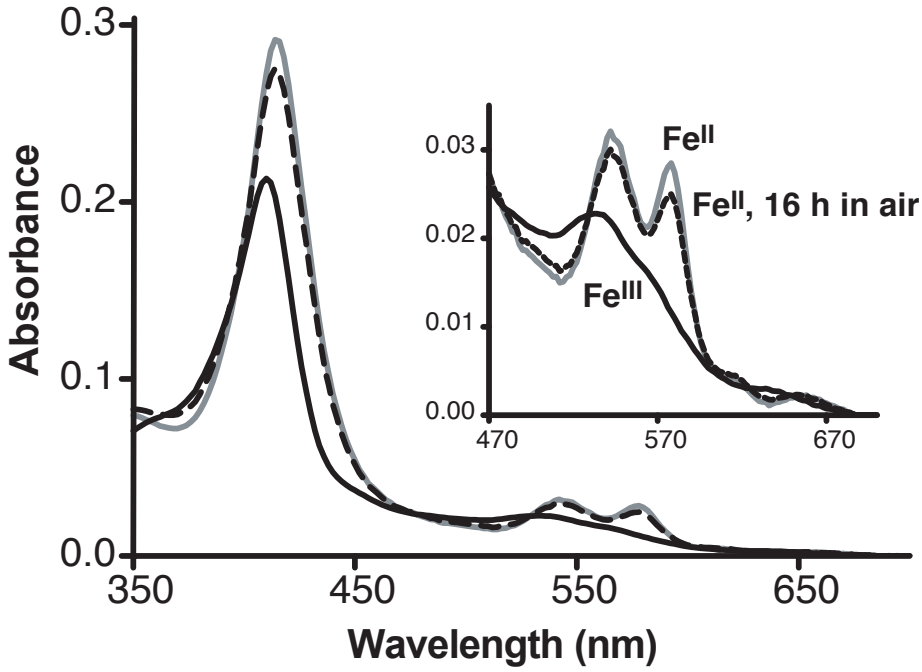

Figure 8.2. **Inertness of DosT to oxidation.** Absorbance spectra of DosT in air in the presence of the electron shuttler methyl-viologen (5 μM) at time zero (gray curve) and after 16 h (dashed black curve). Also shown is the spectrum of ferric DosT produced by oxidation with ferricyanide (solid black curve). Analysis of these spectra by multiple-linear-regression analysis indicate that < 6 % of DosT had oxidized to the ferric form after 16 h in the absence of methyl -viologen, while only ~ 17 % of DosT had oxidized to the ferric form after 16 h in the presence of methyl-viologen. The inset shows an expansion of the 470 - 700 nm region of the spectrum. Spectra were recorded in 50 mM Tris-HCl (pH 8.0) at 37 °C.

***Table 8.2*. Equilibrium and kinetic parameters for DosT and DevS.**

	O_2				CO			NO	ATP
	k_{on} ($\mu M^{-1}s^{-1}$)	k_{off} (s^{-1})	K_d (μM)	k_{ox} (h^{-1})	k_{on} ($\mu M^{-1}s^{-1}$)	k_{off} (s^{-1})	K_d (μM)	K_d (nM)	K_M (μM)
DosT [a]	0.79	20[#]	26	<0.01	0.05	0.06	0.94	5.0	39
DevS [a]	8.8	12.5	3.0	0.17	1.8	0.06	0.036*	20	73
*Bj*FixL [b]	0.14	20	140	2.7	0.0050	0.045	9		47
SW Mb [c]	14	16	1.2	0.060[d]	0.50	0.019	0.037	0.0045[e]	

[a] This work (*17*); [b] Gilles-Gonzalez *et al.,* (*14*) and (*170*); [c] Rohlfs *et al.,* (*171*); [d] Brantley *et al.,* (*88*); [e] Olson and Phillips (*172*). [#] Calculated from k_{on} and K_d. [*] Calculated from k_{on} and k_{off}.

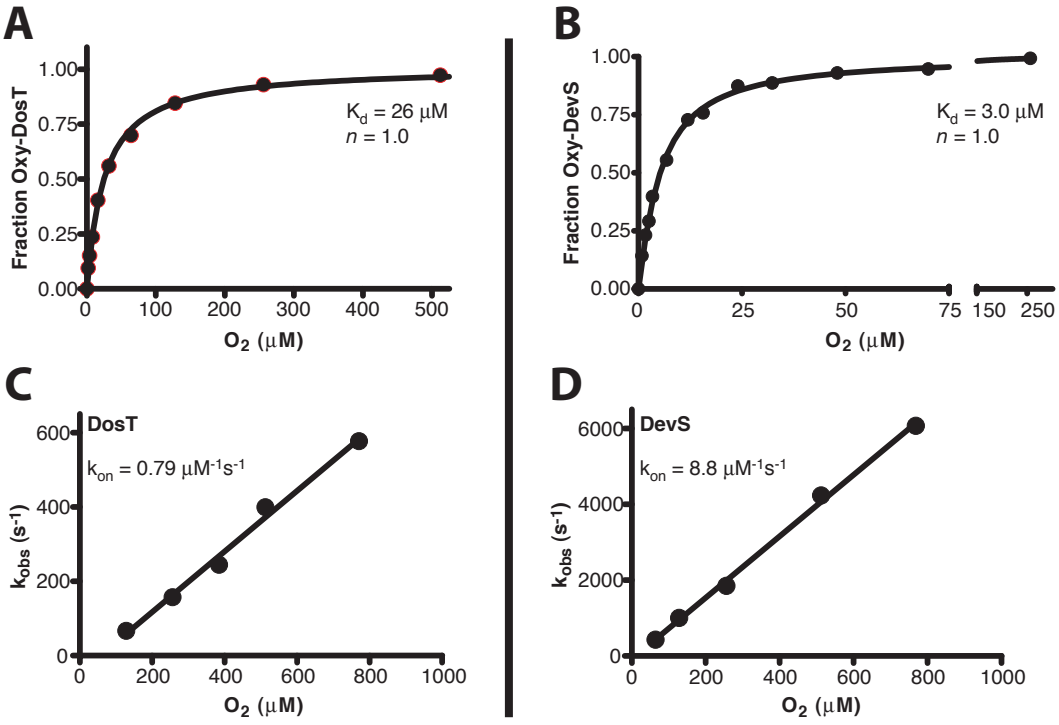

Figure 8.3. **Kinetic and equilibrium parameters for binding of O_2 to DosT and DevS.** **(A)** The DosT $K_d(O_2)$ was determinded by titrating deoxy-DosT (2 μM) with 1 - 1200 μM O_2. Fractional saturations were calculated from multiple linear regression of whole spectra, and data were fit to the Hill equation. **(B)** The DevS $K_d(O_2)$ was determined by titrating deoxy-DevS (2 μM) with 0.8 - 256 μM O_2, with data analysis as in panel A. **(C)** The DosT k_{on} (O_2) was determined by monitoring O_2 rebinding after laser flash photolysis at 435 nm. **(D)** The DevS $k_{on}(O_2)$ was determined as described for panel C. All measurements were at pH 8.0 and 25 °C.

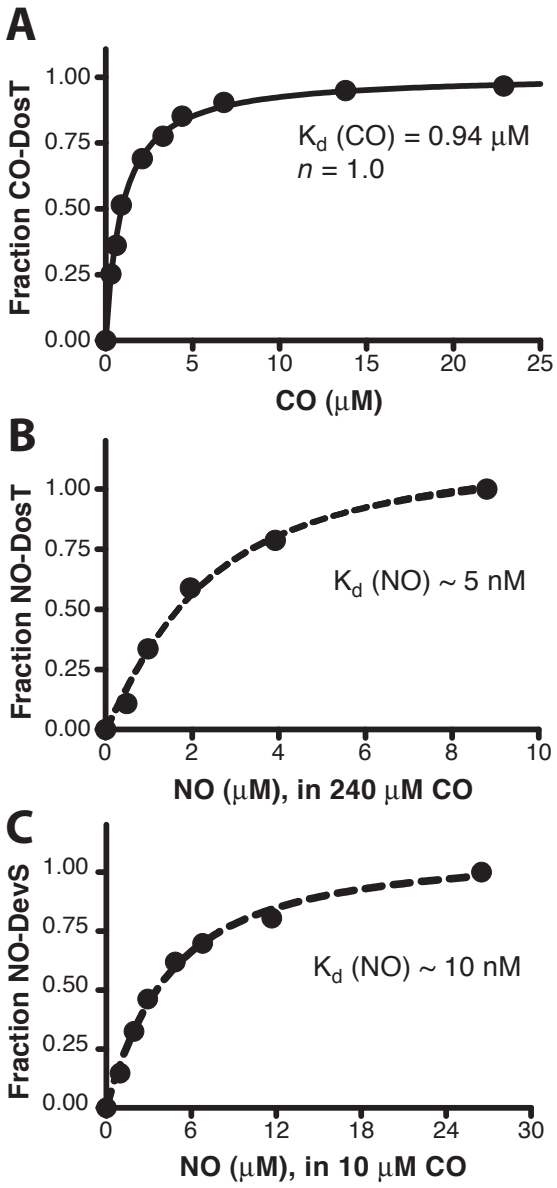

Figure 8.4. **Equilibrium parameters for binding CO and NO to DosT and DevS. (A)** Titration of deoxy-DosT with CO. **(B)** Titration of deoxy-DosT with NO in a background of 240 μM CO. **(C)** Titration of deoxy-DevS with NO in a background of 10 μM CO. All measurements were in 50 mM Tris-HCl, 50 mM KCl, and 5 % (v/v) ethylene glycol at pH 8.0 and 25 ^{o}C.

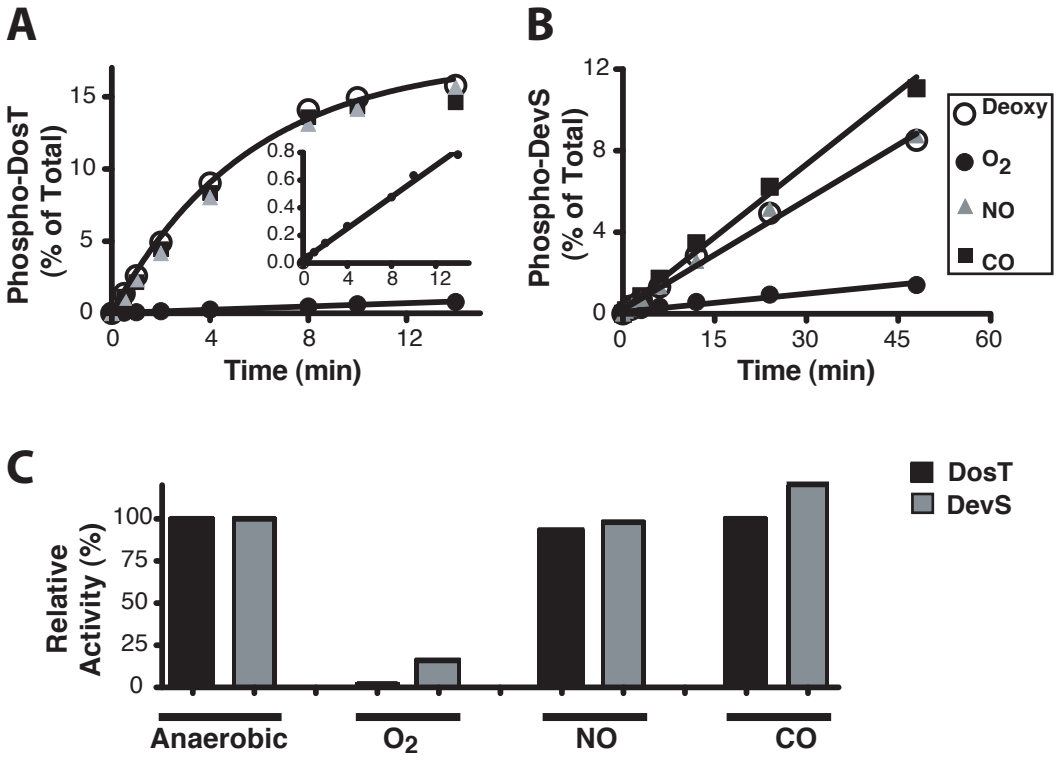

Figure 8.5. **Specific inhibition of DosT and DevS by O_2. (A)** Autophosphorylation of DosT in the deoxy- (open circles), oxy- (closed circles), carbonmonoxy- (squares), and nitrosyl- (triangles) forms. The inset shows a 20-fold expansion of the ordinate for the oxy-DosT autophosphorylation reaction. **(B)** Autophosphorylation of DevS in the deoxy- (open circles), oxy- (closed circles), carbonmonoxy- (squares), and nitrosyl- (triangles) forms. (**C)** Quantification of the autophosphorylation activities of each liganded species as compared to the unliganded form (deoxy, 100 % active). Note the specific inhibition of DosT and DevS autophosphorylation by O_2. All reactions were at pH 8.0 and 23 ^{o}C.

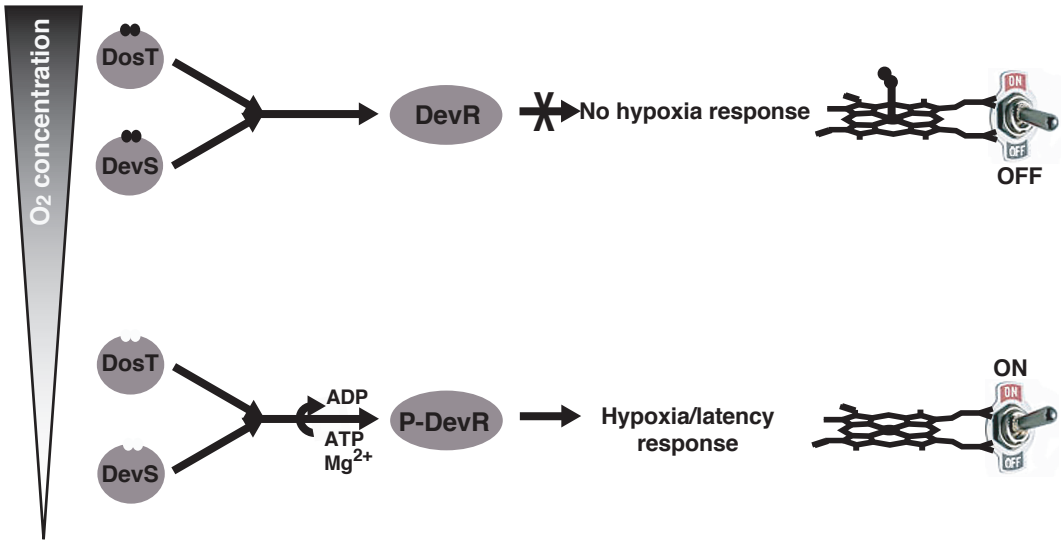

Figure 8.6. **Schematic representation of the effect of O_2 on the DosT/DevS/DevR system.** Under normoxic conditions, i.e., conditions of air saturation (256 μM O_2), both DosT and DevS will be saturated with O_2, and their kinase activity will be switched off (top). Under hypoxic conditions, DosT and DevS will exist primarily in their deoxy states and manifest full kinase activity (bottom). Catalysis of phosphoryl transfer from ATP to DevR, either by DosT or DevS, will trigger the *M. tuberculosis* hypoxic response. This hypoxic response is correlated with *M. tuberculosis* latency *in vivo*.

BIBLIOGRAPHY

1. Pugh, C. W., and Ratcliffe, P. J. (2003) Regulation of angiogenesis by hypoxia: role of the HIF system. *Nat Med 9*, 677-684.
2. Semenza, G. L. (2009) Regulation of vascularization by hypoxia-inducible factor 1. *Ann N Y Acad Sci 1177*, 2-8.
3. Semenza, G. L. (2009) Involvement of oxygen-sensing pathways in physiologic and pathologic erythropoiesis. *Blood 114*, 2015-2019.
4. Weir, E. K., Lopez-Barneo, J., Buckler, K. J., and Archer, S. L. (2005) Acute oxygen-sensing mechanisms. *N Engl J Med 353*, 2042-2055.
5. Lahiri, S., Roy, A., Baby, S. M., Hoshi, T., Semenza, G. L., and Prabhakar, N. R. (2006) Oxygen sensing in the body. *Prog Biophys Mol Biol 91*, 249-286.
6. Lopez-Barneo, J., Ortega-Saenz, P., Pardal, R., Pascual, A., Piruat, J. I., Duran, R., and Gomez-Diaz, R. (2009) Oxygen sensing in the carotid body. *Ann N Y Acad Sci 1177*, 119-131.
7. Semenza, G. L. (2003) Targeting HIF-1 for cancer therapy. *Nat Rev Cancer 3*, 721-732.
8. Semenza, G. L. (2008) Hypoxia-inducible factor 1 and cancer pathogenesis. *IUBMB Life 60*, 591-597.
9. Mole, D. R., and Ratcliffe, P. J. (2008) Cellular oxygen sensing in health and disease. *Pediatr Nephrol 23*, 681-694.
10. Unden, G., Becker, S., Bongaerts, J., Schirawski, J., and Six, S. (1994) Oxygen regulated gene expression in facultatively anaerobic bacteria. *Antonie Van Leeuwenhoek 66*, 3-22.
11. Iuchi, S., and Weiner, L. (1996) Cellular and molecular physiology of *Escherichia coli* in the adaptation to aerobic environments. *J Biochem 120*, 1055-1063.
12. Sawers, G. (1999) The aerobic/anaerobic interface. *Curr Opin Microbiol 2*, 181-187.
13. Green, J., Crack, J. C., Thomson, A. J., and LeBrun, N. E. (2009) Bacterial sensors of oxygen. *Curr Opin Microbiol 12*, 145-151.
14. Gilles-Gonzalez, M. A., Gonzalez, G., Perutz, M. F., Kiger, L., Marden, M. C., and Poyart, C. (1994) Heme-based sensors, exemplified by the kinase FixL, are a new class of heme protein with distinctive ligand binding and autoxidation. *Biochemistry 33*, 8067-8073.

15. Gilles-Gonzalez, M. A., and Gonzalez, G. (2005) Heme-based sensors: defining characteristics, recent developments, and regulatory hypotheses. *J Inorg Biochem 99*, 1-22.
16. Freitas, T. A., Hou, S., and Alam, M. (2003) The diversity of globin-coupled sensors. *FEBS Lett 552*, 99-104.
17. Sousa, E. H., Tuckerman, J. R., Gonzalez, G., and Gilles-Gonzalez, M. A. (2007) DosT and DevS are oxygen-switched kinases in *Mycobacterium tuberculosis*. *Protein Sci 16*, 1708-1719.
18. Iyer, L. M., Anantharaman, V., and Aravind, L. (2003) Ancient conserved domains shared by animal soluble guanylyl cyclases and bacterial signaling proteins. *BMC Genomics 4*, 5.
19. Gilles-Gonzalez, M. A., Ditta, G. S., and Helinski, D. R. (1991) A haemoprotein with kinase activity encoded by the oxygen sensor of *Rhizobium meliloti*. *Nature 350*, 170-172.
20. Gilles-Gonzalez, M. A. (2001) Oxygen signal transduction. *IUBMB Life 51*, 165-173.
21. Gilles-Gonzalez, M. A., and Gonzalez, G. (2004) Signal transduction by heme-containing PAS-domain proteins. *J Appl Physiol 96*, 774-783.
22. Romling, U., Gomelsky, M., and Galperin, M. Y. (2005) C-di-GMP: the dawning of a novel bacterial signalling system. *Mol Microbiol 57*, 629-639.
23. Ross, P., Weinhouse, H., Aloni, Y., Michaeli, D., Weinberger-Ohana, P., Mayer, R., Braun, S., de Vroom, E., van der Marel, G. A., van Boom, J. H., and Benziman, M. (1987) Regulation of cellulose synthesis in *Acetobacter xylinum* by cyclic diguanylic acid. *Nature 325*, 279-281.
24. Ross, P., Mayer, R., and Benziman, M. (1991) Cellulose biosynthesis and function in bacteria. *Microbiol Rev 55*, 35-58.
25. Ross, P., Aloni, Y., Weinhouse, C., Michaeli, D., Weinberger-Ohana, P., Meyer, R., and Benziman, M. (1985) An unusual guanyl oligonucleotide regulates cellulose synthesis in *Acetobacter xylinum*. *FEBS Lett 186*, 191-196.
26. Tal, R., Wong, H. C., Calhoon, R., Gelfand, D., Fear, A. L., Volman, G., Mayer, R., Ross, P., Amikam, D., Weinhouse, H., Cohen, A., Sapir, S., Ohana, P., and Benziman, M. (1998) Three cdg operons control cellular turnover of cyclic di-GMP in *Acetobacter xylinum*: genetic organization and occurrence of conserved domains in isoenzymes. *J Bacteriol 180*, 4416-4425.

27. Simm, R., Morr, M., Kader, A., Nimtz, M., and Romling, U. (2004) GGDEF and EAL domains inversely regulate cyclic di-GMP levels and transition from sessility to motility. *Mol Microbiol 53*, 1123-1134.
28. Ausmees, N., Mayer, R., Weinhouse, H., Volman, G., Amikam, D., Benziman, M., and Lindberg, M. (2001) Genetic data indicate that proteins containing the GGDEF domain possess diguanylate cyclase activity. *FEMS Microbiol Lett 204*, 163-167.
29. Ryjenkov, D. A., Tarutina, M., Moskvin, O. V., and Gomelsky, M. (2005) Cyclic diguanylate is a ubiquitous signaling molecule in bacteria: insights into biochemistry of the GGDEF protein domain. *J Bacteriol 187*, 1792-1798.
30. Schmidt, A. J., Ryjenkov, D. A., and Gomelsky, M. (2005) The ubiquitous protein domain EAL is a cyclic diguanylate-specific phosphodiesterase: enzymatically active and inactive EAL domains. *J Bacteriol 187*, 4774-4781.
31. Costerton, J. W., Stewart, P. S., and Greenberg, E. P. (1999) Bacterial biofilms: a common cause of persistent infections. *Science 284*, 1318-1322.
32. D'Argenio, D. A., and Miller, S. I. (2004) Cyclic di-GMP as a bacterial second messenger. *Microbiology 150*, 2497-2502.
33. Romling, U., and Amikam, D. (2006) Cyclic di-GMP as a second messenger. *Curr Opin Microbiol 9*, 218-228.
34. Jenal, U., and Malone, J. (2006) Mechanisms of cyclic-di-GMP signaling in bacteria. *Annu Rev Genet 40*, 385-407.
35. Ryan, R. P., Fouhy, Y., Lucey, J. F., and Dow, J. M. (2006) Cyclic di-GMP signaling in bacteria: recent advances and new puzzles. *J Bacteriol 188*, 8327-8334.
36. Hengge, R. (2009) Principles of c-di-GMP signalling in bacteria. *Nat Rev Microbiol 7*, 263-273.
37. Galperin, M. Y., Nikolskaya, A. N., and Koonin, E. V. (2001) Novel domains of the prokaryotic two-component signal transduction systems. *FEMS Microbiol Lett 203*, 11-21.
38. Chang, A. L., Tuckerman, J. R., Gonzalez, G., Mayer, R., Weinhouse, H., Volman, G., Amikam, D., Benziman, M., and Gilles-Gonzalez, M. A. (2001) Phosphodiesterase A1, a regulator of cellulose synthesis in *Acetobacter xylinum*, is a heme-based sensor. *Biochemistry 40*, 3420-3426.

39. Tarutina, M., Ryjenkov, D. A., and Gomelsky, M. (2006) An unorthodox bacteriophytochrome from *Rhodobacter sphaeroides* involved in turnover of the second messenger c-di-GMP. *J Biol Chem 281*, 34751-34758.
40. Tanaka, A., Takahashi, H., and Shimizu, T. (2007) Critical role of the heme axial ligand, Met95, in locking catalysis of the phosphodiesterase from *Escherichia coli* (*Ec* DOS) toward cyclic diGMP. *J Biol Chem 282*, 21301-21307.
41. Wan, X., Tuckerman, J. R., Saito, J. A., Freitas, T. A., Newhouse, J. S., Denery, J. R., Galperin, M. Y., Gonzalez, G., Gilles-Gonzalez, M. A., and Alam, M. (2009) Globins synthesize the second messenger bis-(3'-5')-cyclic diguanosine monophosphate in bacteria. *J Mol Biol 388*, 262-270.
42. Qi, Y., Rao, F., Luo, Z., and Liang, Z. X. (2009) A Flavin Cofactor-Binding PAS Domain Regulates c-di-GMP Synthesis in *Ax*DGC2 from *Acetobacter xylinum*. *Biochemistry 48*, 10275-10285.
43. Barends, T. R., Hartmann, E., Griese, J. J., Beitlich, T., Kirienko, N. V., Ryjenkov, D. A., Reinstein, J., Shoeman, R. L., Gomelsky, M., and Schlichting, I. (2009) Structure and mechanism of a bacterial light-regulated cyclic nucleotide phosphodiesterase. *Nature 459*, 1015-1018.
44. Sawai, H., Yoshioka, S., Uchida, T., Hyodo, M., Hayakawa, Y., Ishimori, K., and Aono, S. Molecular oxygen regulates the enzymatic activity of a heme-containing diguanylate cyclase (HemDGC) for the synthesis of cyclic di-GMP. *Biochim Biophys Acta 1804*, 166-172.
45. Sudarsan, N., Lee, E. R., Weinberg, Z., Moy, R. H., Kim, J. N., Link, K. H., and Breaker, R. R. (2008) Riboswitches in eubacteria sense the second messenger cyclic di-GMP. *Science 321*, 411-413.
46. Chan, C., Paul, R., Samoray, D., Amiot, N. C., Giese, B., Jenal, U., and Schirmer, T. (2004) Structural basis of activity and allosteric control of diguanylate cyclase. *Proc Natl Acad Sci U S A 101*, 17084-17089.
47. Ryjenkov, D. A., Simm, R., Romling, U., and Gomelsky, M. (2006) The PilZ domain is a receptor for the second messenger c-di-GMP: the PilZ domain protein YcgR controls motility in enterobacteria. *J Biol Chem 281*, 30310-30314.
48. Lee, V. T., Matewish, J. M., Kessler, J. L., Hyodo, M., Hayakawa, Y., and Lory, S. (2007) A cyclic-di-GMP receptor required for

bacterial exopolysaccharide production. *Mol Microbiol 65*, 1474-1484.

49. Hickman, J. W., and Harwood, C. S. (2008) Identification of FleQ from *Pseudomonas aeruginosa* as a c-di-GMP-responsive transcription factor. *Mol Microbiol 69*, 376-389.
50. Newell, P. D., Monds, R. D., and O'Toole, G. A. (2009) LapD is a bis-(3',5')-cyclic dimeric GMP-binding protein that regulates surface attachment by *Pseudomonas fluorescens* Pf0-1. *Proc Natl Acad Sci U S A 106*, 3461-3466.
51. Leduc, J. L., and Roberts, G. P. (2009) Cyclic di-GMP allosterically inhibits the CRP-like protein (Clp) of *Xanthomonas axonopodis* pv. *citri*. *J Bacteriol 191*, 7121-7122.
52. Krasteva, P. V., Fong, J. C., Shikuma, N. J., Beyhan, S., Navarro, M. V., Yildiz, F. H., and Sondermann, H. *Vibrio cholerae* VpsT regulates matrix production and motility by directly sensing cyclic di-GMP. *Science 327*, 866-868.
53. Weber, H., Pesavento, C., Possling, A., Tischendorf, G., and Hengge, R. (2006) Cyclic-di-GMP-mediated signalling within the sigma network of *Escherichia coli*. *Mol Microbiol 62*, 1014-1034.
54. Sommerfeldt, N., Possling, A., Becker, G., Pesavento, C., Tschowri, N., and Hengge, R. (2009) Gene expression patterns and differential input into curli fimbriae regulation of all GGDEF/EAL domain proteins in *Escherichia coli*. *Microbiology 155*, 1318-1331.
55. Botsford, J. L., and Harman, J. G. (1992) Cyclic AMP in prokaryotes. *Microbiol Rev 56*, 100-122.
56. Imamura, R., Yamanaka, K., Ogura, T., Hiraga, S., Fujita, N., Ishihama, A., and Niki, H. (1996) Identification of the *cpdA* gene encoding cyclic 3',5'-adenosine monophosphate phosphodiesterase in *Escherichia coli*. *J Biol Chem 271*, 25423-25429.
57. Simm, R., Lusch, A., Kader, A., Andersson, M., and Romling, U. (2007) Role of EAL-containing proteins in multicellular behavior of *Salmonella enterica* serovar *Typhimurium*. *J Bacteriol 189*, 3613-3623.
58. Beyhan, S., Odell, L. S., and Yildiz, F. H. (2008) Identification and characterization of cyclic diguanylate signaling systems controlling rugosity in *Vibrio cholerae*. *J Bacteriol 190*, 7392-7405.
59. Kuchma, S. L., Brothers, K. M., Merritt, J. H., Liberati, N. T., Ausubel, F. M., and O'Toole, G. A. (2007) BifA, a cyclic-Di-GMP phosphodiesterase, inversely regulates biofilm formation and

swarming motility by *Pseudomonas aeruginosa* PA14. *J Bacteriol 189*, 8165-8178.

60. Blattner, F. R., Plunkett, G., 3rd, Bloch, C. A., Perna, N. T., Burland, V., Riley, M., Collado-Vides, J., Glasner, J. D., Rode, C. K., Mayhew, G. F., Gregor, J., Davis, N. W., Kirkpatrick, H. A., Goeden, M. A., Rose, D. J., Mau, B., and Shao, Y. (1997) The complete genome sequence of *Escherichia coli* K-12. *Science 277*, 1453-1462.
61. Laemmli, U. K. (1970) Cleavage of structural proteins during the assembly of the head of bacteriophage T4. *Nature 227*, 680-685.
62. Appleby, C. A. (1978) Purification of Rhizobium cytochromes P-450. *Methods Enzymol 52*, 157-166.
63. Jones, G. H., Symmons, M. F., Hankins, J. S., and Mackie, G. A. (2003) Overexpression and purification of untagged polynucleotide phosphorylases. *Protein Expr Purif 32*, 202-209.
64. Kimhi, Y., and Littauer, U. Z. (1968) Purification and properties of polynucleotide phosphorylase from *Escherichia coli*. *J Biol Chem 243*, 231-240.
65. Mayer, R., Ross, P., Weinhouse, H., Amikam, D., Volman, G., Ohana, P., Calhoon, R. D., Wong, H. C., Emerick, A. W., and Benziman, M. (1991) Polypeptide composition of bacterial cyclic diguanylic acid-dependent cellulose synthase and the occurrence of immunologically crossreacting proteins in higher plants. *Proc Natl Acad Sci U S A 88*, 5472-5476.
66. Delgado-Nixon, V. M., Gonzalez, G., and Gilles-Gonzalez, M. A. (2000) Dos, a heme-binding PAS protein from *Escherichia coli*, is a direct oxygen sensor. *Biochemistry 39*, 2685-2691.
67. Gonzalez, G., Dioum, E. M., Bertolucci, C. M., Tomita, T., Ikeda-Saito, M., Cheesman, M. R., Watmough, N. J., and Gilles-Gonzalez, M. A. (2002) Nature of the displaceable heme-axial residue in the *Ec*Dos protein, a heme-based sensor from *Escherichia coli*. *Biochemistry 41*, 8414-8421.
68. Tuckerman, J. R., Gonzalez, G., Sousa, E. H., Wan, X., Saito, J. A., Alam, M., and Gilles-Gonzalez, M. A. (2009) An oxygen-sensing diguanylate cyclase and phosphodiesterase couple for c-di-GMP control. *Biochemistry 48*, 9764-9774.
69. Christen, M., Christen, B., Folcher, M., Schauerte, A., and Jenal, U. (2005) Identification and characterization of a cyclic di-GMP-

specific phosphodiesterase and its allosteric control by GTP. *J Biol Chem 280*, 30829-30837.

70. Yoshimura, T., Sagami, I., Sasakura, Y., and Shimizu, T. (2003) Relationships between heme incorporation, tetramer formation, and catalysis of a heme-regulated phosphodiesterase from *Escherichia coli*: a study of deletion and site-directed mutants. *J Biol Chem 278*, 53105-53111.
71. Sousa, E. H., Tuckerman, J. R., Gonzalez, G., and Gilles-Gonzalez, M. A. (2007) A memory of oxygen binding explains the dose response of the heme-based sensor FixL. *Biochemistry 46*, 6249-6257.
72. Mendez-Ortiz, M. M., Hyodo, M., Hayakawa, Y., and Membrillo-Hernandez, J. (2006) Genome-wide transcriptional profile of *Escherichia coli* in response to high levels of the second messenger 3',5'-cyclic diguanylic acid. *J Biol Chem 281*, 8090-8099.
73. Hou, S., Larsen, R. W., Boudko, D., Riley, C. W., Karatan, E., Zimmer, M., Ordal, G. W., and Alam, M. (2000) Myoglobin-like aerotaxis transducers in Archaea and Bacteria. *Nature 403*, 540-544.
74. Zhang, W., and Phillips, G. N., Jr. (2003) Structure of the oxygen sensor in *Bacillus subtilis*: signal transduction of chemotaxis by control of symmetry. *Structure 11*, 1097-1110.
75. Vinogradov, S. N., Hoogewijs, D., Bailly, X., Mizuguchi, K., Dewilde, S., Moens, L., and Vanfleteren, J. R. (2007) A model of globin evolution. *Gene 398*, 132-142.
76. Shikama, K., and Matsuoka, A. (1989) Spectral properties unique to the myoglobins lacking the usual distal histidine residue. *J Mol Biol 209*, 489-491.
77. Conti, E., Moser, C., Rizzi, M., Mattevi, A., Lionetti, C., Coda, A., Ascenzi, P., Brunori, M., and Bolognesi, M. (1993) X-ray crystal structure of ferric *Aplysia limacina* myoglobin in different liganded states. *J Mol Biol 233*, 498-508.
78. Gong, W., Hao, B., Mansy, S. S., Gonzalez, G., Gilles-Gonzalez, M. A., and Chan, M. K. (1998) Structure of a biological oxygen sensor: a new mechanism for heme-driven signal transduction. *Proc Natl Acad Sci U S A 95*, 15177-15182.

79. Dou, Y., Olson, J. S., Wilkinson, A. J., and Ikeda-Saito, M. (1996) Mechanism of hydrogen cyanide binding to myoglobin. *Biochemistry 35*, 7107-7113.
80. Mansy, S. S., Olson, J. S., Gonzalez, G., and Gilles-Gonzalez, M. A. (1998) Imidazole is a sensitive probe of steric hindrance in the distal pockets of oxygen-binding heme proteins. *Biochemistry 37*, 12452-12457.
81. Antoine, R., Alonso, S., Raze, D., Coutte, L., Lesjean, S., Willery, E., Locht, C., and Jacob-Dubuisson, F. (2000) New virulence-activated and virulence-repressed genes identified by systematic gene inactivation and generation of transcriptional fusions in *Bordetella pertussis*. *J Bacteriol 182*, 5902-5905.
82. Galperin, M. Y. (2005) A census of membrane-bound and intracellular signal transduction proteins in bacteria: bacterial IQ, extroverts and introverts. *BMC Microbiol 5*, 35.
83. Wood, G. E., Khelef, N., Guiso, N., and Friedman, R. L. (1998) Identification of Btr-regulated genes using a titration assay. Search for a role for this transcriptional regulator in the growth and virulence of *Bordetella pertussis*. *Gene 209*, 51-58.
84. Borriello, G., Werner, E., Roe, F., Kim, A. M., Ehrlich, G. D., and Stewart, P. S. (2004) Oxygen limitation contributes to antibiotic tolerance of *Pseudomonas aeruginosa* in biofilms. *Antimicrob Agents Chemother 48*, 2659-2664.
85. Rani, S. A., Pitts, B., Beyenal, H., Veluchamy, R. A., Lewandowski, Z., Davison, W. M., Buckingham-Meyer, K., and Stewart, P. S. (2007) Spatial patterns of DNA replication, protein synthesis, and oxygen concentration within bacterial biofilms reveal diverse physiological states. *J Bacteriol 189*, 4223-4233.
86. Winkler, W. C., Gonzalez, G., Wittenberg, J. B., Hille, R., Dakappagari, N., Jacob, A., Gonzalez, L. A., and Gilles-Gonzalez, M. A. (1996) Nonsteric factors dominate binding of nitric oxide, azide, imidazole, cyanide, and fluoride to the rhizobial heme-based oxygen sensor FixL. *Chem Biol 3*, 841-850.
87. Quillin, M. L., Arduini, R. M., Olson, J. S., and Phillips, G. N., Jr. (1993) High-resolution crystal structures of distal histidine mutants of sperm whale myoglobin. *J Mol Biol 234*, 140-155.
88. Brantley, R. E., Jr., Smerdon, S. J., Wilkinson, A. J., Singleton, E. W., and Olson, J. S. (1993) The mechanism of autooxidation of myoglobin. *J Biol Chem 268*, 6995-7010.

89. Carpousis, A. J., Van Houwe, G., Ehretsmann, C., and Krisch, H. M. (1994) Copurification of *E. coli* RNAase E and PNPase: evidence for a specific association between two enzymes important in RNA processing and degradation. *Cell 76*, 889-900.
90. Py, B., Higgins, C. F., Krisch, H. M., and Carpousis, A. J. (1996) A DEAD-box RNA helicase in the *Escherichia coli* RNA degradosome. *Nature 381*, 169-172.
91. Miczak, A., Kaberdin, V. R., Wei, C. L., and Lin-Chao, S. (1996) Proteins associated with RNase E in a multicomponent ribonucleolytic complex. *Proc Natl Acad Sci U S A 93*, 3865-3869.
92. Regonesi, M. E., Del Favero, M., Basilico, F., Briani, F., Benazzi, L., Tortora, P., Mauri, P., and Deho, G. (2006) Analysis of the *Escherichia coli* RNA degradosome composition by a proteomic approach. *Biochimie 88*, 151-161.
93. Worrall, J. A., Gorna, M., Crump, N. T., Phillips, L. G., Tuck, A. C., Price, A. J., Bavro, V. N., and Luisi, B. F. (2008) Reconstitution and analysis of the multienzyme *Escherichia coli* RNA degradosome. *J Mol Biol 382*, 870-883.
94. Carpousis, A. J. (2007) The RNA degradosome of *Escherichia coli*: an mRNA-degrading machine assembled on RNase E. *Annu Rev Microbiol 61*, 71-87.
95. Huther, F. J., Psarros, N., and Duschner, H. (1990) Isolation, characterization, and inhibition kinetics of enolase from *Streptococcus rattus* FA-1. *Infect Immun 58*, 1043-1047.
96. Jager, S., Fuhrmann, O., Heck, C., Hebermehl, M., Schiltz, E., Rauhut, R., and Klug, G. (2001) An mRNA degrading complex in *Rhodobacter capsulatus*. *Nucleic Acids Res 29*, 4581-4588.
97. Prud'homme-Genereux, A., Beran, R. K., Iost, I., Ramey, C. S., Mackie, G. A., and Simons, R. W. (2004) Physical and functional interactions among RNase E, polynucleotide phosphorylase and the cold-shock protein, CsdA: evidence for a 'cold shock degradosome'. *Mol Microbiol 54*, 1409-1421.
98. Morita, T., Kawamoto, H., Mizota, T., Inada, T., and Aiba, H. (2004) Enolase in the RNA degradosome plays a crucial role in the rapid decay of glucose transporter mRNA in the response to phosphosugar stress in *Escherichia coli*. *Mol Microbiol 54*, 1063-1075.
99. Morita, T., Maki, K., and Aiba, H. (2005) RNase E-based ribonucleoprotein complexes: mechanical basis of mRNA

destabilization mediated by bacterial noncoding RNAs. *Genes Dev 19*, 2176-2186.

100. Stock, J. B., Ninfa, A. J., and Stock, A. M. (1989) Protein phosphorylation and regulation of adaptive responses in bacteria. *Microbiol Rev 53*, 450-490.
101. Parkinson, J. S., and Kofoid, E. C. (1992) Communication modules in bacterial signaling proteins. *Annu Rev Genet 26*, 71-112.
102. Soupene, E., Foussard, M., Boistard, P., Truchet, G., and Batut, J. (1995) Oxygen as a key developmental regulator of *Rhizobium meliloti* N2-fixation gene expression within the alfalfa root nodule. *Proc Natl Acad Sci U S A 92*, 3759-3763.
103. Poole, R. K., and Hill, S. (1997) Respiratory protection of nitrogenase activity in *Azotobacter vinelandii*--roles of the terminal oxidases. *Biosci Rep 17*, 303-317.
104. Appleby, C. A. (1969) Properties of leghaemoglobin *in vivo*, and its isolation as ferrous oxyleghaemoglobin. *Biochim Biophys Acta 188*, 222-229.
105. Wittenberg, J. B., Appleby, C. A., and Wittenberg, B. A. (1972) The kinetics of the reactions of leghemoglobin with oxygen and carbon monoxide. *J Biol Chem 247*, 527-531.
106. Aizawa, S. I., Harwood, C. S., and Kadner, R. J. (2000) Signaling components in bacterial locomotion and sensory reception. *J Bacteriol 182*, 1459-1471.
107. Gilles-Gonzalez, M. A., and Gonzalez, G. (1993) Regulation of the kinase activity of heme protein FixL from the two-component system FixL/FixJ of *Rhizobium meliloti*. *J Biol Chem 268*, 16293-16297.
108. Agron, P. G., Ditta, G. S., and Helinski, D. R. (1993) Oxygen regulation of *nifA* transcription *in vitro*. *Proc Natl Acad Sci U S A 90*, 3506-3510.
109. Reyrat, J. M., David, M., Blonski, C., Boistard, P., and Batut, J. (1993) Oxygen-regulated in vitro transcription of *Rhizobium meliloti nifA* and *fixK* genes. *J Bacteriol 175*, 6867-6872.
110. Galinier, A., Garnerone, A. M., Reyrat, J. M., Kahn, D., Batut, J., and Boistard, P. (1994) Phosphorylation of the *Rhizobium meliloti* FixJ protein induces its binding to a compound regulatory region at the *fixK* promoter. *J Biol Chem 269*, 23784-23789.
111. David, M., Daveran, M. L., Batut, J., Dedieu, A., Domergue, O., Ghai, J., Hertig, C., Boistard, P., and Kahn, D. (1988) Cascade

regulation of *nif* gene expression in *Rhizobium meliloti*. *Cell 54*, 671-683.

112. Wayne, L. G., and Sohaskey, C. D. (2001) Nonreplicating persistence of *Mycobacterium tuberculosis*. *Annu Rev Microbiol 55*, 139-163.
113. Kohler, S., Foulongne, V., Ouahrani-Bettache, S., Bourg, G., Teyssier, J., Ramuz, M., and Liautard, J. P. (2002) The analysis of the intramacrophagic virulome of *Brucella suis* deciphers the environment encountered by the pathogen inside the macrophage host cell. *Proc Natl Acad Sci U S A 99*, 15711-15716.
114. Schnappinger, D., Ehrt, S., Voskuil, M. I., Liu, Y., Mangan, J. A., Monahan, I. M., Dolganov, G., Efron, B., Butcher, P. D., Nathan, C., and Schoolnik, G. K. (2003) Transcriptional adaptation of *Mycobacterium tuberculosis* within macrophages: insights into the phagosomal environment. *J Exp Med 198*, 693-704.
115. Via, L. E., Lin, P. L., Ray, S. M., Carrillo, J., Allen, S. S., Eum, S. Y., Taylor, K., Klein, E., Manjunatha, U., Gonzales, J., Lee, E. G., Park, S. K., Raleigh, J. A., Cho, S. N., McMurray, D. N., Flynn, J. L., and Barry, C. E., 3rd. (2008) Tuberculous granulomas are hypoxic in guinea pigs, rabbits, and nonhuman primates. *Infect Immun 76*, 2333-2340.
116. Stewart, G. R., Robertson, B. D., and Young, D. B. (2003) Tuberculosis: a problem with persistence. *Nat Rev Microbiol 1*, 97-105.
117. Wayne, L. G., and Hayes, L. G. (1996) An in vitro model for sequential study of shiftdown of *Mycobacterium tuberculosis* through two stages of nonreplicating persistence. *Infect Immun 64*, 2062-2069.
118. Voskuil, M. I., Schnappinger, D., Visconti, K. C., Harrell, M. I., Dolganov, G. M., Sherman, D. R., and Schoolnik, G. K. (2003) Inhibition of respiration by nitric oxide induces a *Mycobacterium tuberculosis* dormancy program. *J Exp Med 198*, 705-713.
119. Sherman, D. R., Voskuil, M., Schnappinger, D., Liao, R., Harrell, M. I., and Schoolnik, G. K. (2001) Regulation of the *Mycobacterium tuberculosis* hypoxic response gene encoding alpha-crystallin. *Proc Natl Acad Sci U S A 98*, 7534-7539.
120. Shi, L., Jung, Y. J., Tyagi, S., Gennaro, M. L., and North, R. J. (2003) Expression of Th1-mediated immunity in mouse lungs induces a *Mycobacterium tuberculosis* transcription pattern

characteristic of nonreplicating persistence. *Proc Natl Acad Sci U S A 100*, 241-246.

121. Boon, C., and Dick, T. (2002) *Mycobacterium bovis* BCG response regulator essential for hypoxic dormancy. *J Bacteriol 184*, 6760-6767.
122. Park, H. D., Guinn, K. M., Harrell, M. I., Liao, R., Voskuil, M. I., Tompa, M., Schoolnik, G. K., and Sherman, D. R. (2003) Rv3133c/dosR is a transcription factor that mediates the hypoxic response of *Mycobacterium tuberculosis*. *Mol Microbiol 48*, 833-843.
123. Saini, D. K., Malhotra, V., Dey, D., Pant, N., Das, T. K., and Tyagi, J. S. (2004) DevR-DevS is a bona fide two-component system of *Mycobacterium tuberculosis* that is hypoxia-responsive in the absence of the DNA-binding domain of DevR. *Microbiology 150*, 865-875.
124. Roberts, D. M., Liao, R. P., Wisedchaisri, G., Hol, W. G., and Sherman, D. R. (2004) Two sensor kinases contribute to the hypoxic response of *Mycobacterium tuberculosis*. *J Biol Chem 279*, 23082-23087.
125. Dasgupta, N., Kapur, V., Singh, K. K., Das, T. K., Sachdeva, S., Jyothisri, K., and Tyagi, J. S. (2000) Characterization of a two-component system, devR-devS, of *Mycobacterium tuberculosis*. *Tuber Lung Dis 80*, 141-159.
126. Saini, D. K., Malhotra, V., and Tyagi, J. S. (2004) Cross talk between DevS sensor kinase homologue, Rv2027c, and DevR response regulator of *Mycobacterium tuberculosis*. *FEBS Lett 565*, 75-80.
127. Dye, C., Scheele, S., Dolin, P., Pathania, V., and Raviglione, M. C. (1999) Consensus statement. Global burden of tuberculosis: estimated incidence, prevalence, and mortality by country. WHO Global Surveillance and Monitoring Project. *JAMA 282*, 677-686.
128. Sciotti, M. A., Chanfon, A., Hennecke, H., and Fischer, H. M. (2003) Disparate oxygen responsiveness of two regulatory cascades that control expression of symbiotic genes in *Bradyrhizobium japonicum*. *J Bacteriol 185*, 5639-5642.
129. Gonzalez, G., Gilles-Gonzalez, M. A., Rybak-Akimova, E. V., Buchalova, M., and Busch, D. H. (1998) Mechanisms of autoxidation of the oxygen sensor FixL and *Aplysia* myoglobin:

implications for oxygen-binding heme proteins. *Biochemistry 37*, 10188-10194.

130. Dunham, C. M., Dioum, E. M., Tuckerman, J. R., Gonzalez, G., Scott, W. G., and Gilles-Gonzalez, M. A. (2003) A distal arginine in oxygen-sensing heme-PAS domains is essential to ligand binding, signal transduction, and structure. *Biochemistry 42*, 7701-7708.
131. Becana, M., and Klucas, R. V. (1992) Transition metals in legume root nodules: iron-dependent free radical production increases during nodule senescence. *Proc Natl Acad Sci U S A 89*, 8958-8962.
132. Da Re, S., Schumacher, J., Rousseau, P., Fourment, J., Ebel, C., and Kahn, D. (1999) Phosphorylation-induced dimerization of the FixJ receiver domain. *Mol Microbiol 34*, 504-511.
133. Tuckerman, J. R., Gonzalez, G., and Gilles-Gonzalez, M. A. (2001) Complexation precedes phosphorylation for two-component regulatory system FixL/FixJ of *Sinorhizobium meliloti*. *J Mol Biol 308*, 449-455.
134. Rabin, B. R. (1967) Co-operative effects in enzyme catalysis: a possible kinetic model based on substrate-induced conformation isomerization. *Biochem J 102*, 22C-23C.
135. Frieden, C. (1970) Kinetic aspects of regulation of metabolic processes. The hysteretic enzyme concept. *J Biol Chem 245*, 5788-5799.
136. Frieden, C. (1979) Slow transitions and hysteretic behavior in enzymes. *Annu Rev Biochem 48*, 471-489.
137. Sousa, E. H., Gonzalez, G., and Gilles-Gonzalez, M. A. (2005) Oxygen blocks the reaction of the FixL-FixJ complex with ATP but does not influence binding of FixJ or ATP to FixL. *Biochemistry 44*, 15359-15365.
138. Haapanen, J. H., Kass, I., Gensini, G., and Middlebrook, G. (1959) Studies on the gaseous content of tuberculous cavities. *Am Rev Respir Dis 80*, 1-5.
139. Saini, D. K., Pant, N., Das, T. K., and Tyagi, J. S. (2002) Cloning, overexpression, purification, and matrix-assisted refolding of DevS (Rv 3132c) histidine protein kinase of *Mycobacterium tuberculosis*. *Protein Expr Purif 25*, 203-208.
140. Florczyk, M. A., McCue, L. A., Purkayastha, A., Currenti, E., Wolin, M. J., and McDonough, K. A. (2003) A family of acr-coregulated *Mycobacterium tuberculosis* genes shares a common DNA motif

and requires *Rv3133c* (*dosR* or *devR*) for expression. *Infect Immun 71*, 5332-5343.

141. Parish, T., Smith, D. A., Kendall, S., Casali, N., Bancroft, G. J., and Stoker, N. G. (2003) Deletion of two-component regulatory systems increases the virulence of *Mycobacterium tuberculosis*. *Infect Immun 71*, 1134-1140.
142. Timm, J., Post, F. A., Bekker, L. G., Walther, G. B., Wainwright, H. C., Manganelli, R., Chan, W. T., Tsenova, L., Gold, B., Smith, I., Kaplan, G., and McKinney, J. D. (2003) Differential expression of iron-, carbon-, and oxygen-responsive mycobacterial genes in the lungs of chronically infected mice and tuberculosis patients. *Proc Natl Acad Sci U S A 100*, 14321-14326.
143. Malhotra, V., Sharma, D., Ramanathan, V. D., Shakila, H., Saini, D. K., Chakravorty, S., Das, T. K., Li, Q., Silver, R. F., Narayanan, P. R., and Tyagi, J. S. (2004) Disruption of response regulator gene, *devR*, leads to attenuation in virulence of *Mycobacterium tuberculosis*. *FEMS Microbiol Lett 231*, 237-245.
144. Muttucumaru, D. G., Roberts, G., Hinds, J., Stabler, R. A., and Parish, T. (2004) Gene expression profile of *Mycobacterium tuberculosis* in a non-replicating state. *Tuberculosis (Edinb) 84*, 239-246.
145. Talaat, A. M., Lyons, R., Howard, S. T., and Johnston, S. A. (2004) The temporal expression profile of *Mycobacterium tuberculosis* infection in mice. *Proc Natl Acad Sci U S A 101*, 4602-4607.
146. Voskuil, M. I., Visconti, K. C., and Schoolnik, G. K. (2004) *Mycobacterium tuberculosis* gene expression during adaptation to stationary phase and low-oxygen dormancy. *Tuberculosis (Edinb) 84*, 218-227.
147. Bagchi, G., Chauhan, S., Sharma, D., and Tyagi, J. S. (2005) Transcription and autoregulation of the *Rv3134c-devR-devS* operon of *Mycobacterium tuberculosis*. *Microbiology 151*, 4045-4053.
148. Sohaskey, C. D. (2005) Regulation of nitrate reductase activity in *Mycobacterium tuberculosis* by oxygen and nitric oxide. *Microbiology 151*, 3803-3810.
149. Sharma, D., Bose, A., Shakila, H., Das, T. K., Tyagi, J. S., and Ramanathan, V. D. (2006) Expression of mycobacterial cell division protein, FtsZ, and dormancy proteins, DevR and Acr, within lung

granulomas throughout guinea pig infection. *FEMS Immunol Med Microbiol 48*, 329-336.

150. Brencic, A., and Winans, S. C. (2005) Detection of and response to signals involved in host-microbe interactions by plant-associated bacteria. *Microbiol Mol Biol Rev 69*, 155-194.
151. Dixon, R., and Kahn, D. (2004) Genetic regulation of biological nitrogen fixation. *Nat Rev Microbiol 2*, 621-631.
152. Fischer, H. M. (1994) Genetic regulation of nitrogen fixation in rhizobia. *Microbiol Rev 58*, 352-386.
153. Tuckerman, J. R., Gonzalez, G., Dioum, E. M., and Gilles-Gonzalez, M. A. (2002) Ligand and oxidation-state specific regulation of the heme-based oxygen sensor FixL from *Sinorhizobium meliloti*. *Biochemistry 41*, 6170-6177.
154. Reed, M. B., Gagneux, S., Deriemer, K., Small, P. M., and Barry, C. E., 3rd. (2007) The W-Beijing lineage of *Mycobacterium tuberculosis* overproduces triglycerides and has the DosR dormancy regulon constitutively upregulated. *J Bacteriol 189*, 2583-2589.
155. Ioanoviciu, A., Yukl, E. T., Moenne-Loccoz, P., and Montellano, P. R. (2007) DevS, a heme-containing two-component oxygen sensor of *Mycobacterium tuberculosis*. *Biochemistry 46,* 4250-4260.
156. Sardiwal, S., Kendall, S. L., Movahedzadeh, F., Rison, S. C., Stoker, N. G., and Djordjevic, S. (2005) A GAF domain in the hypoxia/NO-inducible *Mycobacterium tuberculosis* DosS protein binds haem. *J Mol Biol 353*, 929-936.
157. Cole, S. T., Brosch, R., Parkhill, J., Garnier, T., Churcher, C., Harris, D., Gordon, S. V., Eiglmeier, K., Gas, S., Barry, C. E., 3rd, Tekaia, F., Badcock, K., Basham, D., Brown, D., Chillingworth, T., Connor, R., Davies, R., Devlin, K., Feltwell, T., Gentles, S., Hamlin, N., Holroyd, S., Hornsby, T., Jagels, K., Krogh, A., McLean, J., Moule, S., Murphy, L., Oliver, K., Osborne, J., Quail, M. A., Rajandream, M. A., Rogers, J., Rutter, S., Seeger, K., Skelton, J., Squares, R., Squares, S., Sulston, J. E., Taylor, K., Whitehead, S., and Barrell, B. G. (1998) Deciphering the biology of *Mycobacterium tuberculosis* from the complete genome sequence. *Nature 393*, 537-544.
158. Eich, R. F., Li, T., Lemon, D. D., Doherty, D. H., Curry, S. R., Aitken, J. F., Mathews, A. J., Johnson, K. A., Smith, R. D., Phillips, G. N., Jr., and Olson, J. S. (1996) Mechanism of NO-induced

oxidation of myoglobin and hemoglobin. *Biochemistry 35*, 6976-6983.

160. Schnappinger, D., Schoolnik, G. K., and Ehrt, S. (2006) Expression profiling of host pathogen interactions: how *Mycobacterium tuberculosis* and the macrophage adapt to one another. *Microbes Infect 8*, 1132-1140.
161. Chan, E. D., Chan, J., and Schluger, N. W. (2001) What is the role of nitric oxide in murine and human host defense against tuberculosis? Current knowledge. *Am J Respir Cell Mol Biol 25*, 606-612.
162. Chan, J., and Flynn, J. (2004) The immunological aspects of latency in tuberculosis. *Clin Immunol 110*, 2-12.
163. Nathan, C., and Shiloh, M. U. (2000) Reactive oxygen and nitrogen intermediates in the relationship between mammalian hosts and microbial pathogens. *Proc Natl Acad Sci U S A 97*, 8841-8848.
164. Shiloh, M. U., and Nathan, C. F. (2000) Reactive nitrogen intermediates and the pathogenesis of *Salmonella* and *mycobacteria*. *Curr Opin Microbiol 3*, 35-42.
165. Kwon, O. J. (1997) The role of nitric oxide in the immune response of tuberculosis. *J Korean Med Sci 12*, 481-487.
166. Cevallos, M. A., Encarnacion, S., Leija, A., Mora, Y., and Mora, J. (1996) Genetic and physiological characterization of a *Rhizobium etli* mutant strain unable to synthesize poly-beta-hydroxybutyrate. *J Bacteriol 178*, 1646-1654.
167. Garton, N. J., Christensen, H., Minnikin, D. E., Adegbola, R. A., and Barer, M. R. (2002) Intracellular lipophilic inclusions of mycobacteria *in vitro* and in sputum. *Microbiology 148*, 2951-2958.
168. Garton, N. J., Waddell, S. J., Sherratt, A. L., Lee, S. M., Smith, R. J., Senner, C., Hinds, J., Rajakumar, K., Adegbola, R. A., Besra, G. S., Butcher, P. D., and Barer, M. R. (2008) Cytological and transcript analyses reveal fat and lazy persister-like bacilli in tuberculous sputum. *PLoS Med 5*, e75.
169. Flynn, J. L., and Chan, J. (2005) What's good for the host is good for the bug. *Trends Microbiol 13*, 98-102.
170. Gilles-Gonzalez, M. A., Gonzalez, G., and Perutz, M. F. (1995) Kinase activity of oxygen sensor FixL depends on the spin state of its heme iron. *Biochemistry 34*, 232-236.
171. Rohlfs, R. J., Mathews, A. J., Carver, T. E., Olson, J. S., Springer, B. A., Egeberg, K. D., and Sligar, S. G. (1990) The effects of amino

acid substitution at position E7 (residue 64) on the kinetics of ligand binding to sperm whale myoglobin. *J Biol Chem 265*, 3168-3176.

172. Olson, J.S. and Phillips, G.N. (1997) Myoglobin discriminates between O_2, NO, and CO by electrostatic interactions with the bound ligand. *J Biol Inorg Chem 2*, 544-552.